## REVIEW

Check for updates

# Stability and reliability of perovskite containing solar cells and modules: degradation mechanisms and mitigation strategies†

Sara Baumann, ID *[ab] Giles E. Eperon,[c] Alessandro Virtuani, ID [d] Quentin Jeangros,[d] Dana B. Kern, ID [e] Dounya Barrit, ID [f] Jackson Schall,[eg] Wanyi Nie,‡[h] Gernot Oreski, ID [i] Mark Khenkin,[j] Carolin Ulbrich,[j] Robby Peibst,[ba] Joshua S. Stein[k] and Marc Köntges ID *[b]

Perovskite solar cells have shown a strong increase in efficiency over the last 15 years. With a record power conversion efficiency on small area above 34%, perovskite/silicon tandem solar cells already exceed the efficiency limit of silicon solar cells and their efficiency is expected to increase further. While predicted to take large markets shares in a few years thanks to their high efficiency and low manufacturing cost potential, perovskite/silicon tandem devices are not yet sufficiently reliable, which brings into question the commercial viability of this new technology. This review provides an extensive summary of degradation mechanisms occurring in perovskite solar cells and modules. In particular, instabilities triggered by the presence and generation of mobile ions in the perovskite absorber and/or by extrinsic stress factors are discussed in detail. In addition, mitigation strategies developed so far to improve the reliability of the technology are also presented.

### Broader context

In order to achieve the climate goals, the share of renewable energies in total energy conversion must be increased. Therefore, it is advisable to minimize land consumption by increasing the efficiency of solar modules. Tandem solar modules are suitable in this regard, as they consist of two solar cells with different band gaps which allows to increase efficiency. In combination with conventional silicon technology, perovskite solar cells are particularly well suited, as their band gap can be optimized, they are cost-effective and their raw materials are sufficiently available. With a theoretical efficiency limit around 44%, dual junction perovskite/silicon tandem solar cells have already experimentally exceeded the theoretical limit for single-junction silicon solar cells (*i.e.* 29.5%) and achieved 33.9% efficiency on ~1 cm² areas. Beyond upscaling to larger areas, achieving a sufficient stability and operational service lifetime of 30 years and more is essential for the deployment of perovskite/silicon tandem solar cells. However, the stability of perovskites is presently under scrutiny, as the solar cells made with these novel compounds have so far degraded under various environmental influences such as temperature, humidity, oxygen or light on much smaller timescales. Therefore, a focus of research should now be on optimizing long-term stability.

[a] *Institute for Electronic Materials and Devices, Leibniz University Hannover, 30167 Hannover, Germany. E-mail: sara.baumann@stud.uni-hannover.de*

[b] *Institute for Solar Energy Research Hamelin, 31860 Emmerthal, Germany. E-mail: koentges@isfh.de*

[c] *Swift Solar Inc., San Carlos, CA 94070, USA*

[d] *CSEM, 2002 Neuchâtel, Switzerland*

[e] *Materials Chemical and Computational Science Directorate, National Renewable Energy Laboratory, Golden, CO 80401, USA*

[f] *TotalEnergies OneTech, 91120 Palaiseau, France*

[g] *Department of Physics, Colorado School of Mines, Golden, CO 80401, USA*

[h] *Los Alamos National Laboratory, Los Alamos, NM 87545, USA*

[i] *Polymer Competence Center Leoben GmbH, 8700 Leoben, Austria*

[j] *Helmholtz-Zentrum Berlin for Materials and Energy, 14109 Berlin, Germany*

[k] *Sandia National Laboratories, Albuquerque, NM 87185, USA*

† Electronic supplementary information (ESI) available. See DOI: https://doi.org/10.1039/d4ee01898b

‡ Now with the Department of Physics, SUNY University at Buffalo, Buffalo, NY 14260 USA.

## A. Introduction

Metal halide perovskite (MHP) photovoltaic (PV) cells have been the focus of significant research and development interest as an alternative to crystalline silicon (c-Si) and as an addition to c-Si in tandem structures. This global interest is due to a quick rise in cell efficiency[1] since the first perovskite solar cells (PSCs) were produced in 2009,[2] a potential for low production costs thanks to a certain tolerance to atomic point defects,[3] and the band gap tunability of the perovskite material.[4] While record single-junction (SJ) efficiencies are approaching with c-Si solar cells, the ability of PSCs, especially larger area modules, to survive outdoor operation conditions is still uncertain with a wide variability in reported service life for laboratory samples.[5]

**7566** | *Energy Environ. Sci.*, 2024, **17**, 7566–7599

This journal is © The Royal Society of Chemistry 2024

One reason for this uncertainty lies in the very definition of the technology, which is based on a crystallographic classification rather than composition. Thus, there is a wide variety of MHP compositions being developed and lessons learned may not be transferable. Researchers have demonstrated that MHPs are very sensitive to slight variations in both composition and processing parameters and conditions.[6]

Efforts to scale PSCs to larger area modules have resulted in cell to module losses of as much as −10% absolute PCE[5] mainly due to difficulties in depositing large homogeneous MHP films[7] and also the reliance on transparent conductive oxides (TCOs) and their rather high series resistance.[8] MHP composition, charge transport layers (CTLs) and electrodes must use stable materials that result in both high efficiency PSCs and durable devices. It should be first noted that "stability" refers to the capacity to resist (or slow) changes (*e.g.* reactions) that can lead to degraded performance, while "reliability" (and durability) relate to how long these devices perform to expectations in the environment (*e.g.* outdoors). The focus of many research groups recently shifted from efficiency to stability and reliability while first early companies start ramping their production capacities. There are remaining challenges with respect to selecting stable materials and manufacturing reliable modules, yet still only 10% of the current research on PSCs addresses material stability and reliability issues.[9] While other review articles have provided overviews of PSC degradation mechanisms,[10–12] this article expands the review to module-level, with inclusion of mechanical failures, effects of reverse bias, module design and packaging issues and potential induced degradation (PID). Thereby, the mechanisms are mainly explained on the basis of SJ PSCs, but are also concretized for tandem applications. Furthermore, we include a review of mitigation strategies being considered for solving stability problems and increasing reliability of MHP-containing modules.
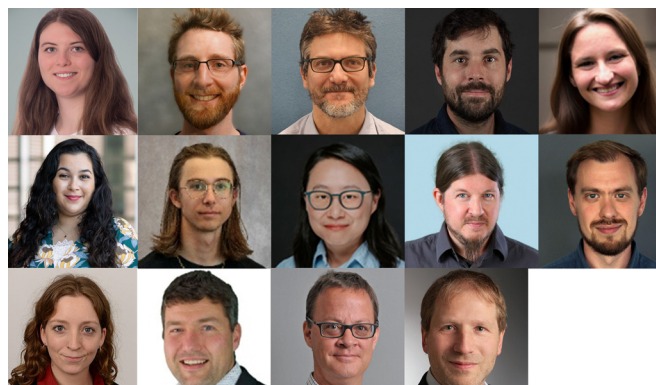
# B. Intrinsic perovskite degradation mechanisms

This first section reviews intrinsically degradation phenomena that occur within the MHP layer. At the end of the section, Table 3 gives and overview of MHP components influencing the stability.

## A. Intrinsic phase instability

The MHP lattice structure forms a cubic, or almost cubic, lattice structure only within a certain range of ionic radii of the three lattice components A, B, and X. This cubic phase is the 'black phase' or 'alpha phase' that is applicable for PV devices, since it readily absorbs light. If any of the A, B, or X components have a too large or small effective ionic radius compared to the other constituents, the cubic structure cannot form, due to physical space constraints. Slight size mismatch can result in undesired secondary crystal phases with non-ideal absorption profile. If the mismatch is significant, the material will not form in the desired $ABX_3$ stoichiometry at all. To predict whether a stable cubic structure is formed, the Goldschmidt tolerance factor can be used, giving a number determined from the ionic radii of the constituent elements.[13] Typically, a tolerance factor of ∼0.85–1 will form a cubic structure, and outside of that regime undesirable phases will form.

MHPs have temperature-dependent tolerance factors. They can be annealed to occupy a desired phase but will always return to their preferred phase under the respective specific (operational) conditions. This change can happen over very long timescales. This can lead to phase instability, where over time the desired black phase degrades to a non-active PV phase. *E.g.*, the pure Formamidinium ($CH(NH_2)_2^+$ or $FA^+$) lead iodide ($FAPbI_3$) MHP composition can be annealed to form the black phase at ∼150 °C, but at room temperature (RT) its tolerance factor is outside the cubic

*LRTB: Sara Baumann (PhD candidate at ISFH, stable perovskite-silicon tandem modules), Dr Giles Eperon (chief science officer at Swift Solar, commercialization of perovskite tandem solar cells), Dr Alessandro Virtuani (reliability of PV modules at CSEM, EPFL and Officina del Sole), Dr Quentin Jeangros (team leader perovskite materials and devices at CSEM), Dr Dana B. Kern (durability of PV materials, cells, and modules at NREL), Dr Dounya Barrit (PV reliability at TotalEnergies), Jackson Schall (PhD candidate at NREL, characterization of perovskites), Dr Wanyi Nie (associate professor at SUNY, perovskite optoelectronic devices), Dr Gernot Oreski (leader of Sustainable Polymer Solutions division at the PCCL and external lecturer at the University of Leoben), Dr Mark Khenkin (Outdoor Performance Group at PVcomB, HZB Berlin, outdoor stability of perovskite-based solar cells), Dr Carolin Ulbrich (leader of Outdoor Performance Group at PVcomB, HZB Berlin), Prof. Dr Robby Peibst (leader of next generation solar cells at ISFH and professorship at the University of Hannover), Dr Joshua Stein (Sandia National Laboratories, director for the Perovskite PV Accelerator for Commercializing Technologies (PACT), independent and unbiased evaluations of perovskite modules), Dr Marc Köntges (leader of PV Reliability at ISFH, characterization methods for PV systems and technologies for reliable tandem modules).*

This journal is © The Royal Society of Chemistry 2024

*Energy Environ. Sci.*, 2024, **17**, 7566–7599 | **7567**

regime, at ~1.02, and will therefore return to a yellow delta phase over days/weeks.[14]

For standard testing under international electrotechnical commission (IEC) 61215 procedures, MHP modules will experience temperatures in the range from −40 °C to +85 °C[15] except for the hot spot test where the reverse voltage protection strategy for shading of the module sets the module temperature during partial shading.[16] If their tolerance factor is close to the edge of the black phase regime at room temperature, it is likely that at some part of the operating temperature range it will degrade to a non-cubic phase.
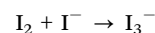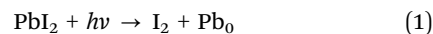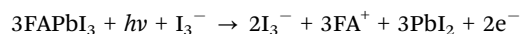
Phase instability can be detected by employing crystallographic methods, *e.g.* X-ray diffraction (XRD) to measure a MHP film's structure, usually as a function of time at room temperature or in operating temperature range. It could be beneficial to employ thermal cycling to accelerate possible phase instabilities, by probing the limits of the operating temperature range.

Preventing phase instability can be accomplished by selecting a composition that is well within the tolerance factor regime for the desired black phase. The tolerance factor can provide rough guidelines for compositions that may be phase stable. Efforts have been made to use a modified, more complex calculation for higher accuracy.[17,18] *E.g.*, Fig. 1 shows how alloying elements can be used for phase stabilization. $FAPbI_3$ (tolerance factor too high) and $CsPbI_3$ (tolerance factor too low) both exhibit different non-cubic phases at room temperature. However, the black phase is produced at room temperature by creating an alloy with an appropriate tolerance factor (represented by averaging ionic radii), as Li *et al.* show.[13] The resulting $FA_xCs_{1-x}PbI_3$ composition is one of the commonly used MHP variations and shows good phase stability. Methylammonium ($CH_3NH_3^+$ or $MA^+$) lead iodide ($MAPbI_3$) and other appropriately chosen $FA_xMA_yCs_{(1-x-y)}PbX_3$ alloys can also sit within this phase-stable regime. However, alloying introduces other problems like phase segregation as described in Section B-C. Recently, progress has been made towards a full phase diagram of these various alloys in combined experimental and theoretical work, including the temperature dependence, by Xu *et al.*[19] Further work is still needed to clearly map the temperature-dependent phase diagrams for a full range of alloys.

## B. Instability induced by leftover MHP precursor and phase impurities

Unconverted $PbI_2$ in MHP films can lead to phase instability and can stem from processing conditions, incomplete mixing during fabrication, or degradation pathways. $PbI_2$ can photolyze under blue or UV light, breaking down into $I_2$ and metallic Pb amongst other byproducts.[20–24] Then $I_2$ can react with the MHP to create more $PbI_2$, thus starting a catalytic breakdown. The photocatalytic breakdown reaction is detailed in equation (1). The presence of $PbI_2$ initiates a photolytic reaction in which MHP material is lost from the film as $I_2$ and deprotonated cations amongst other products[22,23] as depicted in Fig. 2. Table 1 explains the symbols used in all following figures.

$$3FAPbI_3 + h\nu + I_3^- \rightarrow 2I_3^- + 3FA^+ + 3PbI_2 + 2e^-$$
$$PbI_2 + h\nu \rightarrow I_2 + Pb_0 \tag{1}$$
$$I_2 + I^- \rightarrow I_3^-$$

An excess of $PbI_2$ has been used in many cases as a passivation strategy, as it may improve device performance in many cases.[25] However, the observation of this photolytic reaction suggests that this strategy results in unstable films under light, so other passivation strategies are needed.[23] In addition, it may be difficult to totally remove any $PbI_2$ regions, however small, from MHP films created with typical fabrication approaches, implying that strategies to minimize unreacted $PbI_2$ or remove it afterwards could be critical. A key question for long-term MHP photostability is whether the photolysis reaction can be initiated by MHP itself; if so, this reaction may be unavoidable and the focus should be on slowing down its initiation or reaction rate. Donakowski *et al.* suggest that it could be initiated by at least $FAPbI_3$, but a clear answer to this question does not seem to have been reached.[22]

In addition to $PbI_2$, small inclusions of other phases within MHP can initiate decomposition. Using a multimodal microscopy approach, Macpherson *et al.* showed that nanoscale hexagonal polytypes (MHP composition, but different crystal structure) act as degradation nucleation sites.[26,27] Exposing these under illumination resulted in degradation stemming from sites that were often on the nanometre-scale, making these phases hard to identify. They showed that changing composition and fabrication conditions impacted the density
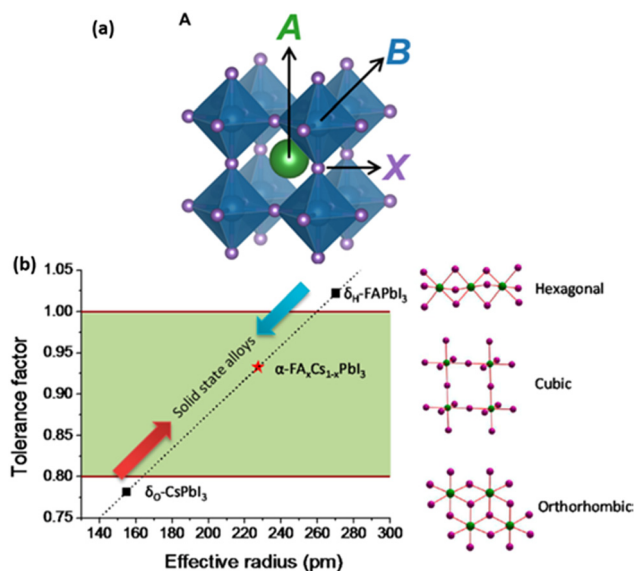


**Fig. 1** (a) Diagram of perovskite crystal lattice showing $A^+$ (*e.g.*, $FA^+$, $MA^+$, $Cs^+$), $B^{2+}$ (*e.g.*, $Pb^{2+}$) and $X^-$ (*e.g.* $I^-$, $Br^-$, $Cl^-$) components reproduced from ref. 17. Copyright 2019 The Authors. (b) Tuning tolerance factor by alloying elements. $CsPbI_3$ and $FAPbI_3$ reside in the non-cubic phase at room temperature (tolerance factor too low/high respectively), but alloying them gives an average tolerance factor within the cubic regime. Reprinted with permission from ref. 13. Copyright 2015 American Chemical Society.
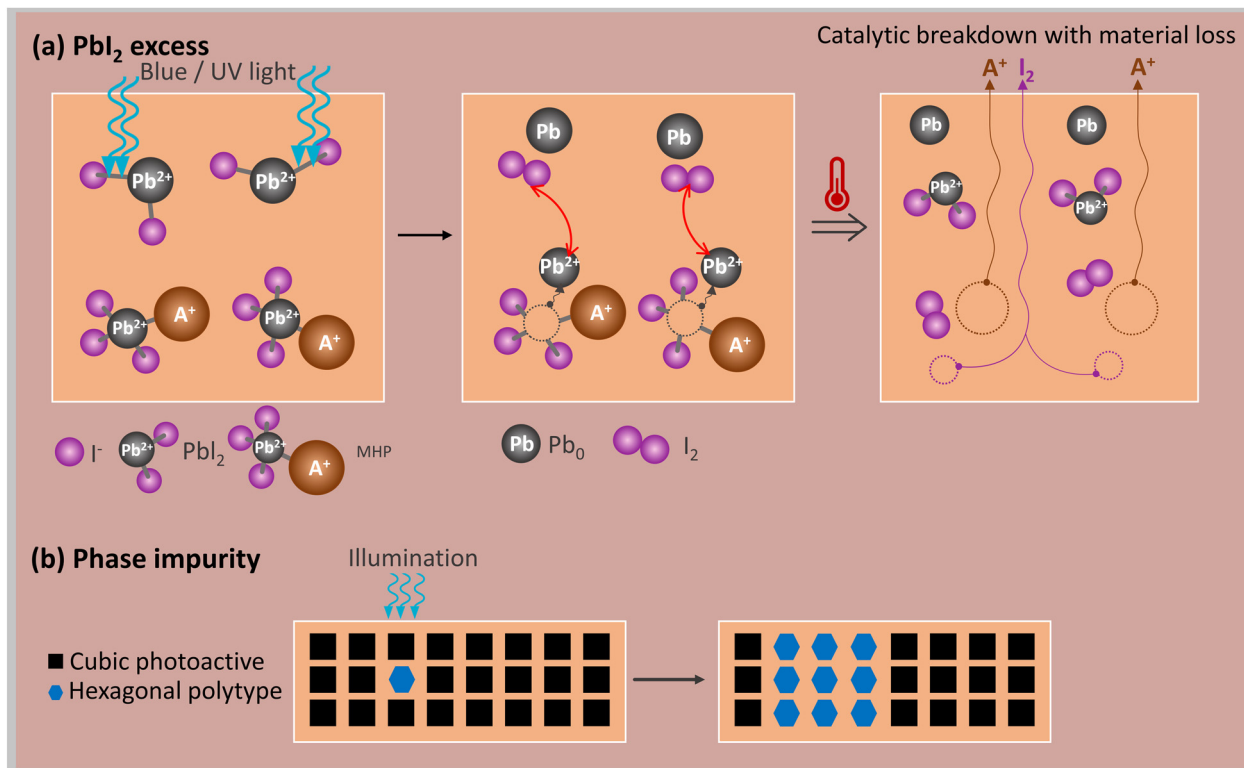
**7568** | *Energy Environ. Sci.*, 2024, **17**, 7566–7599

This journal is © The Royal Society of Chemistry 2024

**Fig. 2** (a) $PbI_2$ residues absorbing blue/UV light can initiate a catalytic breakdown reaction with material loss in the form of $A^+$ and $I_2$. (b) Nanoscale hexagonal polytypes acting as nucleation sites for further degradation of cubic photoactive to hexagonal not photoactive phase.

**Table 1** Symbols used in the following figures

| Symbol | Meaning |
| --- | --- |
| $\Rightarrow$ | Accelerated by |
| | Elevated temperature |
| | Time |
| | Illumination |
| | Electrical bias |
| | Stability problems |
| | Ion Movement |
| | Unwanted reaction between ions |
| | Avoided reaction |
| | Layer has ion blocking characteristics |
| | Material instability |
| $\uparrow/\downarrow$ | Increase/decrease |
| A  X | Regions with higher concentration of $A^+/X^-$ (often not photoactive) |

of such phases, demonstrating the importance to optimize composition and processing to minimize such defects. With sufficient density of impurities (such as excess $PbI_2$ or other phase impurities), these can be detected using XRD or energy dispersive X-ray spectroscopy (EDX).[23] However, several of the studies referenced above suggest that these phases can be problematic even when present at very small fractions that

are only detectable by elaborate electron microscopy-based techniques.[27] Empirical testing of this degradation mode may be accomplished by measuring external quantum efficiency (EQE) while exposing the MHP to light that is absorbed by the impurity – generally any light with a blue or UV component. E.g., for $PbI_2$, wavelengths of $<515$ nm are absorbed.[28] The degradation rate is likely to be temperature sensitive, so a

This journal is © The Royal Society of Chemistry 2024

Energy Environ. Sci., 2024, **17**, 7566–7599 | **7569**

suggested screening protocol might be to place MHP films or PSC devices under blue-containing illumination plus heating to accelerate the reaction with a temperature that would not degrade the specific MHP composition without illumination (*e.g.*, <100 °C for MAPbI$_3$ and <170 °C for FAPbI$_3$) and measure XRD to assess bulk structure degradation.

As briefly mentioned above, the best way to mitigate this mechanism seems unclear thus far. Possible strategies include optimization of composition, stoichiometry[23,26] and the processing to *e.g.* minimize PbI$_2$ residues or, if possible, to avoid them completely. It may also be possible to carry out post-treatments to remove unwanted phases.

## C. Phase segregation

Mixed cation mixed halide MHP compositions are a recent trend to produce high-efficiency PSCs with optimal band gaps for tandem PV with stable crystal structures and extended lifetimes.[29] By analysing literature reports, a prevalent FA:MA cation ratio in the order of 4:1 with <10% Cs stabilization is commonly used.[30–33] Single-halide (*i.e.* pure iodide) PSCs reach efficiencies of 22–26%. However, their relatively low band gap (*e.g.* ~1.5–1.6 eV) is not optimal for MHP/Si tandem solar cells.[34] For MHP/Si tandems the MHP top cell band gap should be ~1.65–1.7 eV and even higher for MHP/MHP tandems,[35] which can *e.g.* be achieved by the incorporation of bromide, chloride or increasing the amount of Cs. However, bromide ratios of more than 20% (at least for MA and MA/FA compositions) bear the risk of halide segregation.[35] Thus, the bromide ratio for stable devices should be limited to ~14–17% to obtain SJ power conversion efficiencies (PCEs) of 18–24%.[32,36–41] This allows obtaining band gaps of about 1.63 eV to 1.70 eV,[32,36,42] which are suitable for MHP/Si tandems. Using Cs/FA or Cs/FA/MA on the A-site probably allows for higher Br ratios as Cs$_{0.17}$FA$_{0.83}$Pb(I$_{0.73}$Br$_{0.27}$)$_3$ was shown to be stable under 1.5 sun illumination.[43] Knight *et al.* state that the higher stability of

triple cation MHPs against halide segregation might be a result of their high crystallinity.[44]

With site-alloyed compositions, even when the average tolerance factor encourages black phase formation, it can be energetically unfavourable in operating conditions for the MHP constituent elements to remain well-mixed in the alloy. This can result in spatial segregation into two or more phases of different composition. While it is possible that this could result in multiple phases that are both black phase, the more problematic and more likely scenario is that one or both segregated phases will have a preferred phase within the operating temperature range that is not the black phase. This segregated phase(s) will then degrade to the non-black phase, causing optical and likely electronic losses. Small fractions of phase segregation can initiate larger scale segregation over time as sketched in Fig. 3. To test if a given composition will phase-segregate under operating conditions, crystallographic studies as a function of time under realistic operational conditions have been performed. Adding a spatial compositional or structural analysis technique such as nano-XRD or time-of-flight secondary ion mass spectroscopy (ToF-SIMS) can detect the scale, morphology, and composition of segregated products.[45] In order to avoid phase segregation, energetic calculations can be carried out on a given composition to determine which are more or less likely to de-mix.

**Cation segregation.** The A site of MHP structures is typically occupied by cations such as FA$^+$, MA$^+$ or Cs$^+$. Those cations can segregate – either caused by an energetically unfavourable composition, or by compositional heterogeneity resulting from the fabrication process, as detailed by Mundt *et al.*[46] The fabrication procedure can be optimized to avoid heterogeneity resulting from deposition conditions by decreasing nucleation sites for segregation. Depending on the magnitude of driving energy, minimizing nucleation sites may be enough to prevent a segregation-prone composition from segregating, but the success of such an approach seems unclear so far. Choosing
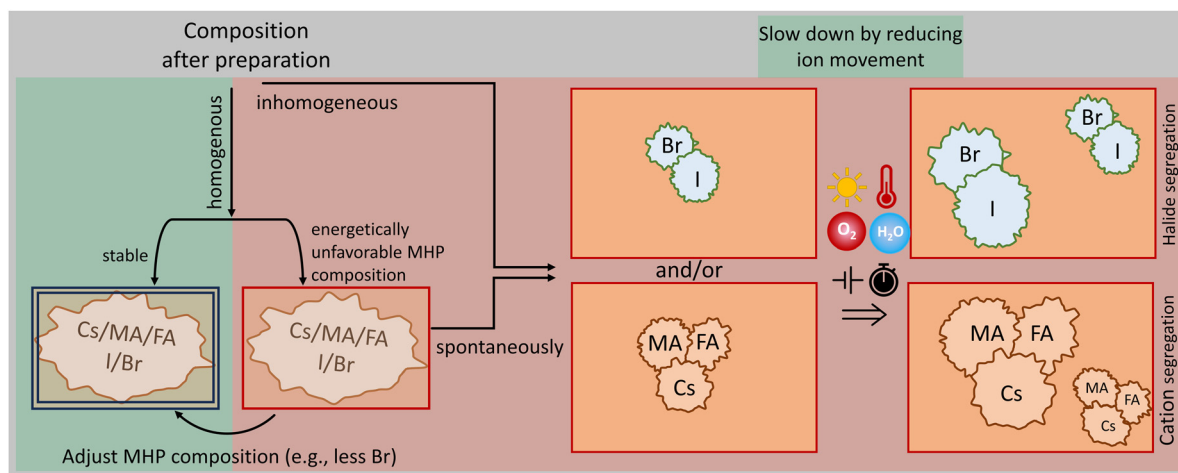


**Fig. 3** Phase segregation in mixed cation and/or halide MHP films can either occur directly at MHP formation due to inhomogeneous mixing during preparation or spontaneously if the composition is energetically unfavourable (at certain temperatures). In both cases, phase segregation will proceed with time and be accelerated by external influences whereas (halide) segregation can be slowed down by reducing ion movement.

**7570** | *Energy Environ. Sci.*, 2024, **17**, 7566–7599

This journal is © The Royal Society of Chemistry 2024

an energetically stable mixed is likely the best approach. Schelhas *et al.* found that compositions such as $FA_a$-$MA_bCs_{1-a-b}PbI_3$ are possibly the best candidates in this regard, though $FA_aMA_bPbI_3$ and $FA_aCs_bPbI_3$ mixed cation compositions may have some regimes in the compositional space where they are stable.[45] A large compositional screen by Zhao *et al.*[47] assessing the stability of a large number of MHP compositions under temperature and light stressing supported this suggestion, and also indicated that having mixed halides appeared to change the regimes of energetic stability.

**Halide segregation.** Similar to cation segregation, alloyed X-site halides (*e.g.* $I^-$, $Br^-$ or $Cl^-$) can segregate into macroscopic phases to minimize overall free energy.[48–51] Halide segregation in the common iodide–bromide system generally occurs with a Br ratio of $\geq$15–20%, depending on exact composition.[35,50] Halide segregation occurs through ion migration (see Section B-D) in defective sites as vacancies,[52] accelerated by external triggers like light or electrical fields. Environmental factors such as oxygen and moisture also strongly impact halide segregation as will be discussed later. Local strain relaxation, particularly with Br concentration below 50%, activates halide segregation, while a strain-free mixed halide crystal prevents light-induced segregation.[53] The A-cation also influences the energy barrier for phase segregation. MA-based MHP have a low barrier for cation segregation, which can initiate halide segregation. It has been shown that crystal phase is a good, but not complete, predictor for halide segregation susceptibility.[50]

To probe halide segregation, XRD and photoluminescence (PL) are commonly used to measure the change in the lattice parameter and optical band gaps, respectively. In the mixed halide structure, the main XRD peaks should be located between the peaks of the pure phases, presenting as a single peak. Upon segregation, the single peak can split into two peaks corresponding to the individual pure phases.[48] By mixing bromide into the pure iodide phase, the optical band edge in PL measurements systematically blue-shifts. Light-induced halide segregation, as reported by Hoke *et al.*,[48] involves reversible band gap redshift due to an iodine-rich phase. PL and transient absorption spectroscopy can also be used to detect changes in recombination kinetics due to halide segregation. Once iodide phases are separated from the mixed halide phase, the majority of the carriers can be trapped in this phase promoting a more intense PL from the lower energy gap.[48,54]

PCE of PSCs and operational lifetime are closely linked to halide segregation. The open-circuit voltage ($V_{OC}$) depends on the optical band gap and radiative recombination efficiency, which is influenced by defect creation within the band gap.[55] Such defects in segregated films cannot always be recognized by decreased radiative recombination and the electroluminescence yield can even be increased. Depending on the composition and stack, different losses may dominate. In some cases $V_{OC}$ losses from halide segregation is less significant than increased interfacial non-radiative recombination.[56] Mahesh *et al.*'s analysis shows that iodide-rich phases formed *via* halide segregation have a smaller band gap, thus reducing $V_{OC}$ overall.[57] Despite possible defect creation, radiative

recombination yield in a segregated film is not necessarily suppressed, potentially improving the external quantum efficiency (EQE) for electroluminescence. As well as $V_{OC}$ loss, in some cases, halide-segregated regions can hinder charge extraction, severely impacting photocurrent.[51]

To suppress halide segregation in mixed halide PSCs, there are two main strategies as summarized in Fig. 3. (a) Choose a composition in which halide segregation is not energetically favourable (typically Br <20%). For MHPs not containing MA/FA up to 40% Br might be possible. Triple halide MHPs, containing Cl in addition to I and Br, are promising to suppress halide segregation.[58,59] (b) Mitigate ion migration by decreasing defect densities. Growing single crystal quality MHPs, such as the recent method by Chen *et al.* and Alsalloum *et al.* for MHP single crystal thin films (pure halide), can stabilize mixed halide phases.[60,61] Defects near surfaces and grain boundaries can be mitigated by passivating halide vacancies with another material. Introducing $Cs^+$,[62] $Rb^+$, or $K^+$[63] in the mixed cation formula may prove effective for defect passivation. Growing 2D MHPs over 3D structures has emerged as a promising strategy to stabilize interfaces, providing strain relaxation for halide phase stabilization.[64–66] Varying cation sizes and anion tuning are crucial for suppressing halide segregation.

### D. Ion migration

MHP materials are mixed electronic/ionic conductors with a low activation energy for the formation of mobile ions.[67,68] The presence of mobile ions has been shown to result in several types of phenomena, from the presence of hysteresis when scanning the current density–voltage ($J$–$V$) properties of a PSC,[69,70] giant photoinduced low-frequency capacitance,[71] PL quantum yield changes, halide segregation in wide band gap MHP absorbers under illumination,[48] to various irreversible changes in the PSC performance occurring over time as a result of external stresses as discussed in the next sections.[72,73]

Experimentally, the density of mobile ions has been estimated to be typically in the order of $1 \times 10^{15}$ $cm^{-3}$ to $1 \times 10^{17}$ $cm^{-3}$ in polycrystalline MHP thin-films used as the absorber of PSCs.[74–80] For comparison, these defect concentrations are higher by a few orders of magnitude compared to typical values found in conventional semiconductors (Si, CdTe, III–V).[81] However, despite containing higher defect concentrations, MHP thin films exhibit excellent optoelectronic properties characterized with a sharp absorption edge[82] and long charge carrier diffusion lengths.[83] From density functional theory (DFT) calculations, it could be inferred that dominant defects with low formation energies induce trap states close to the band edges, while more harmful deeper defect states acting as non-radiative recombination centres have a higher formation energy.[68] This peculiar behaviour is due to the strong antibonding coupling between the Pb s and I p orbitals forming the valence band maximum (VBM) and the high ionicity of the MHP material. As a result, the VBM finds itself shifted upwards to a point where most acceptor states form only shallow states.

From simulation and experimental data, A-site organic cations and the X-site halides are the main ionic defects present in MHP $ABX_3$ thin films, with the former forming in slightly

This journal is © The Royal Society of Chemistry 2024

*Energy Environ. Sci.*, 2024, **17**, 7566–7599 | 7571

higher concentrations but exhibiting a lower diffusion coefficient compared to halide-related defects.[77] Experimentally, halide-related mobile ions have been observed to migrate as a function of external stresses (voltage, light, temperature) – first within the MHP absorber itself,[70,84–86] but then also into the neighbouring contact layers,[87,88] altering their selectivity and the PSC built-in voltage, and towards the electrodes, where e.g. halides may react with the metal electrode to form insulating compounds.[72,73,89] A-site cation migration has also been shown to cause similar reversible[90] or non-reversible changes in PSCs under illumination.[91] Focusing on ion migration in the MHP absorber, experiments and simulations have shown that several competing photochemical processes may occur, leading to the healing of certain types of defects and/or the formation of degradation phases as a result of photoinduced defect formation reactions.[92]

The initial concentration of mobile ions is heavily dependent on the processing conditions,[68] but this concentration may also increase in time when operating the cell under light as a result of several mechanisms. E.g., a reaction between neutral iodine species and photogenerated holes may lead to the formation of iodine vacancies and interstitials.[67] In addition, the photolysis of unconverted lead halide residues, one of the MHP precursors, may induce the release of mobile iodine into the MHP film[93] as depicted in Fig. 2. In some cases, mobile ions may screen the electric field in the solar cell, leading to lower PCE.[94] Furthermore, mobile ions may migrate into the active area of a PSC from a neighbouring dead area through a migration process driven by lateral differences in the electric field between the active and inactive regions of a solar cell.[95]

Overall, while not necessarily impacting the performance of metal halide PSCs in the as-deposited state thanks to a tolerance to point defects, the presence and migration of charged defects impacts the long-term operational stability of PSCs, as it will be detailed in the upcoming sections.

Multiple strategies have been explored for the mitigation of ion migration,[96] including MHP compositional engineering, e.g. inclusions of large A-site cations,[97,98] reducing MHP dimensionality,[99,100] increasing the grain size and grain boundaries modification,[101,102] using additives such as ionic liquids,[103] polymers,[104] or potassium salts.[105,106] As described later the introduction of passivation and blocking layers for interface engineering[107,108] is one strategy to reduce the negative impact of mobile ions. To summarize, a precise control of the MHP absorber composition (low initial density of mobile defects, no PbI$_2$ traces in the as-deposited state, single halide composition to avoid phase segregation, etc.) and microstructure (large grains), as well the use of passivation/barrier layers neighbouring the MHP, are the most promising routes to minimize detrimental effects induced by the migration of mobile ions.

### E. Thermal decomposition

When exposed to high temperatures, MHPs decompose e.g. into gaseous carbon and nitrogen compounds and solid PbI$_2$ whereby the exact decomposition products depend on MHP composition and temperature.[109] The threshold temperature of this process depends on the MHP composition and whether the

PSC is illuminated or not. Schwenzer et al. observed that MA containing MHPs are less thermally stable compared to FAPbI$_3$ and FACsPbI$_3$.[110] Abdelmageed et al. showed that MAPbI$_3$ decomposition starts at 75 °C under illumination, whereas it only decomposes at 95 °C in the dark.[111] Conings et al. showed with DFT calculations that the thermal energy at 85 °C is close to the formation energy of MAPbI$_3$ and proved with EDX that PbI$_2$, conductive Pb$_{(0)}$ and I$_2$ are part of the decomposition products.[112] Abdelmageed et al. observed metallic Pb when MAPbI$_3$ was exposed to 75 °C under illumination whereas only PbI$_2$ formed in dark experiments.[111] Conductive atomic force microscopy (c-AFM) shows that PbI$_2$ areas are non-conducting.[112] The decomposition begins at the surface, continues in the bulk and is faster in ambient air than in inert atmosphere.[112]

Conventional industry qualification standards such as IEC 61215:2021 require long term stability at 85 °C[15] as this can be reached during outdoor operation. There are several reports of PSCs based on MAPbI$_3$ being unstable under temperatures up to 85 °C.[110,112,113] At 60 °C for 22 h or 55 h respectively, thermal degradation of PSCs or MHP/Si tandems has been observed[114,115] leading to a reduced shunt resistance and indication of the formation of metallic phases.[115]

Thermal instability can be mitigated by additives or blocking layers that suppress ion migration. E.g., dimethylammonium formate (DMAFo) was shown to increase stability under 85 °C and illumination.[116] Thermotropic liquid crystals like 3,4,5-trifluoro-4′-(trans-4-propylcyclohexyl)biphenyl (TFPCBP) passivate MHP grain boundaries and thus enable 94% retainment of initial PCE after 1000 h at 85 °C in nitrogen atmosphere whereas the control device lost 22% rel. of its PCE.[117] Cheng et al. introduced CsPbI$_{1.85}$Br$_{1.15}$ quantum dots between MHP and NiO$_x$ in n–i–p PSCs to improve the stability of unencapsulated devices aged at 85 °C and 50% RH in ambient air. PSCs with quantum dots showed higher initial PCEs and retained 85% of their PCE after 400 h while the PCE of PSCs without this modification decreased much faster and reached 85% the of initial value after 150 h.[118] Bi et al. inserted tri-s-triazine-based graphitic carbon nitride (g-C$_3$N$_4$) as a 2D diffusion barrier between an Ag electrode and MAPbI$_3$ and obtained PSCs with higher PCEs compared to devices without the barrier. They simulated that this layer suppresses iodide diffusion by a factor of ~10$^7$ and demonstrated with ToF-SIMS that nearly no iodide moved to the Ag electrode. Therefore, encapsulated PSCs with g-C$_3$N$_4$ blocking layers retained 95% of their initial power after 1000 h damp heat (85 °C, 85% RH), whereas PSCs without this layer showed significant degradation after 100 h damp heat and lost 60% of the initial efficiency after 500 h.[119]

Additionally, Bi et al. observed better stability for FA$_{0.85}$MA$_{0.15}$Pb(I$_{0.85}$Br$_{0.15}$)$_3$ MHP than for MAPbI$_3$. Thus, thermal stability of PSCs can be significantly improved by introducing suitable blocking layers for ion migration and adjustment of MHP composition.

### F. Mechanical properties

The hardness determined by nanoindentation of MHP is low (see Table 2) compared to Si (~13 GPa[120]) and similar to that of

7572 | Energy Environ. Sci., 2024, **17**, 7566–7599

This journal is © The Royal Society of Chemistry 2024

**Table 2**  Hardness of different MHP compositions determined by nanoindentation

| MHP structure | Hardness [GPa] from nanoindentation depending on crystal orientation |
|---|---|
| 2D Layered $(C_6H_5CH_2NH_3)_2PbCl_4$:H | 0.27–0.38[123] |
| MAPbI$_3$ | 0.42–0.46,[124] 0.47,[125] 0.55–0.57,[126] 0.76,[127] 1.0[128] |
| MAPbCl$_3$ | 0.25–0.29[124] |
| MAPbBr$_3$ | 0.26–0.31,[124] 0.32[125] 0.36,[126] 0.54[127] |
| CsPbBr$_3$ | 0.34[126] |
| MAPbI$_{0.1}$Br$_{2.9}$ | 0.63[125] |
| MAPb(I$_{0.7}$Br$_{0.3}$)$_3$ | 0.57[125] |
| FA$_{0.23}$MA$_{0.77}$PbBr$_3$ | 0.37[125] |
| FA$_{0.54}$MA$_{0.46}$PbBr$_3$ | 0.43[125] |
| FAPbBr$_3$ | 0.36[125] |

cell interconnect coatings like eutectic SnPb (0.2 GPa[121]). This implies that cell interconnectors, *e.g.* made from Cu with ~2 GPa hardness,[122] might be pushed through the MHP layer and shunt the PSC at even low pressures (*e.g.* soldering/gluing, during module lamination or finger screen printing). It can be assumed that MHPs behave similarly under tensile forces and that tension caused by cell interconnect ribbons therefore may cause cohesion fracture of the MHP layer.

We suggest investigating whether there are harder MHP compositions – ideally harder than the interconnectors (*e.g.* >2 GPa) – and, if applicable, if PSCs made out of such MHPs are easier to interconnect to strings. However, one needs to make sure that the hardness of MHP brings no other disadvantages. Sun *et al.* observed superior hardness for MAPbI$_3$ single crystals compared to MAPbBr$_3$ and MAPbCl$_3$.[124] Rakita *et al.* state that the mechanical properties mainly depend on the metal–halide bond rather than on the A-site cation being organic (*e.g.* MA$^+$) or inorganic (*e.g.* Cs$^+$).[126] Ma *et al.* showed that the mixture of Br/Cl significantly increases the hardness of MAPbBr$_x$Cl$_{3-x}$ MHPs and that the MA/FA ratio influences the hardness of FAMAPbBr$_3$ MHPs.[125] According to Tu *et al.* 2D MHPs have an even lower hardness than their 3D counterparts as some of the inorganic layers are replaced by soft organic layers. However, increasing the number of inorganic layers from 1 to 5 in 2D MHP structures can increase their hardness from ~0.3 GPa up to ~1 GPa.[129] Another mitigation strategy is the use of methods where the interconnect on top of the MHP cannot connect the underlying electrode *e.g.* by introducing a hard, insulating layer below the interconnection area as in the electrically isolated buried contact (EIBC) concept.[130]

## C. Cell-level specific degradation mechanisms

In the following, degradation mechanisms introduced pertaining to the interaction of cell device layers, and their associated mitigation strategies are explained.

### A. Charge transport and passivation layer reactions

Charge transport layers (CTLs) must remain stable and allow good functionality of the PSC under operational stressors: illumination, heating, electrical potential across the cell, and mechanical stress. There are a variety of ways in which a given

material could exhibit instability. *E.g.* the doping levels in the electron transport layers (ETL) TiO$_2$ are unstable under UV illumination, which changes its defect densities and affect its operation in a cell.[140,141] Some self-assembled monolayers (SAMs), which are currently very popular hole transport layer (HTL) choices, appear to be unstable under illumination due to an electrically isolated electron-rich moiety.[142] Non-fullerene acceptors, also candidates for ETLs, suffer from photochemical reactivity due to the presence of a vinyl linker in their structure.[143]

The interactions between CTL and the MHP layer introduce more varied reaction pathways. Acid–base reactions can occur between elements of the MHP lattice and the CTL. *E.g.*, acidic poly(3,4-ethylenedioxythiophene) polystyrene sulfonate (PEDOT:PSS) has been observed to react with tin-containing MHPs, causing device degradation under extended heating at 85 °C.[144] ZnO, an amphoteric ETL, can react to deprotonate MA cations in MA-containing MHP compositions, which is accelerated under heating and causes PbI$_2$ formation.[145] NiO$_x$, a base, can also react in the same way to deprotonate MHP cations.[146]

It may seem desirable to add dopants to CTLs to improve conductivity. However, introduction of dopant species can also cause more degradation pathways: due to the ionic nature of the MHP material, CTL dopants may diffuse into the MHP. This can cause de-doping of the CTL and can also cause degradation if the dopant is reactive with the MHP material.[147] Furthermore, direct contact with the MHP material leads to the diffusion of ionic species from the MHP, most notably iodine, into the CTL. While in some cases this may be beneficial, iodine ingress is thought to be one of the main causes of drastic instability of the extremely common and highly-performing 2,2′,7,7′-tetrakis(*N*,*N*-di-*p*-methoxyphenylamine)-9,9′-spiro-bifluorene (spiro-OMeTAD) HTL. The iodide species can effectively de-dope the spiro-OMeTAD resulting in rapid degradation of performance when heating to 60 °C.[148,149] The common use of hygroscopic dopants in spiro-OMeTAD is also a likely degradation route – bringing moisture directly into the MHP.[150]

As well as chemical interactions, mechanical interactions can be a degradation route. A mismatch in thermal expansion coefficients or poor adhesion can cause delamination or mechanical deformation of CTL layers upon heating. Schloemer *et al.* showed that MoO$_x$, part of an HTL stack, buckled and

This journal is © The Royal Society of Chemistry 2024

*Energy Environ. Sci.*, 2024, **17**, 7566–7599 | 7573

**Table 3** Rough guidelines on stability of different MHP compositions. Note that stability also highly depends on processing conditions. Illum. means illumination and RT room temperature

| | MHP Composition | Band gap | Stable[a] | Comments on phase stability | Conclusions |
|---|---|---|---|---|---|
| **Single-Cation** | $CsPbI_3$ | 1.77 eV[131] | ≥ 35 °C[132] | Rather **low efficiency**, prone to phase change to inactive compound and air sensitive, but higher heat & moisture resistance and photostability compared to organic MHP | Multi cation or other stabilization methods needed to obtain stable structures in whole operating temperature range |
| | $FAPbI_3$ | 1.47 eV[131] | Not @RT[13], but @150 °C | Higher heat resistance compared to $MAPbI_3$  **High** reported **SJ efficiencies** | |
| | $MAPbI_3$ | 1.55 eV[131] | Not @ 75 °C + illum.[110] | Stable in operating temperature range in the dark, Phase stable, but **degradation under heat + light** | |
| | $MAPb(I_{0.8}Br_{0.2})_3$ | 1.66 eV[133] | Not @ 75 °C + illum. | Improved moisture stability compared to $MAPbI_3$[134] as water adsorption increased for I compared to Br[133]  **Halide segregation for Br/I > 0.2**[44] (e.g., Fig. 4 in[134]) | |
| **Single-Halide (Iodine)** | $FA_{0.8}MA_{0.2}PbI_3$ | 1.53 eV[135] | @RT up to ~ 25% MA[19] | MA exhibits low light + heat and moisture resistance, stability to be investigated for whole operating temperature range | **MA-free** MHP might have increased light + heat & moisture resistance[136]  **Triple cations** might be more stable against phase segregation compared to double cation MHPs[44,45] |
| | $Cs_{0.15}FA_{0.85}PbI_3$ | 1.51 eV[137] | Probably up to ~ 18% Cs (see Fig. 6a in[19]) | Higher structural stability, increased heat & moisture resistance compared to MA-based MHP  Cation segregation under 1 sun illum. was observed for $Cs_{0.15}FA_{0.85}PbI_3$ (with $PbI_2$ residues in the as-deposited state)[45] | |
| | $Cs_{0.10}FA_{0.85}MA_{0.05}PbI_3$ | 1.56 eV[131] | @RT (see Fig. 6b in[19]) | $Cs_{0.091}FA_{0.758}MA_{0.152}PbI_3$ same Goldschmidt tolerance factor as $Cs_{0.15}FA_{0.85}PbI_3$, but more stable against cation segregation under 1 sun illum.[45], probably lower heat resistance due to MA decomposition | |
| **Single-Cation** | $FA_{0.85}MA_{0.15}Pb(I_{0.85}Br_{0.15})_3$ | 1.63 eV[36] | To be investigated | Higher heat resistance compared to $MAPbI_3$[119]  **Stability under constant illum. highly depending on film morphology/processing**[36]; more prone to phase segregation than Cs/FA or MA/FA/Cs MHPs[44] | **Br** to **increase band gap** to be suitable for **MHP/Si tandems**  **High Br/I ratio** may lead to **halide segregation**  Increase band gap by high Cs ratio instead of Br: probably less phase segregation |
| | $Cs_{0.17}FA_{0.83}Pb(I_{0.73}Br_{0.27})_3$ | 1.72 eV[43] | | Stable under 1.5 sun illum.[43]  **Higher heat resistance than with MA** | |
| | $Cs_{0.05}FA_{0.8}MA_{0.15}Pb(I_{0.75}Br_{0.25})_3$ | **1.68 eV**[138] | | **Triple cations** (high crystallinity) might be most promising in terms of **preventing halide segregation**[44] | |
| | $Cs_{0.17}FA_{0.83}Pb(I_{0.6}Br_{0.4})_3$ | 1.75 eV[42] | | CsFA allows higher Br/I ratios without phase segregation compared to MA (still less than 50% @0.5 sun illum.)[139] | |
| | $Cs_{0.4}FA_{0.6}Pb(I_{0.7}Br_{0.3})_3$ | 1.75 eV[42] | | Probably increased photostability with low Br and high Cs ratio[35]  Be careful with cation segregation  See Fig.1g in[35] for exact impact of Cs/Br ratio on band gap | |
| **Triple Halide** | e.g. $Cs_{0.22}FA_{0.78}Pb(I_{0.85}Br_{0.15})_3$ + 5% $MAPbCl_3$[59] | **1.67 eV**[58] | | **Optimal band gap for MHP/Si tandem solar cells**  Increased stability under light + heat[58] | **Triple halide** might be less prone to halide segregation |

[a] e.g., phase stable for Goldschmidt tolerance factor between 0.85 - 1.0 in operating temperature range (-40 °C to +85 °C) or thermodynamically calculated stable alloying

deformed causing degradation when heated at 70 °C.[151] Mechanical weakness of the common $C_{60}$ ETL has been shown to be a weak point where delamination can occur in the MHP stack.[152]

Several promising options for improved stability are reported: for HTLs – undoped PTAA and other polymers, modified NiO,[153] and some SAMs designed for photostability[142] and for ETLs – $SnO_x$, $C_{60}$ (note point above regarding mechanical stability), and modified $TiO_2$.[47,154]

A common strategy to improve performance is to insert a thin passivation layer in between the MHP and ETL, HTL, or both[155] as it is sketched in Fig. 4. In-depth studies of the influence of passivation layers on stability are yet to appear, but some important findings are becoming apparent already.

**7574** | *Energy Environ. Sci.*, 2024, **17**, 7566–7599

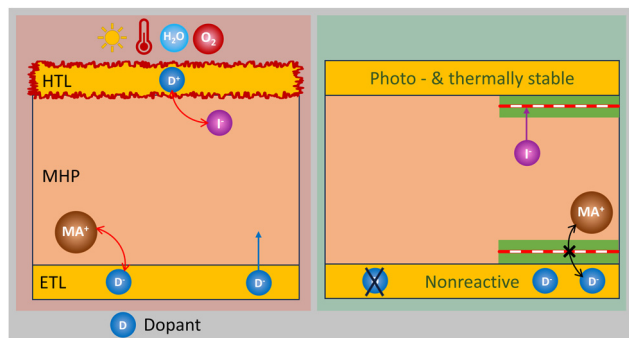This journal is © The Royal Society of Chemistry 2024

Fig. 4 CTLs, especially doped ones, can react with MHP ions. This can be mitigated by using not reactive, intrinsically stable CTLs (without dopants) and/or introducing stable passivation layers between the CTL and MHP layer that block these reactions.

Passivation layers can also introduce instability pathways. It has been shown that some passivation materials undergo similar redox reactions as CTLs, and that some may diffuse into the MHP in similar ways.[156,157]

In all cases discussed above, degradation is caused or accelerated by illumination and/or heating. Therefore, to test empirically whether a proposed CTL or passivation layer is stable when incorporated into a device stack, we propose that a combined heat + light stability test will be most effective as a screening tool. To make rational choices for stable CTLs, it is desirable to choose an intrinsically stable material, minimize reactivity with the MHP by selecting a material that is preferably not acidic/basic, and run heat and light screening tests to check for unexpected degradation routes. The most stable CTLs for PSCs will probably be inorganic rather than organic, e.g. metal oxides[158] or sulphides even though they do not reach highest efficiencies yet.[159]

## B. Electrode-induced degradation

Within a PSC, differences in energy levels and chemical gradients in the electrode, CTLs, and MHP absorber can actively facilitate the exchange of ions across these layers.[160] Migration of electrode atoms into the MHP layer can induce chemical reactions or changes in the potential landscape, which impact device performance and stability. The mobility and reactivity of electrode atoms/ions may be accelerated by factors such as temperature and built-in or external electrical fields.[161,162] Concurrently, degradation pathways are influenced by factors like local defect density, the accumulation of MHP absorber degradation products, and the composition of electrode materials.[73] Typically, low work function metals such as Au, Ag, Cu, Ni, and Al are favored as electrodes due to high conductivity, high reflectivity, and closely matched work function with CTLs. For these reasons, architectures with metal electrodes, Au and Ag specifically,[163,164] produce the highest PCE devices. Au, Ni[165] and Cu[166] are shown to enable the most stable devices. Due to an unmatched work function and its tendency for oxidation Ni limits the maximum performance of a device.[161] Though, regardless of the work function mismatch,

recent reports have shown Cu electrodes enabling high performing and stable devices, comparable with the PCE of devices with Au electrodes.[166]

While some metals are relatively stable in contact with the MHP structure (e.g. Au), almost all metals are reactive with MHP decomposition products (such as MAI, HI, $CH_3I$, and $I_2$).[72,167,168] E.g., it is well known that Ag electrode devices suffer severe degradation due to the formation of AgI both within the absorber and electrode.[169,170] Furthermore, metal atoms can diffuse into the bulk of the MHP absorber layer and create deep trap states, or insulating metal halide species which decrease device performance and stability.[154,161] E.g., from the reaction of iodide/iodine with Cu, Al, Ag, and Au can lead to the formation of an insulating layer at the interface.[171]

Various characterization techniques can be employed to detect and quantify metal electrode diffusion, including ToF-SIMS,[154,161] EDX,[172,173] XRD,[167,174] X-ray photoelectron spectroscopy (XPS).[167,175] These methods provide valuable insights for evaluating the extent of electrode material migration into the MHP or CTLs and gauging its consequential impact on device performance. Performing EDX on cross-sectional samples is useful in detecting the distribution of electrode atoms diffusing between layers. E.g., Liu et al. show significant Ag diffusion into the absorber after thermal deposition of the electrode, resulting in a severe loss in $V_{OC}$ using scanning transmission electron microscopy (STEM)-EDX.[173] Domanski et al. identified with ToF-SIMS significant gold migration through spiro-MeOTAD into the MHP layer at 70 °C causing an irreversible loss in $V_{OC}$, short-circuit current ($I_{SC}$), and fill factor (FF).[161] Insulating metal halide layers as e.g. enhanced formation of CuI at the MHP/electrode interface when a device is exposed to air can in some cases be detected by XRD.[174]

Additionally, Kerner et al. detected rapid formation of $Pb^0$ at the surface of a gold electrode in contact with $MAPbI_3$ MHP with XPS.[175] Not only the MHP degrades, but also the conductivity of Ag electrodes is shown to decrease by two orders of magnitude due to corrosion by iodide within 500 h at elevated temperatures.[119]

Mitigating electrode ion diffusion and preventing the reaction of the electrode with mobile ions from the MHP layer is crucial for extending the operational lifetime of PSCs and is summarized in Fig. 5. The most common strategy to address these challenges is the introduction of a diffusion barrier. As shown by Chen et al. the utilization of titanium between $MAPbI_3$ and Au or Cu cathodes can passivate the MHP interface and prevent metal cathode atoms from diffusing into the absorber. The devices with a Ti interlayer maintained 90% of their initial PCE for 15 days, while devices without this interlayer lost 100% of their PCE after only 5 days.[176] Metal oxides also show promise in reducing electrode migration into the MHP layer. Liu et al. show a dramatic improvement in $V_{OC}$ by the introduction of a ZnO layer between the ETL and Ag electrode[173] (however, notice that ZnO can react with MHPs[145]). Additionally, Kaltenbrunner et al. and Bi et al. introduced a $Cr–Cr_2O_3$[177] or $g-C_3N_4$[119] interlayer that effectively protects the metal top contacts from reactions with the MHP

This journal is © The Royal Society of Chemistry 2024

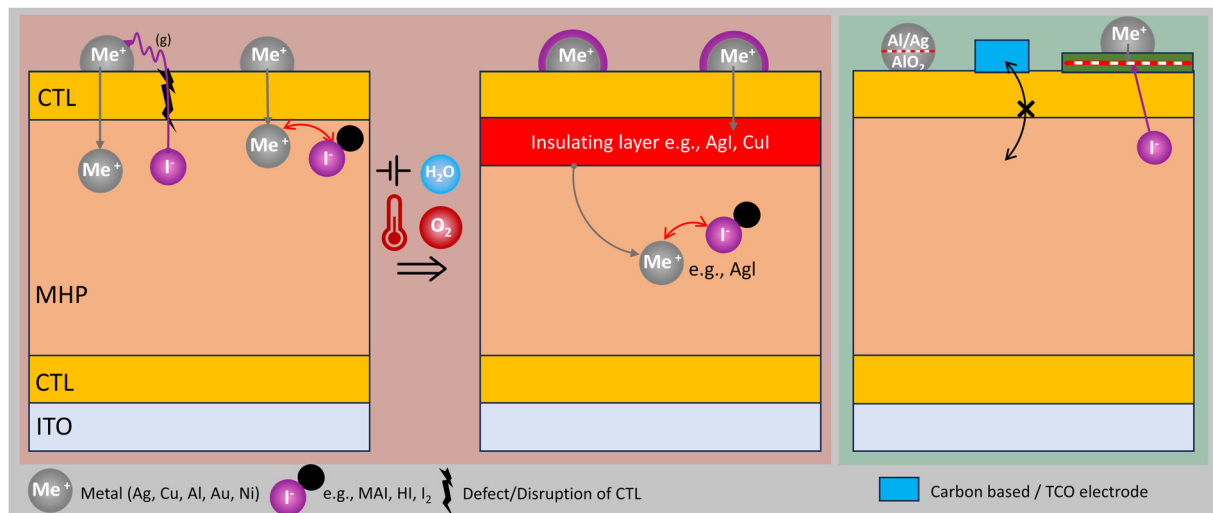Energy Environ. Sci., 2024, **17**, 7566–7599 | **7575**

**Fig. 5** MHP constituents, especially iodide and MHP degradation products react with the metals typically used as electrodes. Thereby, insulating layers may form and hinder efficient charge extraction. Mitigation strategies are the introduction of blocking layers between the MHP and the electrodes or the usage of carbon based/TCO electrodes. However, ITO can be reduced to $In^0$ by $A^+$ ions.

degradation products. Similarly, several research groups use $MoO_x$ interlayer to protect an Al electrode.[154,178] Several organic cathode interlayers between PCBM and Ag or Al electrodes were suggested to prevent reactions to metals in p–i–n PSCs. *E.g.*, some carbolong derivatives,[179] polyoxometalate complexes[180] and rhodamine-functionalized dodecahydro-closo-dodecaborate derivate[181] have been shown to extend the device lifetime compared to the control devices with metal directly deposited on top of ETL. ALD deposited $SnO_2$[182] as well as indium tin oxide (ITO) (or indium zinc oxide (IZO)) layers and Lewis-acid layers between electrode and a dopant-free polymer[183] can also serve as a blocking layer, but only if they are dense and uniform.[160,184] However, the diffusion of cations from the MHP absorber (such as $MA^+$ and $FA^+$) can cause the acid-mediated ITO reduction to $In^0$.[185,186] This was hypothesized to cause the degradation in PSCs where the CTL does not provide sufficient ion blocking.[187]

Further investigations include alloying metal electrodes or creating bi-layer metal configurations to enhance electrode stability. Alloying Ag and Al is shown to form an $AlO_x$ layer at the CTL/electrode interface preventing migration of Ag atoms into the MHP. Using this strategy, Jiang *et al.* report significant stability improvement with almost no change in the $V_{OC}$ after 360 h aging in air with 10% humidity, while comparable devices with an Ag contact show a $V_{OC}$ drop by 85% in the same conditions.[188] Similarly, the insertion of a thin layer of Cu[189] or Au[190] below an Ag electrode considerably lowers the diffusion of MHP decomposition products into the CTL and Ag electrode. Depositing Cr between the spiro-MeOTAD (HTL) and the Au electrode has similar stability enhancing effects. Domanski *et al.* showed that with a 10 nm-thin layer of Cr no Au traces can be found in the MHP after 12 h at 75 °C and 1 sun illumination with inductively coupled plasma mass spectroscopy (ICP-MS).[161]

Even with a diffusion barrier, reactions at the interfaces MHP/CTL and electrode/CTL can alter the charge extraction and carrier recombination properties of the CTL interface. The

inherent tendency of metals to react with MHP and their decomposition products is a critical challenge to solve. Due to this, efforts have been undertaken to eliminate elemental metal from the device stack entirely. The use of carbon-based electrodes[191–193] and TCOs[194,195] leads to a promising increase in reliability compared to elemental metal. Highly transparent conducting electrodes typically exhibit higher electrical losses than metals. However, SJ PSCs often have anyway a TCO on the illuminated side such that a metal contact on the other side does not significantly decrease the resistive losses. In case of MHP/Si tandem solar cells, four times higher resistances in the contacts can be accepted due to the halved current compared to Si. Furthermore, some TCOs can prevent reactions between MHP and metal, *i.e.* metal grids can be placed atop of the TCO so that the charge carriers only need to pass short distances within the TCO and the higher resistance of the TCO can easily be tolerated.

### C. Instability due to strain induced by differences in coefficient of expansion

The thermal expansion coefficients (CTE) of different materials used in MHP or MHP/Si tandem modules vary significantly as summarized in Table 4. The CTE of MHP (depending on the composition) is much higher than that of glass, silicon or ETLs. Typically, the MHP structure is formed at 100 °C on a substrate with much smaller CTE such as glass or Si. Therefore, the MHP cannot contract as it would without the substrate and tensile strain results during cooling to room temperature[196] as sketched in Fig. 6. The lattice strain is significantly smaller on a polyethylene terephthalate (PET) substrate than on ITO/glass due to the larger CTE of PET compared to ITO/glass.[196] Forming the MHP at room temperature results in unstrained MHP films, which is important for stability as strain lowers the activation energy for ion migration.[196] Since the ITO surface is rougher than the bare glass surface, strain relaxation is slower

**7576** | *Energy Environ. Sci.*, 2024, **17**, 7566–7599

This journal is © The Royal Society of Chemistry 2024

**Table 4** Thermal expansion coefficients (CTEs) of several materials of MHP (-Si Tandem) modules

| Material | CTE (10–60 °C) $[10^{-6}\ K^{-1}]$ |
|---|---|
| Glass | $3.7^{[196]}$ |
| Si | $2.6^{[197]}$ |
| PET | $20$–$80^{[196,197]}$ |
| ITO | $8.5^{[196]}$ |
| MAPbI$_3$ | $61,^{[196]}\ 58.2^{[198]}$ |
| MAPbBr$_3$ | $32^{[198]}$ |
| MAPbCl$_3$ | $29.6^{[198]}$ |
| FAPbI$_3$ | $202^{[199]}$ |
| FAPbBr$_3$ | $150^{[200]}$ |
| CsPbI$_2$Br | $84^{[201]}$ |
| CsPbCl$_3$ | $134^{[202]}$ |
| CsPbBr$_3$ | $50^{[200]}$ |
| SnO$_2$ | $3.7^{[203]}$ |
| TiO$_2$ | $11^{[203]}$ |
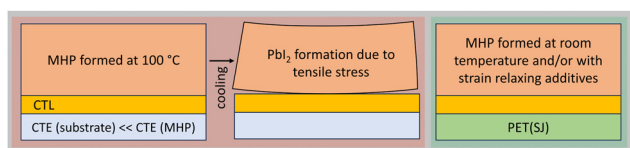


**Fig. 6** MHP formation at elevated temperatures on substrates with significantly lower CTE than MHP (like Si and glass) results in tensile stress within the MHP layer that leads to PbI$_2$ formation over time. Furthermore, stress can be decreased by MHP formation at room temperature and for SJ PSCs on PET substrates.

for MHP/PTAA on ITO/glass than on glass. On glass the strain is shown to relax after 7 days and continuous illumination, which accelerates strain relaxation.[196] On ITO/glass, however, no relaxation was observed after two weeks and the PbI$_2$ XRD peak increased, which means that the MHP decomposes[196] (possibly also due to additional effects besides the strain).

Mitigation possibilities might be the replacement of the annealing step for MHP formation by *e.g.* 12 h at room temperature.[204] Furthermore, additives like octylammonium iodid (OAI) can be incorporated into A-site vacancies of FA$_{0.85}$MA$_{0.15}$Pb(I$_{0.85}$Br$_{0.15}$)$_3$to decrease tensile stress by over 40%. Alternatively, phenethylammoniumiodide (PEAI) can mitigate instabilities due to strain.[205] However, it was shown that post-annealing to 120 °C might lead to a reformation at the MHP/substrate interface and resulting strain.[206] Therefore, it needs to be evaluated whether a high temperature step during module lamination leads to detaching of the MHP from substrates with a large CTE mismatch and whether the above-mentioned relaxing additives can also mitigate this form of stress.

# D. Extrinsic induced degradation mechanisms

The following degradation mechanisms occur when PSCs are exposed to external environmental influences such as external voltages or ambient air that contains water vapor and oxygen.

## A. Degradation due to illumination

The exposition of PSCs to light, visible light sometimes combined with UV light, and elevated temperatures typically leads to an irreversible degradation and belongs to the most critical stressors for PSCs. A feature often observed is that PSCs are stable when illuminated at room temperature or when exposed to elevated temperatures (*e.g.* 85 °C) in the dark but not when the two effects are combined. In other words, the combination of photogenerated charges and elevated temperatures usually drives the degradation of the device. Indeed, photoelectrochemical processes have been found to occur when PSCs are illuminated, with photogenerated charge carriers impacting the ionic dynamics, a temperature-dependent process.[92]

Various failure modes are triggered or significantly accelerated by the combination of illumination and heat, including many of the degradation pathways already discussed in this review. In summary, PbI$_2$ precursor residues not converted to a MHP phase can decompose under blue light, with the photolysis degradation products triggering a degradation of the neighbouring MHP regions.[20] As already mentioned above, mixed MHP materials can undergo a phase segregation process when illuminated, with low bandgap regions then dominating the photoluminescence properties of the material.[207] While the process is mostly reversible, extended phase segregation may lead to irreversible changes in the materials properties as a result of a reorganization of the material[208] and likely a loss of material (through outgassing, see below).[208] In addition, illumination leads to the generation and redistribution of mobile ions depending on the electric field, which can eventually screen the electric field in the absorber, hindering the extraction of photogenerated charge carriers.[94]

The outgassing of volatile decomposition products, typically through cracks/disruptions in the electrode deposited on the MHP, has also been observed.[20] These iodine-based gaseous compounds may then react with the metal electrode, forming insulating AgI$_x$ compounds as discussed beforehand.[20] It is worth noting that the use of a lamination foil should effectively block the transport of gaseous species.

Several researches indicate the particular role of the UV part of the spectrum in causing PSC degradation.[209]

The sun-facing contact and electrode materials may also degrade when exposed to light, especially in the presence of UV light.[209] A notorious example is the UV-induced degradation of the TiO$_x$ electron transport layer used in the first generation of PSCs as reviewed by Boyd *et al.*,[10] particularly in the UV-B range[210]

The use of a UV blocker (*e.g.*, in the encapsulation material) should alleviate some of these issues. However, this would limit the fraction of the solar spectrum available for the absorber and, therefore, decrease the device $J_{SC}$ and PCE of the cell. Alternatively, the UV downshifting materials that absorb the light in the UV region and re-emit visible photons could be used. They could simultaneously achieve favourable optical properties and improved device stability.[211] However, this topic is still in the early stages of development and today there are no efficient and cost-competitive solutions yet.

This journal is © The Royal Society of Chemistry 2024

*Energy Environ. Sci.*, 2024, **17**, 7566–7599 | **7577**

Despite these challenges, the operational stability of PSCs when exposed to light and elevated temperature in the laboratory has been progressing over the years. The use of inorganic or hybrid organic–inorganic single-halide perovskites, in both cases with 2D capping layers, has enabled the demonstration of small-scale PSCs with excellent durability when illuminated at 85 °C or more (e.g., 97% of the initial stability retained after 1000 hours at 85 °C).[132,212] The challenge now is to replicate these promising results with large-area industrial modules and then validate in the field their improved reliability.

### B. Reactions with water vapor

The $NH_3^+$ group within $MA^+$ is hydrophilic[213] such that the bond between $MA^+$ and metal or halide ions is broken by $H_2O$[214] and an intermediate monohydrate and in the following a dihydrated MHP phase can form.[72,215,216] Those reactions are reversible but once the MHP is moisture saturated, the hydration will become irreversible. $MAPbX_3$ ($X = I^-/Br^-/Cl^-$) e.g. will decompose to aqueous MAX and solid $PbX_2$.[214,217] The intermediate monohydrate $MAPbI_3 \cdot H_2O$ can be recognized by its yellow colour and all degradation products can be confirmed with XRD.[218]

Water adsorption is stronger for $I^-$ than for $Br^-$ ions. Noh et al. reported that $MAPb(I_{1-x}Br_x)_3$ solar cells with 20% and 29% Br fraction have much improved dark storage stability in air with RH between 35% and 55% compared to cells with lower Br composition.[72,133] However, moisture-induced surface defects assist halide migration, trapping ions and creating $Br^-$ and $I^-$ rich domains.[219,220] Therefore, high humidity accelerates halide segregation.[221] Fig. 7 summarizes the effects of water vapor on PSCs and mitigation strategies. As $FA^+$ and $Cs^+$ are less polar compared to $MA^+$, water adsorption can be lowered by modifying this part of the MHP composition.[213]

In addition, the contact layers also impact the stability of PSCs under humid conditions. A common HTL, spiro-OMeTAD, is doped with hygroscopic lithium-bis-(trifluoro-methane)sulfonimide (Li-TFSI) and is therefore unstable in humid environments.[222] $TiO_2$ (often used as ETL) is hydrophilic as well and the ETL material [6,6]-phenyl C61 butyric acid methyl ester (PCBM) also accelerates degradation with moisture because it is water absorbing.[214] Therefore, CTLs should be carefully chosen taking their stability into account. Furthermore, the MHP degradation products due to moisture like $PbI_2$ react with the metal electrode[172,223] as it is described in Section C-B.

Several reports of devices passing damp heat tests suggest that a sufficient encapsulation can mitigate moisture degradation.[224–226] Possible encapsulation processes include glass-glass modules with an edge seal[224,226] which will be described in Section E-C. An alternative strategy is the application of thin films directly onto PSCs. An ALD grown $Al_2O_3$ capping layer not only protects PSCs from moisture but can even improve hole transport as it infiltrates spiro-OMeTAD.[227] 45 nm sputtered $SiO_2$ barriers on top of $MAPbI_3$ and 300 nm $SiO_2$ on top of a triple-cation MHP significantly improved stability in nitrogen atmosphere with 85% RH whereby the degradation was imaged by laser beam-induced current (LBIC).[228] However, these capping layers are often not scalable to large areas and might damage MHP layers during application.[214] It has been shown that 1 nm thick $MgF_x$ interlayers between MHP and ETL can also increase stability, with 95% of their initial PCS being retained after >1000 h at 85 °C and 85% RH.[229]

For flexible modules, packaging is an even bigger challenge as no glass can be used and the flexibility of capping layers such as $Al_2O_3$ needs to be considered.[230]

There are several reports on an improvement of the crystallinity of MHP and therefore the PCE of PSCs due to a certain level of humidity during fabrication or a posttreatment with water.[231,232] However, there is no universal rule for optimal humidity levels, and it might strongly depend on the processing route. The atmosphere during preparation should be controlled to obtain consistent results. The stability of PSCs themselves against moisture might be improved by using 2D/quasi 2D MHPs[233] or inserting a 2D MHP layer between ETL and MHP.[226] Furthermore, optimizing the MHP composition with additives can improve moisture stability. The additive TFPCBP e.g. leads to retainment of 96% initial PCE after 3000 h at 45% RH in ambient for unencapsulated devices compared to 75% for control devices and to 86% (with TFPCBP) compared to 51% (control) for encapsulated devices after 1200 h in 85% RH and 85 °C, respectively.[234] Cheng et al. also observed an improvement from 62% of initial PCE after 1000 h damp heat test at 85 °C and 85% RH for encapsulated modules to 86% by adding MHP quantum dots between the MHP and the $NiO_x$ HTL.[118] PSCs with these quantum dots even retained their black colour after dipping into water for 45 min without encapsulation. Additionally, CTLs should be as hydrophobic or non-hygroscopic as possible. Therefore, $NiO_x$ is shown to be much better suited than PEDOT:PSS.[235]

### C. Reactions with oxygen

The exact degradation mechanisms of PSCs in an oxygen-containing atmosphere are not fully understood but they are
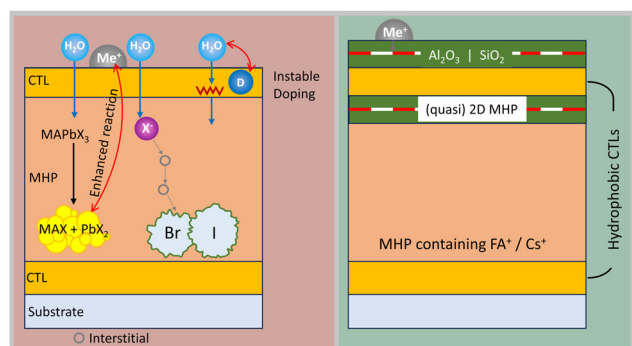


**Fig. 7** Water vapor can react with the MHP resulting in decomposition in, among others, $PbX_2$ visible by a yellow colour. Decomposition products are highly reactive with metal electrodes. Furthermore, water vapor can induce instabilities in (doped) CTLs and moisture induced defects enhance ion movement resulting in halide segregation. Mitigation strategies are barrier layers, hydrophobic CTLs, (quasi) 2D MHP on top of 3D MHP and avoiding of $MA^+$ or encapsulation (see Fig. 11).

**7578** | Energy Environ. Sci., 2024, **17**, 7566–7599

This journal is © The Royal Society of Chemistry 2024

accelerated by exposure to light, heat, and/or applied voltage bias. Reactive oxygen species can be generated which damage the PSC.[30] One of the main degradation mechanisms is the oxidation of the organic cations, such as $MA^+$ or $FA^+$.[236] The reaction with oxygen molecules can form amine oxides or nitro compounds with the N–H bonds in the organic cations. This reaction can cause organic species to decompose or volatilize from the MHP layer resulting in the loss of organic cations and the formation of vacancies or defects in the MHP structure, which is depicted in Fig. 8. These defects can decrease MHP crystallinity, decrease conductivity, and enhance phase segregation.[12,237]

Another degradation mechanism is the oxidation of metal halides, such as $PbI_2$. Oxygen can react with metal halides and form oxyhalides or metal oxides, such as PbO or $PbO_2$, which decreases the conductivity and stability of the MHP layer.[238] Furthermore, oxygen molecules can interact with the trapped charges in the MHP layer generated by light irradiation or bias voltage. In the dark, higher stability of PSCs upon exposure to oxygen has been observed.[239] Trapped charges can disrupt the crystal structure of the MHP material and create defects or vacancies facilitating the diffusion of oxygen or other molecules into the MHP layer and resulting in reversible degradation in dry air.[240,241] Organic CTL layers are often susceptible to oxygen-induced loss of conductivity, where oxygen reacts with the C–H bonds in the organic materials and forms carbonyl or carboxyl groups, which affect their carrier mobility, and contact quality.[242–244] Typically at least one CTL in PSCs consists of organic materials or small molecules and polymers, (e.g. poly[bis(4-phenyl)(2,4,6-trimethylphenyl)amine] (PTAA) and spiro-OMeTAD as HTLs

and PCBM as an ETL). Spiro-OMeTAD requires some oxidation to decrease the series resistance in devices. However, as mentioned above, the Li-TFSI dopant of Spiro-OMeTAD is very moisture-sensitive. Therefore, a $Li^+$-free hydrophobic HTL was proposed by using a preoxidized salt of the hole transporter itself (e.g. Spiro-OMeTAD$^+$ TFSI$^-$).[72,154] PTAA and poly(3-hexylthiophene-2,5-diyl) (P3HT) on the other hand, act as better barriers for oxygen than Spiro-OMeTAD slowing down the rate of decomposition as reported by Kundu et al.[239,245]

Looking at inorganic CTLs, oxide transport layers such as $TiO_2$, $SnO_2$, $MoO_x$, and $NiO_X$ are often used for efficient devices. For instance, metal oxides such as $TiO_2$, especially under UV light, favour the photoinduced desorption of $O_2$ out of the metallic oxide, generating vacancies that serve as deep electronic trap-states for charge accumulation and recombination across the ETL. But it also leads to the $TiO_2$-mediated photocatalytic decomposition of organic materials in the MHP absorber layer.[72,246,247] $SnO_2$ is now a popular choice as an ETL as it minimizes the intrinsic UV activated deep traps leading to more stable devices.

Reactive oxygen species can also migrate from one layer to another through diffusion or electric fields, causing cross-layer degradation in PSCs. Furthermore, oxygen molecules can oxidize the metal electrodes or contacts of the PSCs, such as Cu or Ag. This forms oxides that can increase series resistance or decrease the shunt resistance of the device.[248,249] Similarly, the X-site species formed due to the degradation of the MHP layer under oxygen diffuse to the metal electrodes and contacts leading to their corrosion, especially in the presence of an electric field.[30]
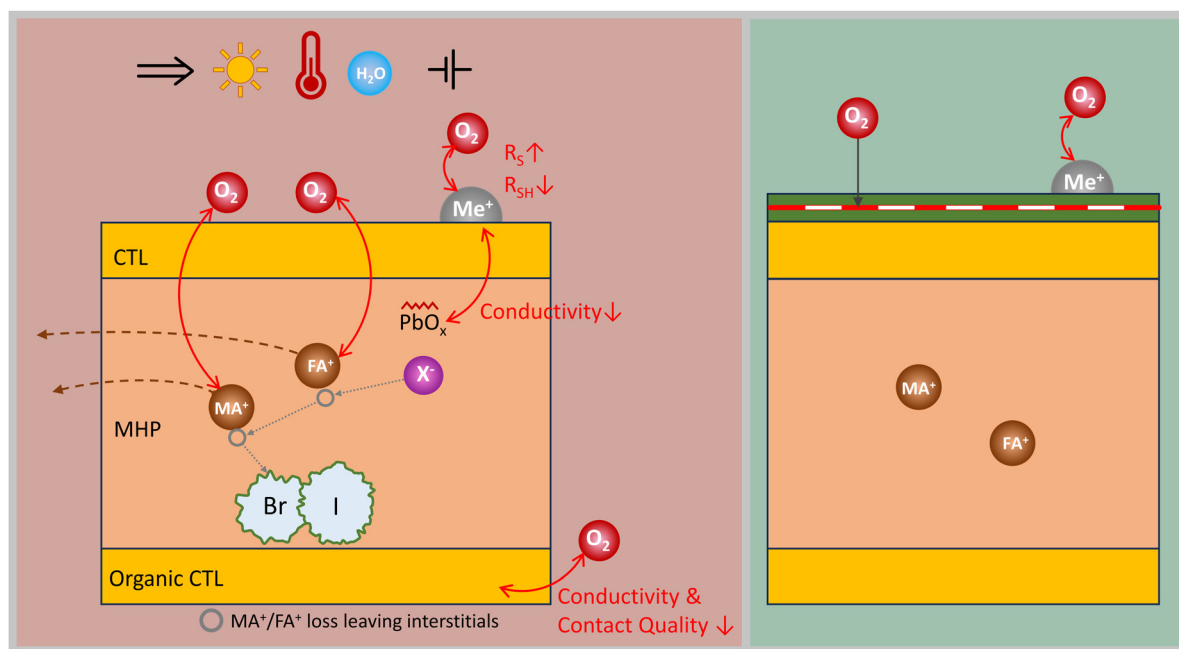


Fig. 8 Organic components can be removed from MHP due to oxidation of $MA^+$ or $FA^+$. The resulting interstitials enhance halide segregation. Additionally, oxygen can react with Pb, with the metal electrodes or CTLs negatively impacting conductivity, stability and/or contact quality.

Sn-based MHPs are especially sensitive to oxygen because Sn(II) is susceptible to oxidation to the Sn(IV) state even under encapsulation. The development and understanding of Sn and mixed Pb–Sn MHPs is crucial due to their ideal band gaps as bottom sub cell of all-MHP tandem PV. Therefore, a lot of effort was made to mitigate their oxidation. For instance, $SnF_2$ was used as an additive to suppress the oxidation of $Sn^{2+}$ to $Sn^{4+}$ induced by the formation of Sn vacancies and interstitials. Lim *et al.* studied the degradation pathways of Sn-only and mixed Pb–Sn MHPs under ambient air. They suggest that the degradation mechanisms of the Sn-only films can be solely related to Sn-vacancy formation and self-doping effects, while in the mixed Pb–Sn films, it involves the formation of deep trap states corresponding to the defect chemistry present in Pb-only MHP.[72,250]

The combination of light, high temperature, high humidity, and/or applied voltage accelerates the degradation of MHP films under oxygen to a greater extent.[239] Therefore, it is important to study the stability of PSCs under different conditions and find ways to improve their durability and reliability. In that context, several strategies have been investigated such as using more stable MHP materials by compositional tuning (cation or halide) that can resist oxygen-induced degradation better than pure MA or FA-based MHPs.[239,240] Furthermore, protective coatings and effective encapsulation materials (such as polymers, glasses, or metals) or techniques that can prevent or lower the ingress of oxygen can protect the MHP layer and the electrodes from oxidation.[12,236] Other mitigation techniques include additives or passivation agents that decrease the formation of defects or vacancies in the MHP layer and improve its electronic properties. In addition, adding dopants to the charge transport layers, such as ionic liquids, metal oxides, or carbon nanotubes, can hinder oxygen penetration.[239]

### D. Reverse bias

As it will be further described in Section E-B, solar cells need to withstand negative bias voltage. However, it has been shown that even less than −5 V of reverse bias may lead to degradation of PSCs[251,252] in contrast to Si solar cells which enable stable modules up to their breakdown voltage $V_{bd} \approx -13$ V to −20 V.[16,253] In Si $V_{bd}$ is the threshold voltage of avalanche breakdown whereas the breakdown in PSCs is suggested to be caused by trap-assisted tunnelling.[252,254] For PSCs Bowering *et al.* defined $V_{bd}$ as the voltage at which the current density ($J$) in dark $J$–$V$ curves is below −1 mA cm$^{-2}$.[251,255] An overview of several published $V_{bd}$ for PSCs ranging from −0.2 V to −8 V can be found in Wang *et al.*[256] and a $V_{bd}$ of −15 V was recently reported by Jiang *et al.*[257] Furthermore, $V_{bd}$ depends on the types of contact employed and density of mobile ions.[251,252]

According to Bowring *et al.* and Bertoluzzi *et al.*, applying reverse bias to a PSC leads to band bending probably resulting in cation accumulations (mainly iodine vacancies due to their low activation energy) at the interface between MHP and HTL and an anion excess close to the ETL.[251,252] The band bending increases with higher negative applied voltages until holes might tunnel from the ETL conduction band into the MHP

valence band likely assisted by traps.[252] This tunnelling might lead to an excess of holes over electrons (about 20 times), which may lead to an oxidation of iodide.[252] Even short exposure to reverse bias can result in the unusual $J$–$V$ curve distortion, characteristic of a tunnel diode (with partially negative differential resistance).[258] Prolonged exposure even to small reverse biases results in a MHP decomposition assigned to iodine loss.[254] As long as the iodine does not leave the PSC, the reaction is reported to be (partially) reversible.[251,259] Also, iodine has been detected in the C60 layer after reverse biasing experiments, which altered the $J$–$V$ properties of the shaded cell.[87] Henzel *et al.* observed that the reverse bias current and degradation rate (PCE loss/time of reverse bias application) are both exponentially dependent on the applied voltage and therefore suggest that the reverse bias degradation is current driven.[255] The degradation rate reached up to 3%/min even under low reverse bias current densities below 2 mA cm$^{-2}$.[255] An extrapolation to −20 mA cm$^{-2}$ and reverse bias slightly above $V_{bd}$ would mean half PCE loss in 3 min.[255]
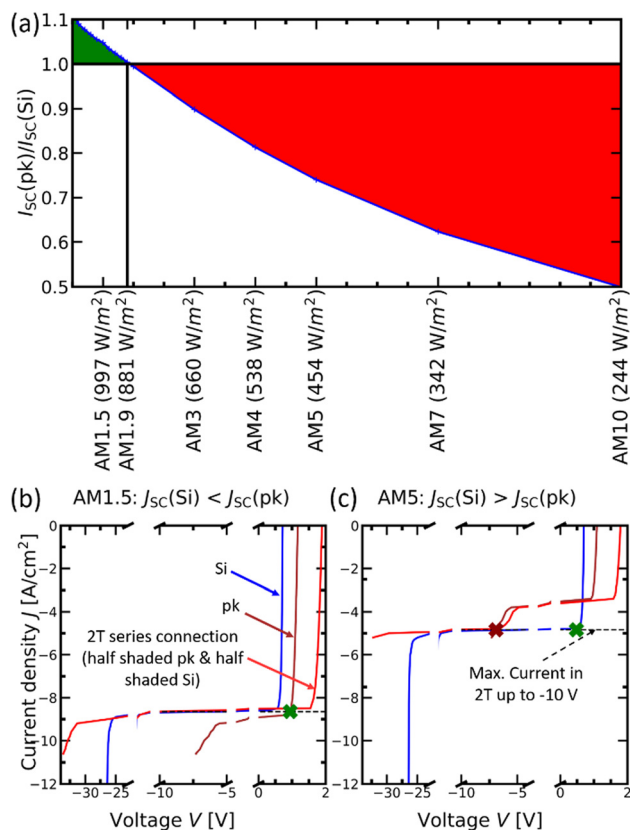
Compared to c-Si, thin-film technologies are more difficult to protect by bypass diodes as their integration into the monolithic interconnection using laser scribing (see Section E-A) is more complex. These technologies are also more prone to reverse bias degradation due to the small layer thicknesses employed in the stack. Indeed, in thin-film PV modules based on CIGS or CdTe materials, small irregularities in the thin-film coatings such as voids or pinholes form preferential current pathways in reverse bias, inducing thermal damage as a result of the large power dissipated locally at these defects.[260]

Similar shunting degradation has been observed in SJ PSCs, with devices often shunting in a few regions after only seconds/minutes at mild reverse voltages of a few volts[87,251] and ascribed to the position of local defects, *e.g.* extrinsic impurities. These may possibly result from the migration and accumulation of mobile ions in the MHP absorber triggered by lateral differences in the electric field around the impurities.[95] The local conductive pathways in reverse bias typically increases temperature beyond the MHP thermal budget, which leads to a decomposition of the neighbouring MHP material to $PbI_2$[254] and to the formation of additional shunt pathways.[87]

MHP devices with a metal electrode are particularly prone to rapid shunting under reverse bias,[87,251] likely due to a redistribution of the conductive metal electrode in the absorber material. Metal-free devices, *e.g.*, using a carbon-based electrode, have been shown to be more resilient to partial shading conditions, with some devices even passing the IEC61215:2016 hotspot test requirements and withstanding up to −9 V and close to 70 mA cm$^{-2}$ for up to 30 min.[254] These carbon-based modules eventually degraded due to a loss of iodine and a local decomposition of the MHP to $PbI_2$, but only when surpassing a reverse voltage around −9 V.

Finally, several theoretical studies investigated the impact on reverse bias resilience of specific cell and module designs (PSC SJ, MHP/Si tandem with 2-terminal (2T, two electrical contacts) and 4-terminal (4T, top and bottom cells have distinct

**7580** | *Energy Environ. Sci.*, 2024, **17**, 7566–7599

This journal is © The Royal Society of Chemistry 2024

**Fig. 9** Simulation of (a) $J_{SC}$(PSC)/$J_{SC}$(Si) ratio in dependence of air mass. Green area (AM1.0–AM1.9) corresponds to situation (b) and the red area to (c). (b) $J$–$V$ characteristics of a half shaded 2T MHP/Si tandem solar cell at AM1.5 with $J_{SC}$(Si) $<$ $J_{SC}$(PSC). The dashed black line shows the maximum working current for a 2T tandem (red) which is only exceeded at more than −10 V and is limited by the Si bottom cell (blue). The green cross visualizes that the PSC (brown) stays in forward bias at this current. (c) When $J_{SC}$(Si) $>$ $J_{SC}$(PSC) (e.g. at AM5) the PSC is current limiting until −7 V and therefore gets reverse biased even when low negative voltages are applied to the 2T tandem, whereas the Si cell stays in forward bias (green cross). The red cross marks the working point of the PSC at which the Si cell starts to be current limiting under this light condition.

electrical contacts; 4 in total) architectures).[261,262] The tolerance to reverse voltages of MHP materials greatly increased in monolithic 2-terminal MHP/Si tandem solar cells due to the presence of the bottom Si cell, whereby over 95% of the reverse voltage is dropped at the latter in dark conditions.[263]

We point out that the protection effect by the c-Si solar cell only applies for shading of a whole cell (as conducted in Xu *et al.*[263]) or partial shading of a cell under light conditions where the short-circuit current density $J_{SC}$(c-Si) $<$ $J_{SC}$(PSC). Fig. 9(a) illustrates that for AM spectra below 1.9, $J_{SC}$(PSC)/ $J_{SC}$(Si) becomes $<$1 for PSC and c-Si solar cells that are current-matched at AM1.5 spectrum. As shown in Fig. 9(b), the maximum current density in a half-shaded 2T MHP/Si solar cell is limited by the Si sub cell at AM1.5 so that the PSC stays in forward bias up to $\approx V_{bd}$(Si). However, at AM5 spectrum (see Fig. 9(c)) the current in the same 2T MHP/Si tandem solar cell is limited by the PSC to a voltage at which the PSC already

experiences reverse bias (see red cross as an example with −10 V applied to the tandem solar cell). The Si solar cell only protects the PSC from experiencing even higher reverse currents for higher reverse bias voltages than −7 V applied at the tandem solar cell (for this example) up to its own $V_{bd}$. The external quantum efficiency (EQE) for the $J_{SC}$ calculation was hereby simulated with SUNRAYS[264,265] and the spectra were simulated with SMARTS[266] for a 37° tilted, south-facing area in the US. Therefore, the reverse bias stability of PSCs should be considered in SJ as well as in tandem applications.

Strategies for the improvement of reverse bias stability are metal-free[254] or inert Au instead of Ag electrodes[267] and single halide MHP.[87,254] Further enhancement was shown by a hole blocking layer between ETL and MHP,[259] a TCO between HTL and metal electrode,[267] polymer HTLs like relatively thick PTAA-layers that block electrons more efficiently than *e.g.* the SAM (2-(3,6-dimethoxy-9*H*-carbazol-9-yl)ethyl)phosphonic acid (MeO-2PACz)[257] or modifying the MHP surface in a way that mitigates ion migration through the MHP surface (*e.g.* by 3-mercaptopropyl(dimethoxy)methylsilane (MDMS)).[268] However, there is still a decrease by more than 25% in PCE after 2 min at −1 V.[268] It might be useful to produce PSCs with low $V_{bd}$ to dissipate the power generated by the illuminated segment homogeneously over the shaded cell area (rather than locally through shunts). Further mitigation strategies on module level will be described in Section E-B.
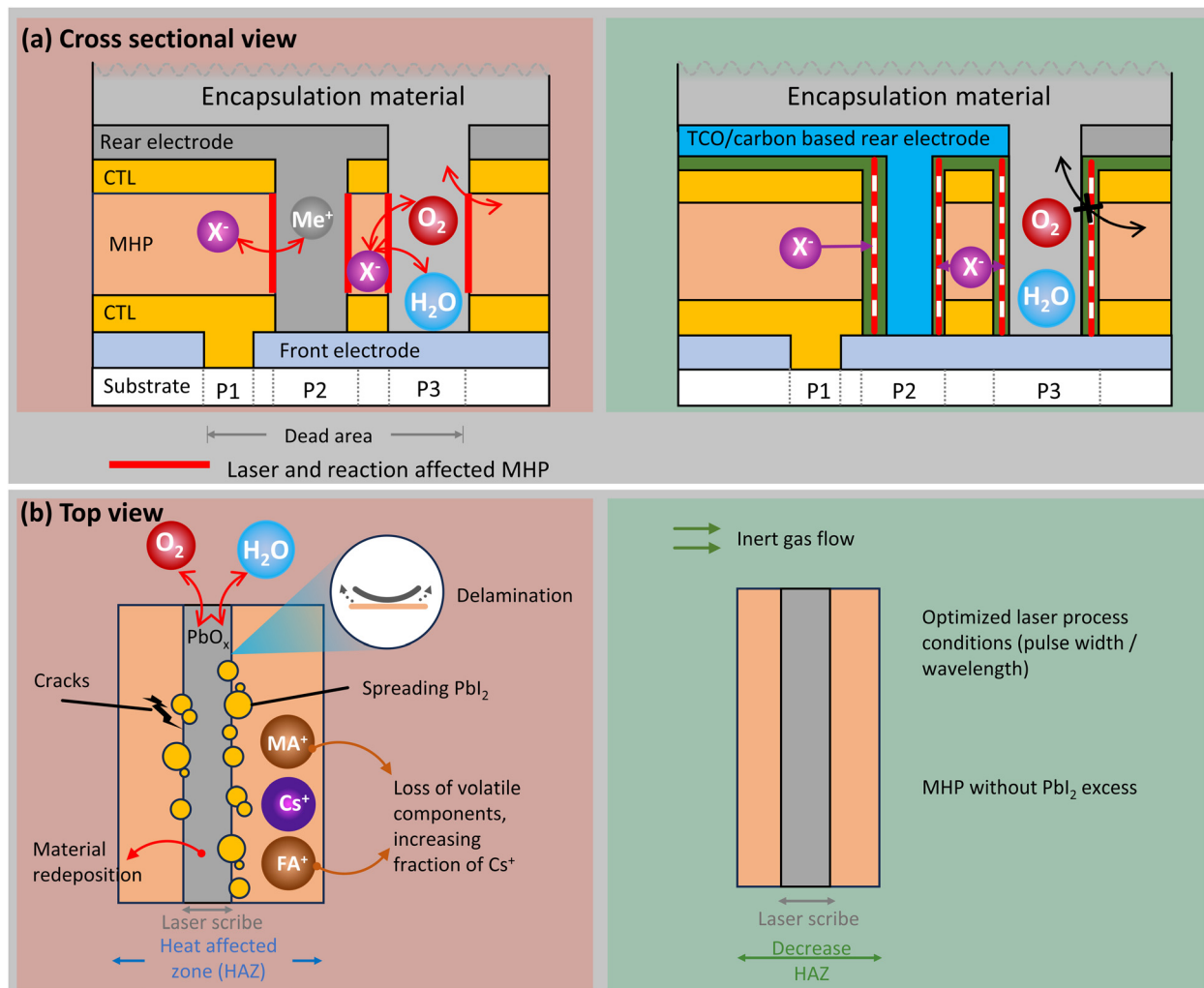
# E. Module-level specific degradation mechanisms

This section provides an overview of degradation mechanisms that become visible when integrating PSCs into solar modules.

## A. Cell interconnection and degradation related to scribe processing

The electrical interconnection of PV cells into strings can introduce degradation pathways at the cell-to-cell interconnects[269,270] decreasing both efficiency and operational lifetime.[271,272] Neighbouring solar cells in thin film technologies (including SJ-PSCs) can be monolithically interconnected, whereby the size and form of a solar cell can be varied. This process is generally achieved by the so-called P1, P2, P3 (and P4) scribing lines[273] depicted in Fig. 10(a). P1/P3 scribes isolate the front/rear contacts of each cell while the P2 scribe provides an electrical series connection from the rear of one cell to the front of the next. A P4 scribe may be introduced perpendicular to P1–P3, which separates long cells into shorter segments, generating parallel-connected strings of series-connected cells.[274,275] It is possible to create scribes using mechanical or laser processing. Laser scribing is more scalable for high throughput manufacturing along with less tool wear, greater reproducibility, precision, cleanliness, and adaptability to various materials. Mechanical scribing could result in durability concerns due to defects such as delamination, chipping, and irregular scribe edges.[274,276,277]

This journal is © The Royal Society of Chemistry 2024

*Energy Environ. Sci.*, 2024, **17**, 7566–7599 | **7581**

**Fig. 10** (a) Side view: P1, P2 and P3 laser scribe interconnection of SJ PSCs introduce metal/MHP interfaces at P2 and MHP/ambient or MHP/ encapsulation material interfaces where instabilities can occur when not mitigated by barrier layers or TCO/carbon-based electrodes. (b) Top view: Laser scribing can cause delamination and cracks and, for P2 or P3, $PbI_2$ spreading along the scribe line and an increasing fraction of $Cs^+$ in the HAZ as $MA^+$ and $FA^+$ are more volatile than $Cs^+$. Inert gas flow can cool the PSC and thus decrease HAZ. Further mitigation strategies are optimizing laser process parameter and avoiding $PbI_2$ excess in MHP.

An abundance of work strives to optimize scribing to improve performance by minimizing cell to module losses *via* low series resistance and small dead areas.[278,279] Possible defects from laser scribing include incomplete ablation, material changes within the heat-affected zone (HAZ), microcracks, delamination, and residues/redeposition.[274,276,277] In addition to durability concerns associated with laser-modified materials chemistry and microstructure, there is also the concern of new interface types introduced at scribed interconnects (particularly for P2 and P3), as we describe below.

Ultrafast laser pulse widths are desired to achieve "cold" ablation due to minimized transfer of the electronic energy to thermal motion *via* electron–phonon scattering.[280,281] It has been shown for MHPs that the HAZ decreases with decreasing pulse width from nanosecond to sub-picosecond time ranges.[282–284] The extent of the HAZ during laser processing likely impacts the durability and degradation mechanisms in MHP modules.

While nanosecond lasers ablate primarily *via* thermally-driven melting, picosecond laser ablation transitions toward a mechanical stress-assisted lift-off mechanism. This may result in steep edges and less redeposition/residue but also possible defects such as delamination and microcracks that can generate shunts inside the groove.[277,282,283] Mechanical lift-off ablation can also occur by laser processing from the glass-side rather than film-side. Even with picosecond laser ablation, studies show heat-induced changes in MHP composition in the range of 1–5 μm away from ablation craters or scribe lines,[276,285] and additional impacts of secondary interactions with volatile or redeposited species up to 10 μm away.[285]

Pulse wavelength also impacts the ablation mechanism and associated module durability concerns. In particular, short wavelengths may lead to breaking of chemical bonds and ablation *via* photochemical decomposition of molecules.[277] *E.g.*, Udalova *et al.* show that resonant absorption during laser processing induces a greater extent of chemical degradation

**7582** | *Energy Environ. Sci.*, 2024, **17**, 7566–7599

This journal is © The Royal Society of Chemistry 2024

products compared to infrared (IR) irradiation below the MHP band gap.[285] This is attributable to photodegradation induced by excitation of electronic energy levels as well as the electron–phonon interactions that lead to heating.

The chemical species produced in laser-affected areas will influence decomposition pathways near module interconnects. Laser ablation can volatilize or decompose organic species more easily than the inorganic components of the MHP. For multi-cation compositions containing Cs along with organic cations such as FA and MA, this can result in enhanced fraction of Cs in the HAZ and in any re-solidified material.[276] Indeed, additional studies suggest that compositions including Cs cations have smaller laser-affected areas due to greater thermal stability and fewer volatile degradation products.[285]

Many studies show that the edges of laser-ablated scribes and craters decompose to $PbI_2$, forming a type-I heterojunction with surrounding MHP.[276,284,285] Greater PL intensity near the laser-ablated edge may result both from type-I charge transfer and passivating effects of $PbI_2$ in small quantities.[284] Interestingly, Kosasih et al. find that any existing $PbI_2$ grains may grow in size upon laser processing, but that no new $PbI_2$ grains were formed if the MHP layer was initially $PbI_2$ free.[276] Degradation related to mechanical and laser scribing can be investigated with optical profilometry, scanning electron microscopy (SEM), and EDX to visualize larger-scale issues (e.g. delamination, burrs, edge irregularities, large compositional changes).[286] Finer details of crystal structure and phase inhomogeneities characterized using methods such as STEM[276] and XRD.[282] Modified chemical bond environment and associated decomposition products have been identified with Raman spectroscopy.[285]

As devices scale up in size to the module level, microscopic analysis risks studying isolated areas unrepresentative of the dominant durability concerns. Pairing rapid large-area analysis, or eventually in-line screening, with detailed microscopy promises a pathway toward scalable durability optimization. E.g., dark lock-in thermography and luminescence imaging have been applied to distinguish intra-cell defects from interconnect defects.[269,270,287] Light-beam induced current mapping has also been used.[288] Examples of defects at laser scribes detected with macroscale imaging include interruption or shorting along P1 or P3 by redeposition of conductive material, incomplete scribes causing resistance or re-routing of current pathways, burrs/irregularities along scribe edges, inactive cells due to interconnect faults, and current crowding along interconnects after thermomechanical stress.[269,270,287] Pairing these analysis tools with accelerated stress testing and outdoor aging is a fruitful path toward selecting laser process conditions to optimize beyond initial performance and also improve durability.[12,289]

The atmosphere during laser ablation impacts degradation products and potential subsequent degradation pathways. In ambient atmosphere, MHP may decompose to $PbO_x$ under laser processing, which is mechanically rigid and electrically insulating.[285] The dihydrated MHP phase may also form due to interaction with moisture.[290] In inert atmosphere, degradation

products are observed such as $PbI_2$ and polyiodides (e.g. $I_3^-$, $MAI_x$) which may form via decomposition of the inorganic sublattice to create $I_0$ and $I_2$ that further react with the MHP[285] as described in equation (1). Furthermore, volatile components may be re-deposited either from cooling or laser pulse shielding, resulting in accumulation of chemical species that can further react with undegraded MHP. These include degradation products such as $PbO_x$, $PbI_2$, $I_2$, and (for certain compositions) methylamine ($CH_3NH_2$), hydrogen cyanide (HCN), and formamidine ($H_2NCHO$).[285] Inert gas flow can decrease the laser-affected area by removing such laser-induced decomposition products and decreasing sample temperature.

New interfaces formed within laser-processed interconnects pose additional durability considerations. P3 scribing can oxidize metal contacts and promote reactions between metal and MHP, e.g. leading to products such as AgI or $(MA)_2Au_2I_6$.[285] Such degradation near P3 can decrease the active area and provide a pathway for further decomposition initiated at the scribe edges of the rear metal contact. For bifacial constructions with TCO as the rear electrode, laser scribing at P3 may induce thermomechanical stress, which may create another durability concern.[286] P3 also represents an area where the MHP absorber becomes exposed to atmosphere enabling reaction with moisture or oxygen during processing.[73] Fenske et al. suggest that increased heating from using nanosecond laser for P3 scribing may improve performance by generating $PbI_2$ and a thin Br-rich interfacial layer that passivate the MHP,[278] but it is unclear if this would also impact long-term stability. Upon module encapsulation, MHP or metal decomposition products at P3 may come into direct contact with polymers used for lamination at elevated temperatures. Some common encapsulants are known to produce detrimental degradation products such as acetic acid from ethylene vinyl acetate (EVA)[291] or methacrylic acid from surlyn,[10] which could react with the MHP at P3 during module aging.[292] At the P2 scribe, a new interface is introduced such that the MHP absorber may directly touch the metal.[293] As discussed in Section C-B, electrode migration into the MHP absorber can cause severe degradation. Such decomposition can increase resistance, which may lead to Joule heating that promotes further degradation at interconnects during module operation. Therefore, scribe interconnects would ideally avoid direct contact between metal and MHP along P2. Strategies for this include rear electrodes composed of carbon-based material[294] or TCOs.[286,295] An alternative strategy is to introduce a diffusion barrier inside P2. Bi et al. demonstrated diffusion barriers made of $Al_2O_3$ nanoparticles, polydimethylsiloxane (PDMS), or carbon nitride.[119] CTL materials could also be used within P2 to separate metal from the MHP at the interconnect.[296] Fig. 10 summarizes the here mentioned degradation mechanisms and mitigations.

However, for 2T MHP/Si tandem solar cells the interconnection of cells will likely resemble that of c-Si wafer-based technology, which generally uses screen-printed fingers and busbars on the solar cells. The front busbars are then

connected through Sn-alloy coated Cu ribbons to the metallization on the rear side of the neighbouring solar cell. Normally, depending on the screen-printing paste and coating alloy, the fingers are fired and the ribbons are soldered at relatively high temperatures (*e.g.* about 700 °C and 350 to 450 °C, respectively[273]). To avoid damaging the different layers in the PSC stack, it is highly recommended to avoid high-temperature processes. A valid alternative to soldering is offered by the use of electrically conductive adhesives (ECA, *i.e.* silver containing pastes) that are already effectively used for the ribbon-stringing of the silicon heterojunction (HJT) technology. The fingers can either be formed with low-temperature screen-printing pastes[297] that typically have a lower conductivity than standard pastes or can be applied onto an insulating layer on the Si bottom cell before PSC fabrication.[130] With the latter option, the firing temperature is only limited by the Si bottom cell and not by the thermal stability of PSC components which allows higher conductivity for front contacts.

## B. Insertion of Bypass diodes

The individual cells of a PV module may become partially shaded during operation, *e.g.* due to a neighbouring tree or building element. In these conditions, the illuminated cells of the string will continue producing a photocurrent. Due to the series connection of the cells in the string, the shaded cell(s) will be driven to reverse bias conditions to pass this photo-generated current. As described in Section D-D, PSCs are greatly sensitive to reverse bias and the number of integrated bypass diodes (BPDs) therefore needs to be evaluated carefully. The most reliable, but very expensive way would suggest the adoption of one BPD per 1–2 PSCs, compared to the typical ratio of 1 BPD per 20–24 cells adopted for conventional c-Si solar cells.[298]

A more realistic module layout with 1 BPD per 24 MHP/Si tandem solar cells with an area of $(15.6 \text{ cm})^2$ is proposed by Qian *et al.*[262] They simulated PSC temperatures of more than 170 °C for all shading ratios >15% of one solar cell in a string and 207 °C for 30% shading as worst-case scenario.[262] However, considering that power dissipation in PSCs is observed to be not homogeneous over the whole shaded area[254] even higher temperatures can be expected at local shunt paths.[262] The shade protection design thus needs to be adapted to the thermal stability of the PSCs (see Section B-E).

According to Qian *et al.* using half-size 2T MHP/Si tandem solar cells (15.6 cm × 7.8 cm) can decrease the worst-case PSC temperature from 207 °C to 186 °C (*i.e.* 1 BPD per 48 half-size MHP/Si tandem solar cells) and further to 134 °C by implementing 6 instead of 3 BPDs.[262] Another mitigation strategy is the optimization of segments (by laser scribe patterning) in SJ or 4T modules in a way that shading of a whole segment becomes difficult during typically shading events.[261] This is *e.g.* simulated by Qian *et al.* with 191.6 cm × 2 cm wide PSC cell strips vertically orientated which overlap the Si bottom cell, that is partially shaded, with less than 1/12 of their cell area. This decreases the PSC worst-case temperature in 4T to 137 °C compared to 207 °C in 2T with same shading conditions and c-Si bottom solar cell. This temperature can further be lowered

to 73 °C by using IBC Si-bottom solar cells[262] that can act as a BPD due to their breakdown at low reverse bias.[261,262] However, the segment form needs to be chosen carefully, *e.g.* line-shaped shadows can lead to 116 °C for 4T IBC modules.[262]

## C. Module packaging

Solar cell strings are packaged into modules to protect them from atmospheric agents such as oxygen and water vapor. In addition, the packaging avoids the release of potentially harmful elements, such as Pb, to the environment. Packaging also provides mechanical support to solar cell strings[273] and electrically insulates the solar cells from the environment.

An optimal packaging structure for PSC should avoid any water and preferably oxygen ingress into the module laminate. Therefore, a glass–glass structure with an edge seal, as depicted in Fig. 11, might be favoured, or backsheets with diffusion barriers – which will have a weight advantage – are required. However, standard edge seal materials based on butyl rubber are optimized towards low water vapor ingress but are not a good barrier towards oxygen. In comparison, standard PV backsheets based on polyethylene terephthalate have an oxygen transmission rate around 10 $cm^2 g^{-1} d^{-1}$,[299] while butyl rubber has a value 10 times higher.[300]

EVA, the encapsulant with historically the largest market share, tends to photodegrade over time generating acetic acid. The acid cannot be released by a glass/glass structure as it would in the case of using a permeable polymeric backsheet.[301] Therefore, encapsulant materials as *e.g.* polyolefins (PO) that do not produce acetic acid should be favoured for PSCs.[224,302,303] Another reason for not adopting EVA as an encapsulant is the relatively high lamination processing temperature of 150 °C (and relatively long processing times of ∼20 min) needed to complete the cross-linking.[304] This processing conditions are largely incompatible with the thermal instability of MHPs. Another advantage of POs over EVAs is that this class of
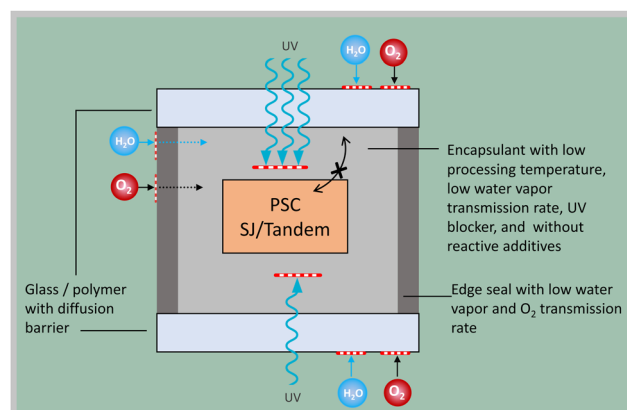


**Fig. 11** Module packaging with glass–glass or backsheets with diffusion barriers protect SJ PSCs or MHP/Si tandem solar cells from water vapor and oxygen. An edge sealing and encapsulation material with low WVTR and low oxygen transmission rates prevent water and oxygen ingress from the side. The encapsulation material needs to be unreactive with MHPs and be processable at low temperatures.

**7584** | *Energy Environ. Sci.*, 2024, **17**, 7566–7599

This journal is © The Royal Society of Chemistry 2024

polymers have a lower water vapor transmission rate (WVTR) and oxygen transmission rate,[273] which might in principle decrease the need for an edge seal. Still, edge seals for PSC are highly recommended. To prevent water ingress in the PSC, moisture barriers such as $AlO_x$ or $SiO_x$ have also been proposed, but likely their adoption should be a supplement but not a substitute of an encapsulation material with a low WVTR.

The generation of harmful by-products by POs or other alternative encapsulants over time is not yet well known since the long-term field experience of this technology in the solar industry is still limited. So far, from indoor durability tests using different PO based encapsulants, no harmful degradation products such as acetic acid have been observed yet.[305–314] Observed chemical reactions include reactions of additives and stabilizers,[307,312,314] or the formation of double bonds, various carbonyl groups and hydroxyl groups on the polymer chain.[310–312] However, a link of volatile PO degradation products to power degradation of a PV module has not been reported yet. Further, compared to the relatively standardized formulation of EVA after 35 years of production, process reproducibility might be lower with alternative encapsulants like POs, due to the lack of experience. The storage conditions of the encapsulant prior to lamination should also be chosen to minimize any moisture uptake from the environment.[301]

As a precaution, several research groups prefer to use thermoplastic PO (TPOs), because thermosetting polyolefin elastomers (POEs) might release thermally activated peroxides (during and after the lamination process), which are added to enable crosslinking and whose effect on PSCs is largely unknown.

Due to the sensitivity of PSC to high temperatures, the optimal encapsulation material should have relatively low melting and processing temperatures (ideally 110 °C to 130 °C). Besides having a good transmittance ($T > 90\%$), the ideal encapsulant might contain UV blockers and likely have a high UV cut-off ($>380–400$ nm) to avoid (or delay) UV induced degradation.[269] However, the UV blocking additives and their degradation products might introduce potential chemical interaction with PSCs and not being able to use the higher energy photons for generating current decreases energy yield.

CTE mismatches can result in internal stresses within the PV module that may cause various failure mechanisms, including fractured cells, broken interconnectors as well as delamination.[315] An additional risk are cohesive failures inside the PSC stack (e.g. at the $MHP/C_{60}/SnO_2$ interface[152]). Furthermore, the long-term adhesion of the encapsulant to the glass and to the cell is critical and needs to be addressed properly.[316–318] Choosing the right encapsulant with appropriate thermo-mechanical properties is crucial to minimize internal stresses and prevent aforementioned failure mechanisms.[319] Moreover, the thermal expansion behaviour of encapsulants is crucial for ensuring a stable lamination process during the production of MHP PV modules. Excessive shrinkage or thermal expansion of the encapsulant, as well as anisotropic behaviour during heating can lead to stresses that may result in damaged cell layers or delamination.[320–322] The careful selection of encapsulant materials, but also of the different layers of the PSC stack (see Section C-C) to minimize CTE mismatch is essential to mitigate internal stresses, prevent production loss and early-stage failures, and ensure the overall reliability and quality of solar modules.

Moreover, encapsulants should ideally be designed to have a low shear viscosity in the molten or liquid state, so that the encapsulant can easily flow without transferring stresses to the top cell causing irreversible damage.

## D. Potential induced degradation (PID)

In string connected modules high PV system voltages (up to $\pm1500$ V), can build up between grounded module frames and solar cells under operation.[323] The PID qualification test (see IEC 61215:2021[15]) for Si PV (and other inorganic thin films) defines the application in both polarities of the modules' nominated system voltage (generally $\pm1000$ V or $\pm1500$ for power generation applications) between the cells and the

**Table 5** Overview of published PID tests on MHP and MHP/Si-tandem solar cells. P–i–n solar cells are Illuminated through the HTL and n–i–ps through the ETL side

| Cell type | Test conditions | | Degradation | Recovery |
|---|---|---|---|---|
| Tandem[115] | 60 °C, 22 h, +1000 V | | Only thermal | — |
| p–i–n, Al foil on both sides[325] | RT, >5000 h | +1000 V | No | — |
| | | ±500 V | No | — |
| | | −1000 V | >50% EQE loss; PCE degradation starts after several h | — |
| p–i–n[114] | −1000 V, 55 h | 25 °C, 20% RH | 59% PCE loss, 40% EQE reduction, lower shunt resistance | +1000 V, 90 h: 37% to 58% of reference PCE |
| | | 60 °C, 60% RH | > 90% PCE & 60% EQE loss with respect to ref stored at 60 °C, 60% RH | +1000 V, 90 h: ≈10% recovery |
| n–i–p, p–i–n[326] | −1000 V, 60 °C, <60% RH, 18 h | | PCE loss: n–i–p w/o PCBM 65%, n–i–p with PCBM 32%, p–i–n 72% | — |
| n–i–p[327] | −1000 V, 60 °C, <60% RH, 18 h | | Up to 95% PCE loss | +1000 V, 72 h: 80% PCE recovery |
| Tandem[115] | −1000 V, 60 °C, <20% RH, 22 h | | 47% PCE loss (ref stored at 60 °C: 16% PCE loss) | +1000 V, 11 h: 52% to 65% of initial PCE |
| n–i–p[328] | Simulation via defect density of different absorber | | PCS loss: $MAPbI_3$: 61%, $CsPbI_3$: 23%, $CsGeI_3$: 56%, $CsSnI_3$: 94% | — |

This journal is © The Royal Society of Chemistry 2024

*Energy Environ. Sci.*, 2024, **17**, 7566–7599 | **7585**

grounded frame for 96 h at 85% RH and 85 °C (*i.e.* in damp-heat like conditions). The previous IEC 62804 PID standard[324] allows the execution of the test likewise in humid (85% RH, 85 °C for 96 h) or in dry (25 °C for 168 h) conditions.

Table 5 gives an overview of the published PID tests applied for PSCs and MHP/Si tandem solar cells/minimodules. The analysed PSCs feature a front contact on a glass substrate and are enclosed with another glass without a connection to the rear contact in a nitrogen atmosphere. Voltage is applied across an Al foil on the substrate glass and the short-circuited PSC[114,325–327] as sketched in Fig. 12. Tandem solar cells are enclosed with encapsulant material on both sides, with the Al foil wrapped on the front side.[115]

In summary, Brecl *et al.* and Xu *et al.* showed that PID testing with +1000 V did not degrade p–i–n PSCs[325] and MHP/Si tandem solar cells.[115] Brecl *et al.* also observed no damage due to PID testing with ±500 V for more than 5000 h at room temperature. However, PID tests with −1000 V showed strong degradation of PSCs[114,325–327] and MHP/Si tandem solar cells.[115] Hereby, the degradation is enhanced when the voltage is applied at 60 °C instead of room temperature.[114] The negative voltage causes a movement of $Na^+$ ions from soda-lime glass that is in contact with the PSC into the MHP absorber. This has been proven by Nakka *et al.* with EDX[114] and Brecl *et al.* with ToF-SIMS.[325]

The $Na^+$ ions cause recombination centers[326,327] and ion migration results in a higher defect density in the absorber which again causes an increased recombination.[328] Enhanced recombination leads to a strong $J_{SC}$ decrease, but also $V_{oc}$, FF, PCE[114,115,325–328] and the external quantum efficiency (EQE)[114,325,328] are strongly lowered due to PID. Furthermore, the shunt resistance ($R_{sh}$) of the MHP (sub) cell is lowered by (−) type PID.[115,325] However, $R_{sh}$ of the Si sub cell is not

decreased as long as no further treatment is conducted after the (−) type PID test.[115] In contrast to Nakka *et al.* and Brecl *et al.*, Xu *et al.* observed a confinement of the $Na^+$ in-diffusion above the $C_{60}$ layer and also an out-diffusion of $Pb^+$, $Cs^+$, $Br^-$ and $I^-$ ions into the encapsulation material with secondary ion mass spectroscopy (SIMS).[115]

Applying positive voltage after PID tests with negative voltage partially recovers PSCs[114,327] and MHP/Si tandem solar cells[115] as $Na^+$ ions are moving back. In addition to $Na^+$ motion, Nakka *et al.* observed the formation of AgI caused by a movement of $Ag^+$ ions from the back contact during PID with negative voltages. AgI bonds are stronger than those between $Na^+$ and $I^-$; therefore, $Ag^+$ ions do not move back under positive voltage.[114]

Indication for PID in PSCs is a diminished electroluminescence (EL)[115] or PL intensity[326] due to higher recombination as well as a shift in the PL peak intensity. Due to ion movement, the PL peak can red shift when Br is removed or blue shift for Br-rich phases.[114,326] Halide segregation can also result in $PbI_2$ formation.[114]

Degradation due to PID might be mitigated by optimized growth conditions that result in low defect densities (*i.e.* $I^-$ rich synthesis conditions) and a MHP composition with a high tolerance for defects.[328]

Furthermore, an additional barrier layer (*e.g.* PCBM between $SnO_2$ (HTL) and MHP) can significantly decrease impacts of PID as shown by Purohit *et al.*[326] Nakka *et al.* suggest adding inert materials that occupy interstitials in the MHP structure to inhibit $Na^+$ penetration.[114] Brecl *et al.* suggest the application of positive bias during night to drive out $Na^+$ ions from the active layer and thus recover the PSCs.[325] A suitable encapsulation material could also serve as a barrier for $Na^+$ diffusion, and a barrier layer that prevents out diffusion of MHP materials
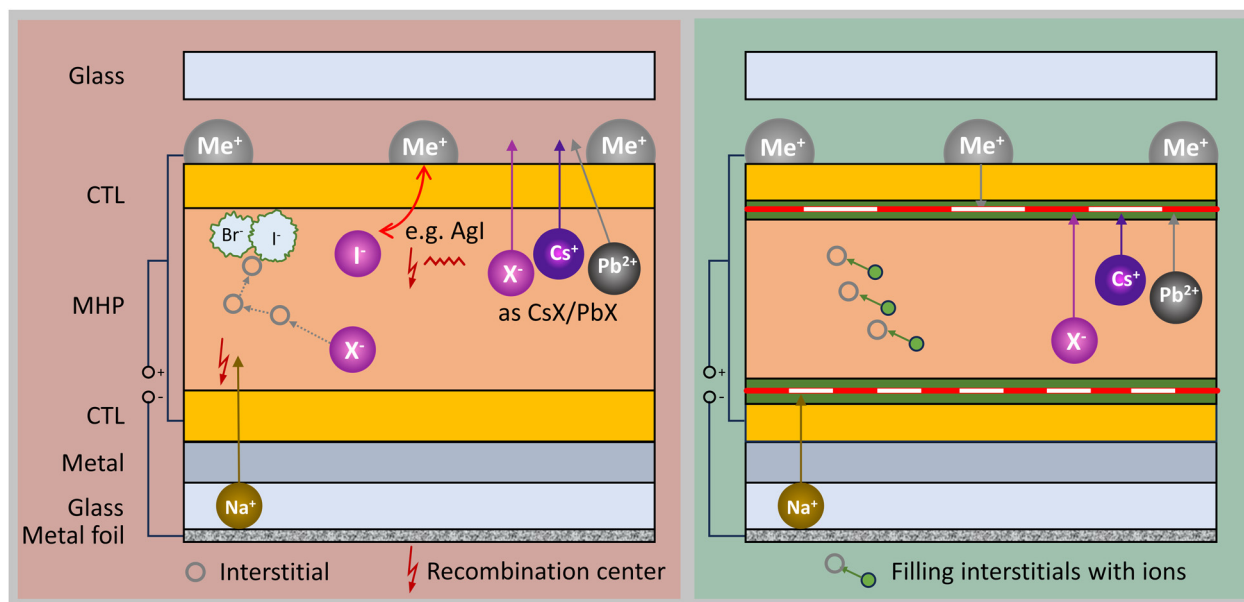


**Fig. 12** PID leads to ion movement, especially of $Na^+$, causing instabilities in the PSC. This can be mitigated by introducing ion blocking layers or by reducing ion migration due to filling of interstitials.

7586 | *Energy Environ. Sci.*, 2024, **17**, 7566–7599

This journal is © The Royal Society of Chemistry 2024

might be useful.[115] According to Xu *et al.* the encapsulant-free NICE encapsulation technology[329] might be a good strategy as the potential bias nearly fully drops at the interface between glass and the inert atmosphere in this case.[115]

Most POs exhibit high volume resistivities due to their non-polar polymer chains based on polyethylene. This might also decrease PID effects, at least for PSCs without glass substrates where the encapsulation foil separates glass and PSC. SJ PSCs may require a proper selection of the glass (*e.g.* non-Na containing glass), the usage of other substrates or the deposition of barrier layers on the glass cover prior to the deposition of the different active layers as shown for CIGS.

### E. Testing and qualification

Recent evidence suggests that modules made of c-Si cells can reach service lifetimes of 25–30+ years in the field.[330,331] As it is not possible to wait 20+ years to replicate the failure modes observed in the field, accelerated-aging testing of PV modules has been introduced to replicate, under controlled laboratory conditions, the most common failures observed after many years of outdoor operation. However, the relevant standards are qualification test aiming at preventing early failures in the fields and not – as often wrongly assumed – life-time tests aiming at predicting the lifetime of the modules. For terrestrial applications, the relevant industry standards are the IEC 61215:2021,[15] covering silicon-based and thin film modules and addressing the reliability of PV modules. They contain accelerated aging protocols including climatic (*e.g.* damp-heat, thermal cycling, humidity-freeze, ...), mechanical (*e.g.* mechanical loads and hail impact) and electrical (*e.g.* PID, wet and dry insulation) tests.

Electrical and mechanical safety requirements are addressed in the IEC 61730:2023.[332] Conformity to these standards is generally considered as a minimum quality requirement and should also be considered as a prerequisite for MHP module commercialization. Some test conditions in the IEC 61215 series may be tailored to cope with technology-specific *meta*-stabilities of PSCs. A typical example is the duration of the stabilization procedures (*i.e.* exposure to light and relaxation times). Therefore, in the long-run, a sub-standard specific to PSC-based modules – as is already the case for other inorganic thin-film PV technologies – may be expected. At the TandemPV 2024 a consensus statement on a minimum stability test and standardized measurement protocols for MHP/Si tandem solar cells was announced to be published soon.[333] Some useful inputs may originate from the ISOS protocols (International Summit on Organic PV Stability[334]), originally designed for organic PV, which are not intended as a replacement of existing qualification standards but are rather aimed at understanding specific failure mechanisms and stability issues, such as ion redistribution under electric fields and reversible degradation.

Pass/fail criteria typically refer to variations in power whereby generally a maximum power loss of 5% is allowed. Thus, the possibility of executing reliable and reproducible as well as accurate and precise power characterization is critical. This will be a challenge for PSCs due to the large variability in their behaviour. Therefore, MHP module characterization protocols should include the development of:[335,336]

● Reproducible stabilization procedures (generally light soaking) to stabilize the power at the maximum power point ($P_{mpp}$) of the device minimizing the impact of metastability

● Procedures to determine the steady-state maximum-power output under continuous illumination rather than relying on conventional $J$–$V$ characteristics, minimizing the impact of hysteresis and transient behaviours

● Procedures to determine the spectral response (SR) of the device and apply a spectral mismatch factor correction. This may be particularly challenging for multi-junction devices, which require the characterization of the SR of each sub-cell.[337]

There are various reports about PSCs and MHP mini modules passing individual (IEC) stability tests.[12,338,339] However, as the MHP technology is not yet industrially mature, still little evidence exists of field-deployed MHP modules, which is the only method to evaluate their actual service life. Further, the rare outdoor monitoring data reported in the literature for MHP solar modules extend normally over a short temporal duration (weeks to months).[340,341] Li *et al.* found instabilities of PSCs under outdoor conditions only occurring during summer months, not in winter.[342] Outdoor tests, therefore, need to cover high operating temperatures. In a recent publication, encapsulated MHP/Si tandem solar cells were monitored over one year in a hot and humid climate (Saudi Arabia), retaining 80% of their initial power after one year.[343] In a temperate climate (Berlin), encapsulated PSCs were monitored outdoors for over 2.5 years exhibiting pronounced seasonal behaviours and *meta*-stable effects.[344] Until now, however, the nature of outdoor studies (*i.e.* mainly the required time) makes it difficult to report about long-term degradation modes of samples in the field so that most of the evidence is available for laboratory-tested prototype modules only.

To conclude, we want to stress that a clear market acceptance of PSCs for power generation applications will only be gained once all the stability (at material level) and reliability (at module level) issues are solved. A first step will be passing the relevant industry standard qualification protocols which – as mentioned – may require some technology specific changes for PSCs. At the same time, potential early adopters (Engineering–Procurement–Construction companies and project developers) will require time series of monitoring data (with a minimum duration of 3 to 5 years) that prove the stability of the MHP modules deployed in the field. Both conditions are minimum requirements to make PSC technology bankable and acceptable.

### F. Limiting factors affecting the lifetime of PSCs and modules

Table 6 summarizes strategies on different levels to improve the stability of PSCs and modules. The prerequisite in the development of long-term stable MHP (SJ or tandem) solar modules is the selection of intrinsically stable materials, especially concerning the MHP composition, but also the full layer stack. It is important to deposit the MHP homogeneously in order to avoid nucleation sites for *e.g.* cation segregation and PbI$_2$

This journal is © The Royal Society of Chemistry 2024

*Energy Environ. Sci.*, 2024, **17**, 7566–7599 | **7587**

**Table 6**

Column groupings: columns under **Enhanced stability with respect to** are split into **Internal effects** (↓, defects/ions ⊗, Residual stress) and **Environmental influences** (↻, temperature 🌡, $H_2O$, $O_2$, light ☀, electrical ⏚).

| Level | Realization | ↓ | ⊗ | Residual stress | ↻ | 🌡 | $H_2O$ | $O_2$ | ☀ | ⏚ | Side effects/Comments |
|---|---|---|---|---|---|---|---|---|---|---|---|
| | | | | | | | | | | | Symbols explained in Table I |
| MHP composition | Energetically favorable alloy (see Table III) with high crystallinity [44] | Probably triple cation [44] | Probably triple halide [58,59] | | | Probably MA-free [136] | Probably MA-free [136] | Probably Sn- & MA-FA-free [236] | M | M | Accept minimal efficiency losses for higher stability |
| MHP processing | Well-mixed components, avoiding $PbI_2$ excess[23] and non-cubic phases[26,27] | M | M | M | | | | | M | | Dispense with passivation by $PbI_2$[25] |
| | Minimizing defect density, Passivating vacancies (e.g., additives) | K+, Rb[63] | K+, Rb[63] | OAI, PEAI[205] | | TFPCBP[117], DMAFo[116] | 2D[233], TFPCBP[234], MDMS[268] | | DMAFo[116] | MDMS[268] | Reduce reactivity with metals |
| | MHP film formation at low temperatures[204] and/or on substrates with similar CTE[196] | M | M | M | | | | | | | |
| CTLs and electrodes | Intrinsically stable material, not interacting with MHP (excluding a lot of dopants): HTL: undoped PTAA, modified NiO[153], some SAMs[142] ETL: $SnO_x$, ($C_{60}$)[47,154] Electrodes: Au, Ni[165], Cu[166], Carbon-based[191–193], TCO[194,195] | | | | | | Hydrophobic (e.g., NiO[235]) | Probably non-organic (e.g., $SnO_2$) | No $TiO_2$ [72,246,247] | Carbon-based[254], Au electrode[26,7] | Dispense with improved conductivity due to CTL doping; Metal oxides or sulfides probably most stable CTLs, but not reaching highest efficiencies[159] Au is expensive, Ni limits efficiency[161] Use materials with good adhesion (not $C_{60}$[152]) |
| | Acting as blocking layer | M | | $SnO_2$[182], ITO, IZO[160,184], $AlO_x$[188] | | M | ITO, IZO[160,184] | PTAA, P3HT[239,245], carbon na-notube[239] | M | TCO, no SAMs, (thick) PTAA[257] | Avoiding reactions with moisture and oxygen reduces vacancies, ion migration and phase segregation |
| Additional blocking layers | Insert between CTL and MHP or electrode | | 2D MHP[64–66] | $MoO_x$[154,178], Ti, Cr-, $Cr_2O_3$[177], $g$-$C_3N_4$[119] | | quantum dots[118], $g$-$C_3N_4$[119] | $MgF_x$,[229] $Al_2O_3$, $SiO_2$, 2D MHP[226], quantum dots[118] | | | PCBM[326]Hole blocking layer; Na+ blocking (PID) | Problems with scalability to large areas, Application might damage MHP Additional processing step |
| Cell interconnection | Optimized laser scribing for SJ monolithic series interconnection | Avoid MA+, FA+ loss, $PbI_2$ spreading[276,284,285] | Avoid cracks, delamination | EIBC[127] | ‡M | < ps pulse[280,281]; inert gas flow | Insert blocking layers[119] | Insert blocking layers[119] | IR wave-lengths[285] | | MHP prone to reaction with metal, $O_2$, $H_2O$ and encapsulant @ P2/P3; ‡Carbon-based[191–193] or TCO[194,195] electrodes, $Al_2O_3$, PDMS, carbon nitride[119] |
| | Low-temperature interconnects (EIBC, electrically conductive adhesives (ECAs)) | | | | | M | | | | | ECAs known from Si-HJT technology |
| Shade protection | Shorter String/Bypass diode, 4T with optimal cell formats, IBC bottom cells | | | | | M | | | | esp. reverse | Costs + space requirement in module |
| Module packaging | Suitable encapsulant (stored in dry atmosphere) | | | ‡M | Probably thermoplastic | Low process temperature | Low water vapor transmission rate | Low oxygen transmission rate | Probably UV-blocking | | Probably PO ‡Minimize CTE mismatch, low shear viscosity in the molten or liquid state |
| | edge seal + glass or polymer with diffusion barrier | | | | | | Butyl-rubber | M | | | Butyl rubber typically have high oxygen transmission rates[300] |

7588 | Energy Environ. Sci., 2024, 17, 7566–7599

This journal is © The Royal Society of Chemistry 2024

propagation. In addition, extreme care should be taken to prevent the emergence of strain during the MHP film formation, *e.g.* by the usage of relaxing additives.

The majority of degradation phenomena in PSCs are caused by ion movement (most prominent iodide) and resulting reactions. We therefore consider the passivation of defects (*e.g.* by additives) and the prevention of ion migration from one layer to another (*e.g.* by inserting ion-blocking layers) to be essential. CTLs that serve as a barrier themselves and thus prevent additional processes might be favoured, but also 2D MHPs might act as efficient barriers. The negative impact of environmental stress factors such as moisture and oxygen can also be tentatively prevented by the adoption of protective layers deposited on top of the PSCs and, in particular, by the adoption of proper module encapsulation structure. Additionally, the mechanical instability of MHPs can be mitigated by inserting insulating layers below the front contact that avoid shunts between front and rear contacts introduced by pressure on top of the front contact as in the EIBC concept.

## F. Conclusions

We propose that large scale screening of various materials and additive combinations is a promising strategy to improve the stability of PSCs. Studying the impact of individual stresses on PSCs is crucial, but it is also important to emphasize that this alone does not predict stability and module reliability. Therefore, testing procedures that combine different stressors for PSCs are proposed such as the ISOS protocols. In addition, testing procedures need to be complemented by reliable outdoor monitoring data, which until now have a limited temporal extension (shorter than three years) and are mostly limited to minimodules (*i.e.* prototype). Even though first outdoor measurements of full-size MHP/Si tandem modules close to commercialization were reported, their long-term stability is still under investigation. Furthermore, specific field stresses must be considered, such as reverse bias due to shading and the resulting hot spots at local shunt paths.

For tandem solar cells, more sophisticated characterization techniques will be needed at module level compared to conventional silicon modules, addressing considerations such as current matching of top and bottom cells throughout the day/year. At the module level, the need for robust packaging structure will require a careful redesign and likely the adoption of an edge seal or the need for more bypass diodes. This should be considered when evaluating the economic viability of MHP/Si tandem modules.

Long-term durability is crucial for industrial implementation and thus minor compromises in maximum efficiency will probably be accepted if these enable increased service life. However, if the durability problems can be solved (without increasing the costs and/or complicating the process), the increased yield per area of MHP/Si tandem modules could provide an additional valuable contribution to further accelerating the energy transition.

After only 15 years of intensive research, small area PSCs exceeded the efficiency of Si solar cells that have been developed and constantly improved for the last 70 years. Several mitigation strategies already exist to address the various instabilities PSCs can experience. It is now time to combine them with a clear focus on reproducibility, reliability and cost-effectiveness in addition to the upscaling of the MHP technology to larger areas. The demonstration of MHP as a reliable technology for terrestrial power generation application needs a focus on reliability development on cell and module level as well as reliability and qualification testing. The close collaboration of various research areas and groups should be funded accordingly.

## Author contributions

## Data availability

The detailed examination of the external quantum efficiencies (EQEs) for the perovskite top solar cell and the silicon bottom solar cell used for Fig. 9 will be published by L. Brockmann (ISFH) in the near future. The evaluation of the spectral intensity for different air masses was conducted with SMARTS 2.9.2 (**https://www.nrel.gov/grid/solar-resource/smarts.html**). The input parameters used are provided as ESI.†

## Conflicts of interest

There are no conflicts to declare.

This journal is © The Royal Society of Chemistry 2024

*Energy Environ. Sci.*, 2024, **17**, 7566–7599 | **7589**

## Acknowledgements

## Notes and references

1 Best Research-Cell Efficiency Chart, https://www.nrel.gov/pv/cell-efficiency.html.

2 A. Kojima, K. Teshima, Y. Shirai and T. Miyasaka, *J. Am. Chem. Soc.*, 2009, **131**, 6050–6051.

3 R. E. Brandt, V. S. Stevanović and D. S. Ginley, *MRS Commun.*, 2015, **5**, 265–275.

4 G. E. Eperon, S. D. Stranks, C. Menelaou, M. B. Johnston, L. M. Herz and H. J. Snaith, *Energy Environ. Sci.*, 2014, **7**, 982.

5 T.-H. Le, H. Driscoll, C.-H. Hou, A. Montgomery, W. Li, J. S. Stein and W. Nie, *Adv. Electron. Mater.*, 2023, **9**, 2300093.

6 K. P. Goetz and Y. Vaynzof, *ACS Energy Lett.*, 2022, **7**, 1750–1757.

7 L. Rakocevic, L. E. Mundt, R. Gehlhaar, T. Merckx, T. Aernouts, M. C. Schubert, S. W. Glunz and J. Poortmans, *Sol. RRL*, 2019, **3**, 1900338.

8 D. Castro, V. C. M. Duarte and L. Andrade, *ACS Omega*, 2022, **7**, 40844–40852.

9 O. Almora, C. I. Cabrera, S. Erten-Ela, K. Forberich, K. Fukuda, F. Guo, J. Hauch, A. W. Y. Ho-Baillie, T. J. Jacobsson, R. A. J. Janssen, T. Kirchartz, M. A. Loi, X. Mathew, D. B. Mitzi, M. K. Nazeeruddin, U. W. Paetzold, B. P. Rand, U. Rau, T. Someya, E. Unger, L. Vaillant-Roca, C. J. Brabec, O. Almora, C. J. Brabec, C. I. Cabrera and S. Erten-Ela, *Adv. Energy Mater.*, 2024, **14**, 2303173.

10 C. C. Boyd, R. Cheacharoen, T. Leijtens and M. D. McGehee, *Chem. Rev.*, 2019, **119**, 3418–3451.

11 N. Ahn and M. Choi, *Adv. Sci.*, 2024, **11**, 2306110.

12 D. Zhang, D. Li, Y. Hu, A. Mei and H. Han, *Commun. Mater.*, 2022, **3**, 58.

13 Z. Li, M. Yang, J. S. Park, S. H. Wei, J. J. Berry and K. Zhu, *Chem. Mater.*, 2016, **28**, 284–292.

14 Q. Han, S.-H. S. Bae, P. Sun, Y.-T. Y. Hsieh, Y. Yang, Y. Seung Rim, H. Zhao, Q. Chen, W. Shi, G. Li, Q. Han, S.-H. S. Bae, P. Sun, Y.-T. Y. Hsieh, Y. Yang, Y. S. Rim, H. Zhao, Q. Chen, G. Li and W. Shi, *Adv. Mater.*, 2016, **28**, 2253–2258.

15 *IEC 61215:2021, Part 1 to 3, Terrestrial photovoltaic (PC) modules – Design qualification and type approval*, 2021.

16 R. Witteck, M. Siebert, S. Blankemeyer, H. Schulte-Huxel, M. Köntges and M. Kontges, *IEEE J. Photovoltaics*, 2020, **10**, 1828–1838.

17 C. J. Bartel, C. Sutton, B. R. Goldsmith, R. Ouyang, C. B. Musgrave, L. M. Ghiringhelli and M. Scheffler, *Sci. Adv.*, 2019, **5**, 1–9.

18 W. Travis, E. N. K. Glover, H. Bronstein, D. O. Scanlon and R. G. Palgrave, *Chem. Sci.*, 2016, **7**, 4548–4556.

19 Z. Xu, Y. Zhao, J. Zhang, K. Chen, C. J. Brabec and Y. Feng, *Phys. Rev. Mater.*, 2020, **4**, 95401.

20 F. Fu, A. Stefano Pisoni, Q. Jeangros, J. Sastre-Pellicer, M. Kawecki, C. Adriana Paracchino, T. Moser, J. Werner, C. Andres, L. Duchêne, P. Fiala, M. Rawlence, S. Nicolay, C. Ballif, N. Ayodhya Tiwari and S. Buecheler, *Energy Environ. Sci.*, 2019, **12**, 3074.

21 R. I. Dawood, A. J. Forty and M. R. Tubbs, *Proc. R. Soc. A*, 1964, **284**, 272–288.

22 A. Donakowski, D. W. Miller, N. C. Anderson, A. Ruth, E. M. Sanehira, J. J. Berry, M. D. Irwin, A. Rockett and K. X. Steirer, *ACS Energy Lett.*, 2021, **6**, 574–580.

23 B. Roose, K. Dey, Y. H. Chiang, R. H. Friend and S. D. Stranks, *J. Phys. Chem. Lett.*, 2020, **11**, 6505–6512.

24 G. Tumen-Ulzii, C. Qin, D. Klotz, M. R. Leyden, P. Wang, M. Auffray, T. Fujihara, T. Matsushima, J. W. Lee, S. J. Lee, Y. Yang and C. Adachi, *Adv. Mater.*, 2020, **32**, 1905035.

25 Y. Chen, Q. Meng, Y. Xiao, X. Zhang, J. Sun, C. B. Han, H. Gao, Y. Zhang, Y. Lu and H. Yan, *ACS Appl. Mater. Interfaces*, 2019, **11**, 44101–44108.

26 S. Macpherson, T. A. S. Doherty, A. J. Winchester, S. Kosar, D. N. Johnstone, Y. H. Chiang, K. Galkowski, M. Anaya, K. Frohna, A. N. Iqbal, S. Nagane, B. Roose, Z. Andaji-Garmaroudi, K. W. P. Orr, J. E. Parker, P. A. Midgley, K. M. Dani and S. D. Stranks, *Nature*, 2022, **607**, 294–300.

27 S. Kosar, A. J. Winchester, T. A. S. Doherty, S. MacPherson, C. E. Petoukhoff, K. Frohna, M. Anaya, N. S. Chan,

7590 | *Energy Environ. Sci.*, 2024, **17**, 7566–7599

This journal is © The Royal Society of Chemistry 2024

J. Madéo, M. K. L. Man, S. D. Stranks and K. M. Dani, *Energy Environ. Sci.*, 2021, **14**, 6320–6328.

28 S. S. Novosad, I. S. Novosad and I. M. Matviishin, *Inorg. Mater.*, 2002, **38**, 1253–1259.

29 D. P. McMeekin, G. Sadoughi, W. Rehman, G. E. Eperon, M. Saliba, M. T. Hörantner, A. Haghighirad, N. Sakai, L. Korte, B. Rech, M. B. Johnston, L. M. Herz and H. J. Snaith, *Science*, 2016, **351**, 151–155.

30 S. Mazumdar, Y. Zhao and X. Zhang, *Front. Electron.*, 2021, **2**, 712785.

31 L. Yang, Q. Xiong, Y. Li, P. Gao, B. Xu, H. Lin, X. Li and T. Miyasaka, *J. Mater. Chem. A*, 2021, **9**, 1574.

32 I. M. Asuo, D. Gedamu, N. Y. Doumon, I. Ka, A. Pignolet, S. G. Cloutier and R. Nechache, *Mater. Adv.*, 2020, **1**, 1866.

33 M. Saliba, T. Matsui, J.-Y. Seo, K. Domanski, J.-P. Correa-Baena, M. Khaja, S. M. Zakeeruddin, W. Tress, A. Abate, A. Hagfeldt and M. Grä, *Energy Environ. Sci.*, 2016, **9**, 1989–1997.

34 E. Aydin, T. G. Allen, M. De Bastiani, L. Xu, J. Ávila, M. Salvador, E. Van Kerschaver and S. De Wolf, *Nat. Energy*, 2020, **5**, 851–859.

35 K. A. Bush, K. Frohna, R. Prasanna, R. E. Beal, T. Leijtens, S. A. Swifter and M. D. Mcgehee, *ACS Energy Lett.*, 2018, **3**, 428–435.

36 S. S. Mali, J. V. Patil, H. Kim, H. H. Kim and C. K. Hong, *Adv. Funct. Mater.*, 2019, **29**, 1–9.

37 F. Zheng, W. Chen, T. Bu, K. P. Ghiggino, F. Huang, Y. Cheng, P. Tapping, T. W. Kee, B. Jia and X. Wen, *Adv. Energy Mater.*, 2019, **9**, 1–11.

38 Z. Hu, Q. An, H. Xiang, L. Aigouy, B. Sun, Y. Vaynzof and Z. Chen, *ACS Appl. Mater. Interfaces*, 2020, **12**, 54832.

39 M. Degani, Q. An, M. Albaladejo-Siguan, Y. J. Hofstetter, C. Cho, F. Paulus, G. Grancini and Y. Vaynzof, *Sci. Adv.*, 2021, **7**, 7930.

40 Y. H. Lin, N. Sakai, P. Da, J. Wu, H. C. Sansom, A. J. Ramadan, S. Mahesh, J. Liu, R. D. J. Oliver, J. Lim, L. Aspitarte, K. Sharma, P. K. Madhu, A. B. Morales-Vilches, P. K. Nayak, S. Bai, F. Gao, C. R. M. Grovenor, M. B. Johnston, J. G. Labram, J. R. Durrant, J. M. Ball, B. Wenger, B. Stannowski and H. J. Snaith, *Science*, 2020, **369**, 96–102.

41 M. Abdi-Jalebi, M. I. Dar, S. P. Senanayak, A. Sadhanala, Z. Andaji-Garmaroudi, L. M. Pazos-Outón, J. M. Richter, A. J. Pearson, H. Sirringhaus, M. Grätzel and R. H. Friend, *Sci. Adv.*, 2019, **5**, 1–9.

42 L. Gil-Escrig, C. Dreessen, F. Palazon, Z. Hawash, E. Moons, S. Albrecht, M. Sessolo and H. J. Bolink, *ACS Energy Lett.*, 2021, **6**, 827–836.

43 Y. Zhou, Y.-H. Jia, H.-H. Fang, M. A. Loi, F.-Y. Xie, L. Gong, M.-C. Qin, X.-H. Lu, C.-P. Wong and N. Zhao, *Adv. Funct. Mater.*, 2018, **28**, 1803130.

44 A. J. Knight and L. M. Herz, *Energy Environ. Sci.*, 2020, **13**, 2024.

45 L. T. Schelhas, Z. Li, J. A. Christians, A. Goyal, P. Kairys, S. P. Harvey, D. H. Kim, K. H. Stone, J. M. Luther, K. Zhu, V. Stevanovic and J. J. Berry, *Energy Environ. Sci.*, 2019, **12**, 1341–1348.

46 L. E. Mundt, F. Zhang, A. F. Palmstrom, J. Xu, R. Tirawat, L. L. Kelly, K. H. Stone, K. Zhu, J. J. Berry, M. F. Toney and L. T. Schelhas, *ACS Energy Lett.*, 2022, **7**, 471–480.

47 Y. Zhao, T. Heumueller, J. Zhang, J. Luo, O. Kasian, S. Langner, C. Kupfer, B. Liu, Y. Zhong, J. Elia, A. Osvet, J. Wu, C. Liu, Z. Wan, C. Jia, N. Li, J. Hauch and C. J. Brabec, *Nat. Energy*, 2022, **7**, 144–152.

48 E. T. Hoke, D. J. Slotcavage, E. R. Dohner, A. R. Bowring, H. I. Karunadasa and M. D. Mcgehee, *Chem. Sci.*, 2015, **6**, 613–617.

49 A. J. Barker, A. Sadhanala, F. Deschler, M. Gandini, S. P. Senanayak, P. M. Pearce, E. Mosconi, A. J. Pearson, Y. Wu, A. Ram, S. Kandada, T. Leijtens, F. De Angelis, S. E. Dutton, A. Petrozza and R. H. Friend, *ACS Energy Lett.*, 2017, **2**, 1416–1424.

50 R. E. Beal, N. Z. Hagström, J. Barrier, A. Gold-Parker, R. Prasanna, K. A. Bush, D. Passarello, L. T. Schelhas, K. Brüning, C. J. Tassone, H. G. Steinrück, M. D. McGehee, M. F. Toney and A. F. Nogueira, *Matter*, 2020, **2**, 207–219.

51 G. F. Samu, C. Janáky and P. V. Kamat, *ACS Energy Lett.*, 2017, **2**, 1860–1861.

52 K. Datta, B. T. Van Gorkom, Z. Chen, M. J. Dyson, T. P. A. Van Der Pol, S. C. J. Meskers, S. Tao, P. A. Bobbert, M. M. Wienk and R. A. J. Janssen, *ACS Appl. Energy Mater.*, 2021, **4**, 6650–6658.

53 Y. Zhao, P. Miao, J. Elia, H. Hu, X. Wang, T. Heumueller, Y. Hou, G. J. Matt, A. Osvet, Y.-T. Chen, M. Tarragó, D. de Ligny, T. Przybilla, P. Denninger, J. Will, J. Zhang, X. Tang, N. Li, C. He, A. Pan, A. J. Meixner, E. Spiecker, D. Zhang and C. J. Brabec, *Nat. Commun.*, 2020, **11**, 6328.

54 S. Joon Yoon, S. Draguta, J. S. Manser, O. Sharia, W. F. Schneider, M. Kuno and P. V. Kamat, *ACS Energy Lett.*, 2016, **1**, 290–296.

55 M. Saliba, T. Matsui, K. Domanski, J.-Y. Seo, A. Ummadisingu, S. M. Zakeeruddin, J.-P. Correa-Baena, W. R. Tress, A. Abate, A. Hagfeldt and M. Grätzel, *Science*, 2016, **354**, 206–209.

56 F. Peña-Camargo, P. Caprioglio, F. Zu, E. Gutierrez-Partida, C. M. Wolff, K. Brinkmann, S. Albrecht, T. Riedl, N. Koch, D. Neher and M. Stolterfoht, *ACS Energy Lett.*, 2020, **5**, 2728–2736.

57 S. Mahesh, J. M. Ball, R. D. J. Oliver, D. P. Mcmeekin, P. K. Nayak, M. B. Johnston and H. J. Snaith, *Energy Environ. Sci.*, 2020, **13**, 258–267.

58 J. Xu, C. C. Boyd, Z. J. Yu, A. F. Palmstrom, D. J. Witter, B. W. Larson, R. M. France, J. Werner, S. P. Harvey, E. J. Wolf, W. Weigand, S. Manzoor, M. F. A. M. Van Hest, J. J. Berry, J. M. Luther, Z. C. Holman and M. D. McGehee, *Science*, 2020, **367**, 1097–1104.

59 S. Mariotti, E. Köhnen, F. Scheler, K. Sveinbjörnsson, L. Zimmermann, M. Piot, F. Yang, B. Li, J. Warby, A. Musiienko, D. Menzel, F. Lang, S. Keßler, I. Levine, D. Mantione, A. Al-Ashouri, M. S. Härtel, K. Xu, A. Cruz, J. Kurpiers, P. Wagner, H. Köbler, J. Li, A. Magomedov, D. Mecerreyes, E. Unger, A. Abate, M. Stolterfoht, B. Stannowski, R. Schlatmann, L. Korte and S. Albrecht, *Science*, 2023, **381**, 63–69.

This journal is © The Royal Society of Chemistry 2024

*Energy Environ. Sci.*, 2024, **17**, 7566–7599 | 7591

60 Y. Chen, Y. Lei, Y. Li, Y. Yu, J. Cai, M.-H. Chiu, R. Rao, Y. Gu, C. Wang, W. Choi, H. Hu, C. Wang, Y. Li, J. Song, J. Zhang, B. Qi, M. Lin, Z. Zhang, A. E. Islam, B. Maruyama, S. Dayeh, L.-J. Li, K. Yang, Y.-H. Lo and S. Xu, *Nature*, 2020, **577**, 209.

61 A. Y. Alsalloum, B. Turedi, K. Almasabi, X. Zheng, R. Naphade, S. D. Stranks, O. F. Mohammed and O. M. Bakr, *Energy Environ. Sci.*, 2021, **14**, 2263–2268.

62 B. Philippe, M. Saliba, J.-P. Correa-Baena, U. B. Cappel, S.-H. Turren-Cruz, M. Grätzel, A. Hagfeldt and H. Kan Rensmo, *Chem. Mater.*, 2017, **29**, 3589–3596.

63 M. Abdi-Jalebi, Z. Andaji-Garmaroudi, A. J. Pearson, G. Divitini, S. Cacovich, B. Philippe, H. Rensmo, C. Ducati, R. H. Friend and S. D. Stranks, *ACS Energy Lett.*, 2018, **3**, 2671–2678.

64 A. A. Sutanto, P. Caprioglio, N. Drigo, Y. J. Hofstetter, I. Garcia-Benito, V. I. E. Queloz, D. Neher, M. K. Nazeeruddin, M. Stolterfoht, Y. Vaynzof and G. Grancini, *Chem*, 2021, **7**, 1903–1916.

65 T. Niu, J. Lu, X. Jia, Z. Xu, M.-C. Tang, D. Barrit, N. Yuan, J. Ding, X. Zhang, Y. Fan, T. Luo, Y. Zhang, D.-M. Smilgies, Z. Liu, A. Amassian, S. Jin, K. Zhao and S. Liu, *Nano Lett.*, 2019, **19**, 7181–7190.

66 S. Sidhik, Y. Wang, M. De Siena, R. Asadpour, A. J. Torma, T. Terlier, K. Ho, W. Li, A. B. Puthirath, X. Shuai, A. Agrawal, B. Traore, M. Jones, R. Giridharagopal, P. M. Ajayan, J. Strzalka, D. S. Ginger, C. Katan, M. A. Alam, J. Even, M. G. Kanatzidis and A. D. Mohite, *Science*, 2022, **377**, 1425–1430.

67 G. Y. Kim, A. Senocrate, T. Y. Yang, G. Gregori, M. Grätzel and J. Maier, *Nat. Mater.*, 2018, **17**, 445–449.

68 W. J. Yin, T. Shi and Y. Yan, *Appl. Phys. Lett.*, 2014, **104**, 063903.

69 B. Chen, M. Yang, S. Priya and K. Zhu, *J. Phys. Chem. Lett.*, 2016, **7**, 905–917.

70 H. Lee, S. Gaiaschi, P. Chapon, A. Marronnier, H. Lee, J. C. Vanel, D. Tondelier, J. E. Bourée, Y. Bonnassieux and B. Geffroy, *ACS Energy Lett.*, 2017, **2**, 943–949.

71 D. A. Jacobs, H. Shen, F. Pfeffer, J. Peng, T. P. White, F. J. Beck and K. R. Catchpole, *J. Appl. Phys.*, 2018, **124**, 225702.

72 C. C. Boyd, R. Cheacharoen, T. Leijtens and M. D. McGehee, *Chem. Rev.*, 2018, **119**, 3418–3451.

73 S. P. Dunfield, L. Bliss, F. Zhang, J. M. Luther, K. Zhu, M. F. A. M. van Hest, M. O. Reese and J. J. Berry, *Adv. Energy Mater.*, 2020, **10**, 1–35.

74 S. A. L. Weber, I. M. Hermes, S. H. Turren-Cruz, C. Gort, V. W. Bergmann, L. Gilson, A. Hagfeldt, M. Graetzel, W. Tress and R. Berger, *Energy Environ. Sci.*, 2018, **11**, 2404–2413.

75 P. Calado, A. M. Telford, D. Bryant, X. Li, J. Nelson, B. C. O'Regan and P. R. F. Barnes, *Nat. Commun.*, 2016, **7**, 1–10.

76 G. Richardson, S. E. J. O'Kane, R. G. Niemann, T. A. Peltola, J. M. Foster, P. J. Cameron and A. B. Walker, *Energy Environ. Sci.*, 2016, **9**, 1476–1485.

77 M. H. Futscher, J. M. Lee, L. McGovern, L. A. Muscarella, T. Wang, M. I. Haider, A. Fakharuddin, L. Schmidt-Mende and B. Ehrler, *Mater. Horiz.*, 2019, **6**, 1497–1503.

78 N. Tessler and Y. Vaynzof, *ACS Energy Lett.*, 2020, **5**, 1260–1270.

79 H. S. Duan, H. Zhou, Q. Chen, P. Sun, S. Luo, T. Bin Song, B. Bob and Y. Yang, *Phys. Chem. Chem. Phys.*, 2015, **17**, 112–116.

80 D. W. DeQuilettes, W. Zhang, V. M. Burlakov, D. J. Graham, T. Leijtens, A. Osherov, V. Bulović, H. J. Snaith, D. S. Ginger and S. D. Stranks, *Nat. Commun.*, 2016, **7**, 11683.

81 T. Zhang, C. Hu and S. Yang, *Small Methods*, 2020, **4**, 1900552.

82 S. De Wolf, J. Holovsky, S. J. Moon, P. Löper, B. Niesen, M. Ledinsky, F. J. Haug, J. H. Yum and C. Ballif, *J. Phys. Chem. Lett.*, 2014, **5**, 1035–1039.

83 S. D. Stranks, G. E. Eperon, G. Grancini, C. Menelaou, M. J. P. Alcocer, T. Leijtens, L. M. Herz, A. Petrozza and H. J. Snaith, *Science*, 2013, **342**, 341–344.

84 Y. Yuan, J. Chae, Y. Shao, Q. Wang, Z. Xiao, A. Centrone and J. Huang, *Adv. Energy Mater.*, 2015, **5**, 1500615.

85 Y. Liu, A. V. Ievlev, N. Borodinov, M. Lorenz, K. Xiao, M. Ahmadi, B. Hu, S. V. Kalinin and O. S. Ovchinnikova, *Adv. Funct. Mater.*, 2021, **31**, 2008777.

86 T. Leijtens, E. T. Hoke, G. Grancini, D. J. Slotcavage, G. E. Eperon, J. M. Ball, M. De Bastiani, A. R. Bowring, N. Martino, K. Wojciechowski, M. D. McGehee, H. J. Snaith and A. Petrozza, *Adv. Energy Mater.*, 2015, **5**, 1500962.

87 R. A. Z. Razera, D. A. Jacobs, F. Fu, P. Fiala, M. Dussouillez, F. Sahli, T. C. J. Yang, L. Ding, A. Walter, A. F. Feil, H. I. Boudinov, S. Nicolay, C. Ballif and Q. Jeangros, *J. Mater. Chem. A*, 2020, **8**, 242–250.

88 Q. Jeangros, M. Duchamp, J. Werner, M. Kruth, R. E. Dunin-Borkowski, B. Niesen, C. Ballif and A. Hessler-Wyser, *Nano Lett.*, 2016, **16**, 7013–7018.

89 M. De Bastiani, E. Van Kerschaver, Q. Jeangros, A. Ur Rehman, E. Aydin, F. H. Isikgor, A. J. Mirabelli, M. Babics, J. Liu, S. Zhumagali, E. Ugur, G. T. Harrison, T. G. Allen, B. Chen, Y. Hou, S. Shikin, E. H. Sargent, C. Ballif, M. Salvador and S. De Wolf, *ACS Energy Lett.*, 2021, **6**, 2944–2951.

90 K. Domanski, B. Roose, T. Matsui, M. Saliba, S. H. Turren-Cruz, J. P. Correa-Baena, C. R. Carmona, G. Richardson, J. M. Foster, F. De Angelis, J. M. Ball, A. Petrozza, N. Mine, M. K. Nazeeruddin, W. Tress, M. Grätzel, U. Steiner, A. Hagfeldt and A. Abate, *Energy Environ. Sci.*, 2017, **10**, 604–613.

91 I. M. Pavlovetc, M. C. Brennan, S. Draguta, A. Ruth, T. Moot, J. A. Christians, K. Aleshire, S. P. Harvey, S. Toso, S. U. Nanayakkara, J. Messinger, J. M. Luther and M. Kuno, *ACS Energy Lett.*, 2020, **5**, 2802–2810.

92 S. G. Motti, D. Meggiolaro, A. J. Barker, E. Mosconi, C. A. R. Perini, J. M. Ball, M. Gandini, M. Kim, F. De Angelis and A. Petrozza, *Nat. Photonics*, 2019, **13**, 532–539.

93 J. Holovský, A. Peter Amalathas, L. Landová, B. Dzurňák, B. Conrad, M. Ledinský, Z. Hájková, O. Pop-Georgievski,

7592 | *Energy Environ. Sci.*, 2024, **17**, 7566–7599

This journal is © The Royal Society of Chemistry 2024

J. Svoboda, T. C. J. Yang and Q. Jeangros, *ACS Energy Lett.*, 2019, **4**, 3011–3017.

94 J. Thiesbrummel, S. Shah, E. Gutierrez-Partida, F. Zu, F. Peña-Camargo, S. Zeiske, J. Diekmann, F. Ye, K. P. Peters, K. O. Brinkmann, P. Caprioglio, A. Dasgupta, S. Seo, F. A. Adeleye, J. Warby, Q. Jeangros, F. Lang, S. Zhang, S. Albrecht, T. Riedl, A. Armin, D. Neher, N. Koch, Y. Wu, V. M. Le Corre, H. Snaith and M. Stolterfoht, *Nat. Energy*, 2024, **9**, 664–676.

95 D. A. Jacobs, C. M. Wolff, X. Y. Chin, K. Artuk, C. Ballif and Q. Jeangros, *Energy Environ. Sci.*, 2022, **15**, 5324–5339.

96 Y. Zhong, J. Yang, X. Wang, Y. Liu, Q. Cai, L. Tan and Y. Chen, *Adv. Mater.*, 2023, **35**, 2302552.

97 S. Tan, I. Yavuz, N. De Marco, T. Huang, S.-J. Lee, C. S. Choi, M. Wang, S. Nuryyeva, R. Wang, Y. Zhao, H.-C. Wang, T.-H. Han, B. Dunn, Y. Huang, J.-W. Lee, Y. Yang, S. Tan, N. De Marco, T. Huang, S. Lee, C. S. Choi, M. Wang, S. Nuryyeva, R. Wang, Y. Zhao, H. Wang, T. Han, B. Dunn, Y. Huang, J. Lee, Y. Yang and I. Yavuz, *Adv. Mater.*, 2020, **32**, 1906995.

98 A. D. Jodlowski, C. Roldán-Carmona, G. Grancini, M. Salado, M. Ralaiarisoa, S. Ahmad, N. Koch, L. Camacho, G. De Miguel and M. Khaja Nazeeruddin, *Nat. Energy*, 2017, **2**, 972–979.

99 P. Liu, Y. Xian, W. Yuan, Y. Long, K. Liu, N. Ur Rahman, W. Li, J. Fan, P. Liu, Y. Xian, W. Yuan, Y. Long, K. Liu, N. U. Rahman, W. Li and J. Fan, *Adv. Energy Mater.*, 2020, **10**, 1903654.

100 Z. Huang, A. H. Proppe, H. Tan, M. I. Saidaminov, F. Tan, A. Mei, C.-S. Tan, M. Wei, Y. Hou, H. Han, S. O. Kelley and E. H. Sargent, *ACS Energy Lett.*, 2019, **4**, 1521–1527.

101 W. Fan, S. Zhang, C. Xu, H. Si, Z. Xiong, Y. Zhao, K. Ma, Z. Zhang, Q. Liao, Z. Kang, Y. Zhang, W. Fan, S. Zhang, C. Xu, H. Si, Z. Xiong, Y. Zhao, K. Ma, Z. Zhang, Q. Liao, Z. Kang and Y. Zhang, *Adv. Funct. Mater.*, 2021, **31**, 2104633.

102 J. Yang, C. Liu, C. Cai, X. Hu, Z. Huang, X. Duan, X. Meng, Z. Yuan, L. Tan and Y. Chen, *Adv. Energy Mater.*, 2019, **9**, 1900198.

103 S. Bai, P. Da, C. Li, Z. Wang, Z. Yuan, F. Fu, M. Kawecki, X. Liu, N. Sakai, J. T.-W. Wang, S. Huettner, S. Buecheler, F. Gao and H. J. Snaith, *Nature*, 2019, **571**, 245.

104 Y. Ma, Y. Cheng, X. Xu, M. Li, C. Zhang, S. Hang Cheung, Z. Zeng, D. Shen, Y.-M. Xie, K. Lok Chiu, F. Lin, S. Kong So, C.-S. Lee, S.-W. Tsang, Y. Ma, X. Xu, M. Li, Z. Zeng, Y. Xie, S. Tsang, Y. Cheng, F. Lin, C. Zhang, S. H. Cheung, K. L. Chiu, S. K. So, D. Shen and C. Lee, *Adv. Funct. Mater.*, 2021, **31**, 2006802.

105 H. Wang, W. Zou, Y. Ouyang, X. Liu, H. Li, H. Luo and X. Zhao, *J. Phys. Chem. Lett.*, 2022, **13**, 8573–8579.

106 J. Cao, S. Xia Tao, P. A. Bobbert, C.-P. Wong, N. Zhao, J. Cao, C. Wong, N. Zhao, S. X. Tao and P. A. Bobbert, *Adv. Mater.*, 2018, **30**, 1707350.

107 S. Yang, S. Chen, E. Mosconi, Y. Fang, X. Xiao, C. Wang, Y. Zhou, Z. Yu, J. Zhao, Y. Gao, F. De Angelis and J. Huang, *Science*, 2019, **365**, 473–478.

108 H. Zai, J. Su, C. Zhu, Y. Chen, Y. Ma, P. Zhang, S. Ma, X. Zhang, H. Xie, R. Fan, Z. Huang, N. Li, Y. Zhang, Y. Li, Y. Bai, Z. Gao, X. Wang, J. Hong, K. Sun, J. Chang, H. Zhou and Q. Chen, *Joule*, 2021, **5**, 2148–2163.

109 L. Ma, D. Guo, M. Li, C. Wang, Z. Zhou, X. Zhao, F. Zhang, Z. Ao and Z. Nie, *Chem. Mater.*, 2019, **31**, 8515–8522.

110 J. A. Schwenzer, T. Hellmann, B. A. Nejand, H. Hu, T. Abzieher, F. Schackmar, I. M. Hossain, P. Fassl, T. Mayer, W. Jaegermann, U. Lemmer and U. W. Paetzold, *ACS Appl. Mater. Interfaces*, 2021, **13**, 15292–15304.

111 G. Abdelmageed, C. Mackeen, K. Hellier, L. Jewell, L. Seymour, M. Tingwald, F. Bridges, J. Z. Zhang and S. Carter, *Sol. Energy Mater. Sol. Cells*, 2018, **174**, 566–571.

112 B. Conings, J. Drijkoningen, N. Gauquelin, A. Babayigit, J. D'Haen, L. D'Olieslaeger, A. Ethirajan, J. Verbeeck, J. Manca, E. Mosconi, F. De Angelis and H.-G. Boyen, *Adv. Energy Mater.*, 2015, **5**, 1500477.

113 N.-K. Kim, Y. H. Min, S. Noh, E. Cho, G. Jeong, M. Joo, S.-W. Ahn, J. S. Lee, S. Kim, K. Ihm, H. Ahn, Y. Kang, H.-S. Lee and D. Kim, *Sci. Rep.*, 2017, **7**, 4645.

114 L. Nakka, W. Luo, A. G. Aberle and F. Lin, *Sol. RRL*, 2023, **7**, 2300100.

115 L. Xu, J. Liu, W. Luo, N. Wehbe, A. Seitkhan, M. Babics, J. Kang, M. De Bastiani, E. Aydin, T. G. Allen, M. Alamer, W. Yan, F. Xu, A. U. Rehman and S. De Wolf, *Cell Rep. Phys. Sci.*, 2022, **3**, 101026.

116 H. Meng, K. Mao, F. Cai, K. Zhang, S. Yuan, T. Li, F. Cao, Z. Su, Z. Zhu, X. Feng, W. Peng, J. Xu, Y. Gao, W. Chen, C. Xiao, X. Wu, M. D. McGehee and J. Xu, *Nat. Energy*, 2024, **9**, 536–547.

117 Y. Yang, C. Liu, Y. Ding, B. Ding, J. Xu, A. Liu, J. Yu, L. Grater, H. Zhu, S. S. Hadke, V. K. Sangwan, A. S. R. Bati, X. Hu, J. Li, S. M. Park, M. C. Hersam, B. Chen, M. Khaja Nazeeruddin, M. G. Kanatzidis and E. H. Sargent, *Nat. Energy*, 2024, **9**, 316–323.

118 F. Cheng, F. Cao, B. Chen, X. Dai, Z. Tang, Y. Sun, J. Yin, J. Li, N. Zheng, B. Wu, F. Cheng, F. Cao, B. Chen, X. Dai, Z. Tang, Y. Sun, J. Yin, J. Li, N. Zheng and B. Wu, *Adv. Sci.*, 2022, **9**, 2201573.

119 E. Bi, W. Tang, H. Chen, Y. Wang, J. Barbaud, T. Wu, W. Kong, P. Tu, H. Zhu, X. Zeng, J. He, S. ichi Kan, X. Yang, M. Grätzel and L. Han, *Joule*, 2019, **3**, 2748–2760.

120 P. M. Nagy, P. Horváth, G. Pető and E. Kálmán, *Mater. Sci. Forum*, 2008, **604–605**, 29–36.

121 J. Gomez and C. Basaran, *Int. J. Solids Struct.*, 2006, **43**, 1505–1527.

122 S. Bansal, E. Toimil-Molares, A. Saxena and R. R. Tummala, *Proc. - Electron. Compon. Technol. Conf.*, 2005, **1**, 71–76.

123 H. Gao, W. Wei, L. Li, Y. Tan and Y. Tang, *J. Phys. Chem. C*, 2020, **124**, 19204–19211.

124 S. Sun, Y. Fang, G. Kieslich, T. J. White and A. K. Cheetham, *J. Mater. Chem. A*, 2015, **3**, 18450–18455.

125 L. Ma, W. Li, K. Yang, J. Bi, J. Feng, J. Zhang, Z. Yan, X. Zhou, C. Liu, Y. Ji, J. C. Huang and X. Han, *APL Mater.*, 2021, **9**, 1–9.

This journal is © The Royal Society of Chemistry 2024

*Energy Environ. Sci.*, 2024, **17**, 7566–7599 | **7593**

126 Y. Rakita, S. R. Cohen, N. K. Kedem, G. Hodes and D. Cahen, *MRS Commun.*, 2015, **5**, 623–629.

127 Z. Dai, M. C. Doyle, X. Liu, M. Hu, Q. Wang, C. E. Athanasiou, Y. Liu, B. W. Sheldon, H. Gao, S. (Frank) Liu and N. P. Padture, *Scr. Mater.*, 2023, **223**, 115064.

128 M. Spina, A. Karimi, W. Andreoni, C. A. Pignedoli, B. Náfrádi, L. Forró and E. Horváth, *Appl. Phys. Lett.*, 2017, **110**, 121903.

129 Q. Tu, I. Spanopoulos, S. Hao, C. Wolverton, M. G. Kanatzidis, G. S. Shekhawat and V. P. Dravid, *ACS Appl. Mater. Interfaces*, 2018, **10**, 22167–22173.

130 S. Baumann, A. Raugewitz, F. Haase, T. Wietler, R. Peibst and M. Köntges, in 2023 *IEEE 50th Photovoltaic Specialists Conference (PVSC)*, 2023.

131 M. Heydarian, M. Heydarian, P. Schygulla, S. K. Reichmuth, A. J. Bett, J. Hohl-Ebinger, F. Schindler, M. Hermle, M. C. Schubert, P. S. C. Schulze, J. Borchert and S. W. Glunz, *Energy Environ. Sci.*, 2024, **17**, 1781.

132 X. Zhao, T. Liu, Q. C. Burlingame, T. Liu, R. Holley, G. Cheng, N. Yao, F. Gao and Y. L. Loo, *Science*, 2022, **377**, 307–310.

133 J. H. Noh, S. H. Im, J. H. Heo, T. N. Mandal and S. Il Seok, *Nano Lett.*, 2013, **13**, 1764–1769.

134 F. Brivio, C. Caetano and A. Walsh, *J. Phys. Chem. Lett.*, 2016, **7**, 1083–1087.

135 J. Dai, C. Xu, H. Zheng, J. Duan, F. Chen, G. Zhu and F. Wang, *J. Mater. Chem. C*, 2017, **5**, 12057.

136 S. H. Turren-Cruz, A. Hagfeldt and M. Saliba, *Science*, 2018, **362**, 449–453.

137 P. F. Ndione, Z. Li and K. Zhu, *J. Mater. Chem. C*, 2016, **4**, 7775.

138 J. Liu, E. Aydin, J. Yin, M. De Bastiani, F. H. Isikgor, A. U. Rehman, E. Yengel, E. Ugur, G. T. Harrison, M. Wang, Y. Gao, J. I. Khan, M. Babics, T. G. Allen, A. S. Subbiah, K. Zhu, X. Zheng, W. Yan, F. Xu, M. F. Salvador, O. M. Bakr, T. D. Anthopoulos, M. Lanza, O. F. Mohammed, F. Laquai and S. De Wolf, *Joule*, 2021, **5**, 3169–3186.

139 C. M. Sutter-Fella, Q. P. Ngo, N. Cefarin, K. L. Gardner, N. Tamura, C. V. Stan, W. S. Drisdell, A. Javey, F. M. Toma and I. D. Sharp, *Nano Lett.*, 2018, **18**, 51.

140 T. Leijtens, G. E. Eperon, S. Pathak, A. Abate, M. M. Lee and H. J. Snaith, *Nat. Commun.*, 2013, **4**, 2885.

141 B. Roose, J. P. C. Baena, K. C. Gödel, M. Graetzel, A. Hagfeldt, U. Steiner and A. Abate, *Nano Energy*, 2016, **30**, 517–522.

142 S. Zhang, R. Wu, C. Mu, Y. Wang, L. Han, Y. Wu and W. H. Zhu, *ACS Mater. Lett.*, 2022, **4**, 1976–1983.

143 P. Jiang, L. Hu, L. Sun, Z. Li, H. Han and Y. Zhou, *Chem. Sci.*, 2022, **13**, 4714–4739.

144 R. Prasanna, T. Leijtens, S. P. Dunfield, J. A. Raiford, E. J. Wolf, S. A. Swifter, J. Werner, G. E. Eperon, C. de Paula, A. F. Palmstrom, C. C. Boyd, M. F. A. M. van Hest, S. F. Bent, G. Teeter, J. J. Berry and M. D. McGehee, *Nat. Energy*, 2019, **4**, 939–947.

145 J. Yang, B. D. Siempelkamp, E. Mosconi, F. De Angelis and T. L. Kelly, *Chem. Mater.*, 2015, **27**, 4229–4236.

146 C. C. Boyd, R. C. Shallcross, T. Moot, R. Kerner, L. Bertoluzzi, A. Onno, S. Kavadiya, C. Chosy, E. J. Wolf, J. Werner, J. A. Raiford, C. de Paula, A. F. Palmstrom, Z. J. Yu, J. J. Berry, S. F. Bent, Z. C. Holman, J. M. Luther, E. L. Ratcliff, N. R. Armstrong and M. D. McGehee, *Joule*, 2020, **4**, 1759–1775.

147 K. Rakstys, C. Igci and M. K. Nazeeruddin, *Chem. Sci.*, 2019, **10**, 6748–6769.

148 G. Tumen-Ulzii, C. Qin, T. Matsushima, M. R. Leyden, U. Balijipalli, D. Klotz and C. Adachi, *Sol. RRL*, 2020, **4**, 2000305.

149 E. Kasparavicius, M. Franckevičius, V. Malinauskiene, K. Genevičius, V. Getautis and T. Malinauskas, *ACS Appl. Energy Mater.*, 2021, **4**, 13696–13705.

150 S. N. Habisreutinger, T. Leijtens, G. E. Eperon, S. D. Stranks, R. J. Nicholas and H. J. Snaith, *Nano Lett.*, 2014, **14**, 5561–5568.

151 T. H. Schloemer, J. A. Raiford, T. S. Gehan, T. Moot, S. Nanayakkara, S. P. Harvey, R. C. Bramante, S. Dunfield, A. E. Louks, A. E. Maughan, L. Bliss, M. D. McGehee, M. F. A. M. Van Hest, M. O. Reese, S. F. Bent, J. J. Berry, J. M. Luther and A. Sellinger, *ACS Energy Lett.*, 2020, **5**, 2349–2360.

152 M. De Bastiani, G. Armaroli, R. Jalmood, L. Ferlauto, X. Li, R. Tao, G. T. Harrison, M. K. Eswaran, R. Azmi, M. Babics, A. S. Subbiah, E. Aydin, T. G. Allen, C. Combe, T. Cramer, D. Baran, U. Schwingenschlögl, G. Lubineau, D. Cavalcoli and S. De Wolf, *ACS Energy Lett.*, 2022, **7**, 827–833.

153 D. Di Girolamo, A. Francesco Di Giacomo, F. Matteocci, A. Giacomo Marrani, D. Dini and A. Abate, *Chem. Sci.*, 2020.

154 J. A. Christians, P. Schulz, J. S. Tinkham, T. H. Schloemer, S. P. Harvey, B. J. Tremolet de Villers, A. Sellinger, J. J. Berry and J. M. Luther, *Nat. Energy*, 2018, **3**, 68–74.

155 A. Rashid, M. Yusoff, M. Vasilopoulou, D. G. Georgiadou, L. C. Palilis, A. Abate and M. K. Nazeeruddin, *Energy Environ. Sci.*, 2021, **14**, 2906.

156 S. M. Park, M. Wei, J. Xu, H. R. Atapattu, F. T. Eickemeyer, K. Darabi, L. Grater, Y. Yang, C. Liu, S. Teale, B. Chen, H. Chen, T. Wang, L. Zeng, A. Maxwell, Z. Wang, K. R. Rao, Z. Cai, S. M. Zakeeruddin, J. T. Pham, C. M. Risko, A. Amassian, M. G. Kanatzidis, K. R. Graham, M. Grätzel and E. H. Sargent, *Science*, 2023, **381**, 209–215.

157 M. Wang, Z. Shi, C. Fei, Z. J. D. Deng, G. Yang, S. P. Dunfield, D. P. Fenning and J. Huang, *Nat. Energy*, 2023, **8**, 1229–1239.

158 A. Das Mahapatra and J.-W. Lee, *CrystEngComm*, 2022, **24**, 7229.

159 B. Roose, Q. Wang and A. Abate, *Adv. Energy Mater.*, 2019, **9**, 1803140.

160 I. Gueye, Y. Shirai, T. Nagata, T. Tsuchiya, D. B. Khadka, M. Yanagida, O. Seo, K. Miyano and O. Sakata, *Chem. Mater.*, 2023, **35**, 1948–1960.

161 K. Domanski, J.-P. Correa-Baena, N. Mine, M. K. Nazeeruddin, A. Abate, M. Saliba, W. Tress, A. Hagfeldt and M. Grätzel, *ACS Nano*, 2016, **10**, 6306–6314.

**7594** | *Energy Environ. Sci.*, 2024, **17**, 7566–7599

This journal is © The Royal Society of Chemistry 2024

162 H. Q. Wang, S. Wang, L. Chen, Z. Yin, S. Mei, Y. Zhong, Y. Yao, N. Li, J. Wang and W. Song, *Sol. Energy Mater. Sol. Cells*, 2021, **230**, 111278.

163 H. Chen, A. Maxwell, C. Li, S. Teale, B. Chen, T. Zhu, E. Ugur, G. Harrison, L. Grater, J. Wang, Z. Wang, L. Zeng, S. Min Park, L. Chen, P. Serles, R. Abbas Awni, B. Subedi, X. Zheng, C. Xiao, N. J. Podraza, T. Filleter, C. Liu, Y. Yang, J. M. Luther, S. De Wolf, M. G. Kanatzidis, Y. Yan and E. H. Sargent, *Nature*, 2023, **613**, 676.

164 W. Zhao, M. Wu, Z. Liu, S. Yang, Y. Li, J. Wang, L. Yang, Y. Han and S. (Frank and) Liu, *Adv. Energy Mater.*, 2023, **13**, 2204260.

165 J. Long, Z. Huang, J. Zhang, A. A. Assi, W. R. Saleh and E. Mohajerani, *IOP Conf. Ser. Earth Environ. Sci.*, 2021, **722**, 012019.

166 F. Cheng, S. Zhan, Y. Cai, F. Cao, X. Dai, R. Xu, J. Yin, J. Li, N. Zheng and B. Wu, *J. Am. Chem. Soc.*, 2023, **145**, 20081–20087.

167 S. Svanström, A. García-Fernández, T. J. Jacobsson, I. Bidermane, T. Leitner, T. Sloboda, G. J. Man, G. Boschloo, E. M. J. Johansson, H. Kan Rensmo and U. B. Cappel, *ACS Mater. Au*, 2022, **2**, 312.

168 N. N. Udalova, E. M. Nemygina, E. A. Zharenova, A. S. Tutantsev, A. A. Sudakov, A. Y. Grishko, N. A. Belich, E. A. Goodilin and A. B. Tarasov, *J. Phys. Chem. C*, 2020, **124**, 24601–24607.

169 Y. Kato, L. K. Ono, M. V. Lee, S. Wang, S. R. Raga and Y. Qi, *Adv. Mater. Interfaces*, 2015, **2**, 1500195.

170 H. Lee and C. Lee, *Adv. Energy Mater.*, 2018, **8**, 1702197.

171 A. Guerrero, J. You, C. Aranda, Y. S. Kang, G. Garcia-Belmonte, H. Zhou, J. Bisquert and Y. Yang, *ACS Nano*, 2016, **10**, 218–224.

172 L. Zhao, R. A. Kerner, Z. Xiao, Y. L. Lin, K. M. Lee, J. Schwartz and B. P. Rand, *ACS Energy Lett.*, 2016, **1**, 595–602.

173 M. Liu, Z. Chen, Y. Yang, H.-L. Yip and Y. Cao, *J. Mater. Chem. A*, 2019, **7**, 17324.

174 S. Svanström, T. J. Jacobsson, G. Boschloo, E. M. J. Johansson, H. Rensmo and U. B. Cappel, *ACS Appl. Mater. Interfaces*, 2020, **12**, 7212–7221.

175 R. A. Kerner, P. Schulz, J. A. Christians, S. P. Dunfield, B. Dou, L. Zhao, G. Teeter, J. J. Berry and B. P. Rand, *APL Mater.*, 2019, **7**, 041103.

176 T. Chen, T. Shi, X. Li, J. Zheng, W. Fan, B. Ni, Y. Wang, J. Dai and Z. Xiao, *Sol. RRL*, 2018, **2**, 1800167.

177 M. Kaltenbrunner, G. Adam, E. D. Głowacki, M. Drack, R. Schwödiauer, L. Leonat, D. H. Apaydin, H. Groiss, M. C. Scharber, M. Schuette White, N. S. Sariciftci and S. Bauer, *Nat. Mater.*, 2015, **14**, 1032.

178 E. M. Sanehira, B. J. Tremolet De Villers, P. Schulz, M. O. Reese, S. Ferrere, K. Zhu, L. Y. Lin, J. J. Berry and J. M. Luther, *ACS Energy Lett.*, 2016, **1**, 38–45.

179 J. Li, J. Wang, Y. Zhou, C. Yu, H. Liu, X. Qi, R. Li, Y. Hua, Y. Yu, R. Chen, D. Chen, L. Mao, H. Xia and H.-L. Wang, *Chem. Front.*, 2022, **6**, 2211.

180 C. Yu, Y. Hu, J. Yang, J. Huang, B. Li, L. Wu, F. Li, C. Yu, J. Yang, B. Li, L. Wu, F. Li, Y. Hu and J. Huang, *Adv. Funct. Mater.*, 2022, **33**, 2209290.

181 N. Liu, J. Xiong, G. Wang, Z. He, J. Dai, Y. Zhang, Y. Huang, Z. Zhang, D. Wang, S. Li, B. Liu, X. Deng, H. Zhang, J. Zhang, N. Liu, J. Xiong, Z. He, J. Dai, Y. Zhang, Y. Huang, Z. Zhang, D. Wang, J. Zhang, G. Wang, S. Li, B. Liu, X. Deng and H. Zhang, *Adv. Funct. Mater.*, 2023, **33**, 2300396.

182 K. O. Brinkmann, J. Zhao, N. Pourdavoud, T. Becker, T. Hu, S. Olthof, K. Meerholz, L. Hoffmann, T. Gahlmann, R. Heiderhoff, M. F. Oszajca, N. A. Luechinger, D. Rogalla, Y. Chen, B. Cheng and T. Riedl, *Nat. Commun.*, 2017, **8**, 13938.

183 J. Luo, B. Liu, H. Yin, X. Zhou, M. Wu, H. Shi, J. Zhang, J. Elia, K. Zhang, J. Wu, Z. Xie, C. Liu, J. Yuan, Z. Wan, T. Heumueller, L. Lüer, E. Spiecker, N. Li, C. Jia, C. J. Brabec and Y. Zhao, *Nat. Commun.*, 2024, **15**, 1234567890.

184 C. C. Boyd, R. Cheacharoen, K. A. Bush, R. Prasanna, T. Leijtens and M. D. Mcgehee, *ACS Energy Lett.*, 2018, **3**, 1772–1778.

185 L. Liu, S. Yellinek, I. Valdinger, A. Donval and D. Mandler, *Electrochim. Acta*, 2015, **176**, 1374–1381.

186 R. A. Kerner and B. P. Rand, *ACS Appl. Energy Mater.*, 2019, **2**, 6097–6101.

187 Q. Jiang, R. Tirawat, R. A. Kerner, E. A. Gaulding, Y. Xian, X. Wang, J. M. Newkirk, Y. Yan, J. J. Berry and K. Zhu, *Nature*, 2023, **623**, 313.

188 Z. Jiang, X. Chen, X. Lin, X. Jia, J. Wang, L. Pan, S. Huang, F. Zhu and Z. Sun, *Sol. Energy Mater. Sol. Cells*, 2016, **146**, 35–43.

189 C.-T. Lin, J. Ngiam, B. Xu, Y.-H. Chang, T. Du, T. J. Macdonald, J. R. Durrant Bcd and M. A. Mclachlan, *J. Mater. Chem. A*, 2020, **8**, 8684.

190 S. Mei, Z. Yin, P. Gu, H.-Q. Wang, J. Wang and W. Song, *ACS Appl. Energy Mater.*, 2021, **4**, 11062–11068.

191 I. Jeon, A. Shawky, S. Seo, Y. Qian, A. Anisimov, E. I. Kauppinen, Y. Matsuo and S. Maruyama, *J. Mater. Chem. A*, 2020, **8**, 11141–11147.

192 J. Yoon, H. Sung, G. Lee, W. Cho, N. Ahn, H. Suk Jung and M. Choi, *Energy Environ. Sci.*, 2017, **10**, 337.

193 H. Zhang, K. Song, L. Zhu and Q. Meng, *Carbon N. Y.*, 2020, **168**, 372–391.

194 Y. J. Noh, J. G. Kim, S. S. Kim, H. K. Kim and S. I. Na, *J. Power Sources*, 2019, **437**, 226894.

195 S. Yoon, H. U. Ha, H.-J. Seok, H.-K. Kim, D.-W. Kang, S. Yoon, D.-W. Kang, H. U. Ha, H.-J. Seok and H.-K. Kim, *Adv. Funct. Mater.*, 2022, **32**, 2111760.

196 J. Zhao, Y. Deng, H. Wei, X. Zheng, Z. Yu, Y. Shao, J. E. Shield and J. Huang, *Sci. Adv.*, 2017, **3**, 1–8.

197 N. Rolston, K. A. Bush, A. D. Printz, A. Gold-Parker, Y. Ding, M. F. Toney, M. D. McGehee and R. H. Dauskardt, *Adv. Energy Mater.*, 2018, 1802139.

198 C. Ge, M. Hu, P. Wu, Q. Tan, Z. Chen, Y. Wang, J. Shi and J. Feng, *J. Phys. Chem. C*, 2018, **122**, 15973–15978.

This journal is © The Royal Society of Chemistry 2024

*Energy Environ. Sci.*, 2024, **17**, 7566–7599 | **7595**

199 D. H. Fabini, C. C. Stoumpos, G. Laurita, A. Kaltzoglou, A. G. Kontos, P. Olycarpos Falaras, G. Kanatzidis, R. Seshadri, D. H. Fabini and R. Seshadri, *Angew. Chem., Int. Ed.*, 2016, **55**, 15392–15396.

200 G. Mannino, I. Deretzis, E. Smecca, A. La Magna, A. Alberti, D. Ceratti and D. Cahen, *J. Phys. Chem. Lett.*, 2020, **11**, 33.

201 D.-J. Xue, Y. Hou, S.-C. Liu, M. Wei, B. Chen, Z. Huang, Z. Li, B. Sun, A. H. Proppe, Y. Dong, M. I. Saidaminov, S. O. Kelley, J.-S. Hu and E. H. Sargent, *Nat. Commun.*, 2020, **11**, 1514.

202 T. H. Johansen, J. Feder and T. Jossang, *Phys. Rev. B: Condens. Matter Mater. Phys.*, 1988, **37**, 5305–5311.

203 P. S. Peercy and B. Morosin, *Phys. Rev. B: Condens. Matter Mater. Phys.*, 1973, **7**, 2779–2786.

204 M. Dailey, Y. Li and A. D. Printz, *ACS Omega*, 2021, **6**, 30214–30223.

205 H. Wang, C. Zhu, L. Liu, S. Ma, P. Liu, J. Wu, C. Shi, Q. Du, Y. Hao, S. Xiang, H. Chen, P. Chen, Y. Bai, H. Zhou, Y. Li, Q. Chen, H. Wang, C. Zhu, L. Liu, S. Ma, P. Liu, J. Wu, C. Shi, Q. Du, Y. Bai, Y. Li, Q. Chen, Y. Hao, S. Xiang, H. Chen, P. Chen and H. Zhou, *Adv. Mater.*, 2019, **31**, 904408.

206 M. D. Mcgehee, D. A. Morales and B. Guo, *APL Energy*, 2023, **1**, 036110.

207 E. T. Hoke, D. J. Slotcavage, E. R. Dohner, A. R. Bowring, H. I. Karunadasa and M. D. McGehee, *Chem. Sci.*, 2015, **6**, 613–617.

208 Z. Li, X. Zheng, X. Xiao, Y. An, Y. Wang, Q. Huang, X. Li, R. Cheacharoen, Q. An, Y. Rong, T. Wang and H. Xu, *Adv. Sci.*, 2022, **9**, 2103948.

209 T. Chen, J. Xie and P. Gao, *Adv. Energy Sustainability Res.*, 2022, **3**, 2100218.

210 A. Farooq, I. M. Hossain, S. Moghadamzadeh, J. A. Schwenzer, T. Abzieher, B. S. Richards, E. Klampaftis and U. W. Paetzold, *ACS Appl. Mater. Interfaces*, 2018, **10**, 21985–21990.

211 F. Bella, G. Griffini, J. P. Correa-Baena, G. Saracco, M. Grätzel, A. Hagfeldt, S. Turri and C. Gerbaldi, *Science*, 2016, **354**, 203–206.

212 S. Sidhik, I. Metcalf, W. Li, T. Kodalle, C. J. Dolan, M. Khalili, J. Hou, F. Mandani, A. Torma, H. Zhang, R. Garai, J. Persaud, A. Marciel, I. A. Muro Puente, G. N. M. Reddy, A. Balvanz, M. A. Alam, C. Katan, E. Tsai, D. Ginger, D. P. Fenning, M. G. Kanatzidis, C. M. Sutter-Fella, J. Even and A. D. Mohite, *Science*, 2024, **384**, 1227–1235.

213 Q. Li, Z. Chen, I. Tranca, S. Gaastra-Nedea, D. Smeulders and S. Tao, *Appl. Surf. Sci.*, 2021, **538**, 148058.

214 W. Chi and S. K. Banerjee, *Chem. Mater.*, 2021, **33**, 4269–4303.

215 A. M. A. Leguy, Y. Hu, M. Campoy-Quiles, M. I. Alonso, O. J. Weber, P. Azarhoosh, M. Van Schilfgaarde, M. T. Weller, T. Bein, J. Nelson, P. Docampo and P. R. F. Barnes, *Chem. Mater.*, 2015, **27**, 3397–3407.

216 A. M. Askar, G. M. Bernard, B. Wiltshire, K. Shankar and V. K. Michaelis, *J. Phys. Chem. C*, 2017, **121**, 1013–1024.

217 J. A. Christians, P. A. Miranda Herrera and P. V. Kamat, *J. Am. Chem. Soc.*, 2015, **137**, 1530–1538.

218 Z. Zhu, V. G. Hadjiev, Y. Rong, R. Guo, B. Cao, Z. Tang, F. Qin, Y. Li, Y. Wang, F. Hao, S. Venkatesan, W. Li, S. Baldelli, A. M. Guloy, H. Fang, Y. Hu, Y. Yao, Z. Wang and J. Bao, *Chem. Mater.*, 2016, **28**, 7385–7393.

219 N. Li, S. Pratap, V. Körstgens, S. Vema, L. Song, S. Liang, A. Davydok, C. Krywka and P. Müller-Buschbaum, *Nat. Commun.*, 2022, **13**, 6701.

220 K. Sun and P. Müller-Buschbaum, *Energy Technol.*, 2023, **11**, 2201475.

221 J. Schlipf, L. Bießmann, L. Oesinghaus, E. Berger, E. Metwalli, J. A. Lercher, L. Porcar and P. Müller-Buschbaum, *J. Phys. Chem. Lett.*, 2018, **9**, 42.

222 X. Guo, J. Li, B. Wang, P. Zeng, F. Li, Q. Yang, Y. Chen and M. Liu, *ACS Appl. Energy Mater.*, 2020, **3**, 970–976.

223 A. Abate, T. Leijtens, S. Pathak, J. Teuscher, R. Avolio, M. E. Errico, J. Kirkpatrik, J. M. Ball, P. Docampo, I. McPherson and H. J. Snaith, *Phys. Chem. Chem. Phys.*, 2013, **15**, 2572–2579.

224 R. Cheacharoen, C. C. Boyd, G. F. Burkhard, T. Leijtens, J. A. Raiford, K. A. Bush, S. F. Bent and M. D. McGehee, *Sustainable Energy Fuels*, 2018, **2**, 2398–2406.

225 L. Shi, T. L. Young, J. Kim, Y. Sheng, L. Wang, Y. Chen, Z. Feng, M. J. Keevers, X. Hao, P. J. Verlinden, M. A. Green and A. W. Y. Ho-Baillie, *ACS Appl. Mater. Interfaces*, 2017, **9**, 25073–25081.

226 R. Azmi, E. Ugur, A. Seitkhan, F. Aljamaan, A. S. Subbiah, J. Liu, G. T. Harrison, M. I. Nugraha, M. K. Eswaran, M. Babics, Y. Chen, F. Xu, T. G. Allen, A. Rehman, C. Wang, T. D. Anthopoulos, U. Schwingenschlögl, M. De Bastiani, E. Aydin and S. De Wolf, *Science*, 2022, **5784**, 1–9.

227 R. Singh, S. Ghosh, A. S. Subbiah, N. Mahuli and S. K. Sarkar, *Sol. Energy Mater. Sol. Cells*, 2020, **205**, 110289.

228 R. H. Ahangharnejhad, Z. Song, T. Mariam, J. J. Gardner, G. K. Liyanage, Z. S. Almutawah, B. M. M. Anwar, M. Junda, N. J. Podraza, A. B. Phillips, Y. Yan, M. J. Heben, R. Hosseinian Ahangharnejhad, Z. Song, T. Mariam, J. J. Gardner, G. K. Liyanage, Z. S. Almutawah, B. M. M. Anwar, M. Junda, N. J. Podraza, A. B. Phillips, Y. Yan and M. J. Heben, *ACS Appl. Energy Mater.*, 2021, **4**, 7571–7578.

229 J. Liu, M. De Bastiani, E. Aydin, G. T. Harrison, Y. Gao, R. R. Pradhan, M. K. Eswaran, M. Mandal, W. Yan, A. Seitkhan, M. Babics, A. S. Subbiah, E. Ugur, F. Xu, L. Xu, M. Wang, A. U. Rehman, A. Razzaq, J. Kang, R. Azmi, A. A. Said, F. H. Isikgor, T. G. Allen, D. Andrienko, U. Schwingenschlögl, F. Laquai and S. De Wolf, *Science*, 2022, **377**, 302–306.

230 H. Wang, Y. Zhao, Z. Wang, Y. Liu, Z. Zhao, G. Xu, T. H. Han, J. W. Lee, C. Chen, D. Bao, Y. Huang, Y. Duan and Y. Yang, *Nano Energy*, 2020, **69**, 104375.

231 G. E. Eperon, S. N. Habisreutinger, T. Leijtens, B. J. Bruijnaers, J. J. Van Franeker, D. W. Dequilettes, S. Pathak, R. J. Sutton, G. Grancini, D. S. Ginger, R. A. J. Janssen, A. Petrozza and H. J. Snaith, *ACS Nano*, 2015, **9**, 9380–9393.

7596 | *Energy Environ. Sci.*, 2024, **17**, 7566–7599

This journal is © The Royal Society of Chemistry 2024

232 W. Zhou, Y. Zhao, C. Shi, H. Huang, J. Wei, R. Fu, K. Liu, D. Yu and Q. Zhao, *J. Phys. Chem. C*, 2016, **120**, 4759–4765.

233 J. Tang, W. Tian, C. Zhao, Q. Sun, C. Zhang, H. Cheng, Y. Shi and S. Jin, *ACS Omega*, 2022, **7**, 10365–10371.

234 Y. Yang, C. Liu, Y. Ding, B. Ding, J. Xu, A. Liu, J. Yu, L. Grater, H. Zhu, S. S. Hadke, V. K. Sangwan, A. S. R. R. Bati, X. Hu, J. Li, S. M. Park, M. C. Hersam, B. Chen, M. K. Nazeeruddin, M. G. Kanatzidis, E. H. Sargent, M. Khaja Nazeeruddin, M. G. Kanatzidis and E. H. Sargent, *Nat. Energy*, 2024, **9**, 316–323.

235 J. You, L. Meng, T.-B. Song, T.-F. Guo, Y. Yang, W.-H. Chang, Z. Hong, H. Chen, H. Zhou, Q. Chen, Y. Liu and N. De Marco, *Nat. Nanotechnol.*, 2016, **11**, 75.

236 L. Duan and A. Uddin, *Mater. Chem. Front.*, 2022, **6**, 400–417.

237 N. Aristidou, C. Eames, I. Sanchez-Molina, X. Bu, J. Kosco, M. S. Islam, S. A. Haque, M. Saiful Islam and S. A. Haque, *Nat. Commun.*, 2017, **8**, 15218.

238 J. S. W. Godding, A. J. Ramadan, Y. H. Lin, K. Schutt, H. J. Snaith and B. Wenger, *Joule*, 2019, **3**, 2716–2731.

239 F. Baumann, S. R. Raga and M. Lira-Cantú, *APL Energy*, 2023, **1**, 011501.

240 K. Kwak, E. Lim, N. Ahn, J. Heo, K. Bang, S. K. Kim and M. Choi, *Nanoscale*, 2019, **11**, 11369–11378.

241 D. G. Zheng and D. H. Kim, *Nanophotonics*, 2023, **12**, 451–476.

242 F. M. Rombach, S. A. Haque and T. J. Macdonald, *Energy Environ. Sci.*, 2021, **14**, 5161–5190.

243 C.-T. Lin, S. Pont, J. Kim, T. Du, S. Xu, X. Li, D. Bryant, M. A. Mclachlan and J. R. Durrant, *Sustainable Energy Fuels*, 2018, **2**, 1686–1692.

244 J. A. Mikroyannidis, A. N. Kabanakis, S. S. Sharma and G. D. Sharma, *Adv. Funct. Mater.*, 2011, **21**, 746–755.

245 S. Kundu and T. L. Kelly, *Mater. Chem. Front.*, 2018, **2**, 81–89.

246 N. Li, X. Niu, Q. Chen and H. Zhou, *Chem. Soc. Rev.*, 2020, **49**, 8235–8286.

247 A. Kumar Jena, A. Kulkarni and T. Miyasaka, *Chem. Rev.*, 2019, **119**, 3036–3103.

248 B. Nath, P. C. Ramamurthy, G. Hegde and D. Roy Mahapatra, *ISSS J. Micro Smart Syst.*, 2022, **11**, 61–79.

249 V. C. Lokande, C. H. Kim, A. C. Lokande, C. D. Lokhande and T. Ji, Oxides for perovskite solar cells in *Chemically deposited nanocrystalline metal oxide thin films*, Springer Verlag, 2021.

250 V. J. Y. Lim, A. M. Ulatowski, C. Kamaraki, M. T. Klug, L. Miranda Perez, M. B. Johnston and L. M. Herz, *Adv. Energy Mater.*, 2023, **13**, 2200847.

251 A. R. Bowring, L. Bertoluzzi, B. C. O'Regan and M. D. McGehee, *Adv. Energy Mater.*, 2018, **8**, 1702365.

252 L. Bertoluzzi, J. B. Patel, K. A. Bush, C. C. Boyd, R. A. Kerner, B. C. O'Regan and M. D. McGehee, *Adv. Energy Mater.*, 2021, **11**, 2002614.

253 R. G. Vieira, F. M. U. de Araújo, M. Dhimish and M. I. S. Guerra, *Energies*, 2020, **13**, 2472.

254 D. Bogachuk, K. Saddedine, D. Martineau, S. Narbey, A. Verma, P. Gebhardt, J. P. Herterich, N. Glissmann,

255 J. Henzel, K. Bakker, M. Najafi, V. Zardetto, S. Veenstra, O. Isabella, L. Mazzarella, A. Weeber and M. Theelen, *ACS Appl. Energy Mater.*, 2023, **6**, 11429–11432.

256 C. Wang, L. Huang, Y. Zhou, Y. Guo, K. Liang, T. Wang, X. Liu, J. Zhang, Z. Hu and Y. Zhu, *Adv. Energy Mater.*, 2023, **13**, 2203596.

257 F. Jiang, Y. Shi, T. R. Rana, D. Morales, I. Gould, D. P. Mccarthy, J. Smith, G. Christoforo, H. Contreras, S. Barlow, A. D. Mohite, H. Snaith, S. R. Marder, J. D. Mackenzie, M. D. Mcgehee and D. S. Ginger, *arXiv*, 2023, preprint, arXiv:2308.08084, DOI: [10.48550/arXiv.2308.08084](10.48550/arXiv.2308.08084).

258 A. Rajagopal, S. T. Williams, C.-C. Chueh and A. K.-Y. Jen, *J. Phys. Chem. Lett.*, 2016, **7**, 46.

259 Z. Ni, H. Jiao, C. Fei, H. Gu, S. Xu, Z. Yu, G. Yang, Y. Deng, Q. Jiang, Y. Liu, Y. Yan and J. Huang, *Nat. Energy*, 2021, **7**, 65–73.

260 S. Johnston, D. Sulas, E. Palmiotti, A. Gerber, H. Guthrey, J. Liu, L. Mansfield, T. J. Silverman, A. Rockett and M. Al-Jassim, in *2018 IEEE 7th World Conference on Photovoltaic Energy Conversion, WCPEC 2018 – A Joint Conference of 45th IEEE PVSC, 28th PVSEC and 34th EU PVSEC*, 2018, pp. 1897–1901.

261 E. J. Wolf, I. E. Gould, L. B. Bliss, J. J. Berry and M. D. McGehee, *Sol. RRL*, 2022, **6**, 2100239.

262 J. Qian, A. F. Thomson, Y. Wu, K. J. Weber and A. W. Blakers, *ACS Appl. Energy Mater.*, 2018, **1**, 3025–3029.

263 Z. Xu, H. Bristow, M. Babics, B. Vishal, E. Aydin, R. Azmi, E. Ugur, B. K. Yildirim, J. Liu, R. A. Kerner, S. De Wolf and B. P. Rand, *Joule*, 2023, **7**, 1992–2002.

264 R. Brendel, *12th EU PV Sol. Energy Conf.*, 1994, 1339.

265 L. Brockmann, private communication, 2023.

266 C. A. Gueymard, SMARTS, version 2.9.5, 2005.

267 C. Jiang, J. Zhou, H. Li, L. Tan, M. Li, W. Tress, L. Ding, M. Grätzel and C. Yi, *Nano-Micro Lett.*, 2023, **15**, 12.

268 X. Guo, N. Li, Y. Xu, J. Zhao, F. Cui, Y. Chen, X. Du, Q. Song, G. Zhang, X. Cheng, X. Tao and Z. Chen, *Adv. Funct. Mater.*, 2023, **33**, 2213995.

269 J. W. Schall, A. Glaws, N. Y. Doumon, T. J. Silverman, M. Owen-Bellini, K. Terwilliger, M. A. Uddin, P. Rana, J. J. Berry, J. Huang, L. T. Schelhas and D. B. Kern, *Sol. RRL*, 2023, **7**, 2300229.

270 L. Rakocevic, L. E. Mundt, R. Gehlhaar, T. Merckx, T. Aernouts, M. C. Schubert, S. W. Glunz and J. Poortmans, *Sol. RRL*, 2019, **3**, 1900338.

271 J. A. Christians, F. Zhang, R. C. Bramante, M. O. Reese, T. H. Schloemer, A. Sellinger, M. F. A. M. Van Hest, K. Zhu, J. J. Berry and J. M. Luther, *ACS Energy Lett.*, 2018, **3**, 2502–2503.

272 Z. Li, T. R. Klein, D. H. Kim, M. Yang, J. J. Berry, M. F. A. M. Van Hest and K. Zhu, *Nat. Rev. Mater.*, 2018, **3**, 18017.

273 S. Guha, *Multijunction Solar Cells and Modules*, Springer Verlag, 2020.

This journal is © The Royal Society of Chemistry 2024

*Energy Environ. Sci.*, 2024, **17**, 7566–7599 | **7597**

274 L. Rakocevic, R. Gehlhaar, M. Jaysankar, W. Song, T. Aernouts, H. Fledderus and J. Poortmans, *J. Mater. Chem. C*, 2018, **6**, 3034–3041.

275 First Solar, First Solar Series 6TM, https://www.firstsolar.com/.

276 F. U. Kosasih, L. Rakocevic, T. Aernouts, J. Poortmans and C. Ducati, *ACS Appl. Mater. Interfaces*, 2019, **11**, 45646–45655.

277 F. Jamaatisomarin, R. Chen, S. Hosseini-Zavareh and S. Lei, *J. Manuf. Mater. Process.*, 2023, **7**, 94.

278 M. Fenske, C. Schultz, J. Dagar, F. U. Kosasih, A. Zeiser, C. Junghans, A. Bartelt, C. Ducati, R. Schlatmann, E. Unger and B. Stegemann, *Energy Technol.*, 2021, **9**, 2000969.

279 F. Di Giacomo, L. A. Castriotta, F. U. Kosasih, D. Di Girolamo, C. Ducati and A. Di Carlo, *Micromachines*, 2020, **11**, 1–13.

280 A. Rousse, C. Rischel, S. Fourmaux, I. Uschmann, S. Sebban, G. Grillon, P. Balcou, E. Förster, J. P. Geindre, P. Audebert, J. C. Gauthier and D. Hulin, *Nature*, 2001, **410**, 65–67.

281 K. Sokolowski-Tinten, J. Bialkowski, A. Cavalleri, D. Von der Linde, A. Oparin, J. Meyer-Ter-Vehn and S. I. Anisimov, *Phys. Rev. Lett.*, 1998, **81**, 224–227.

282 L. Bayer, M. Ehrhardt, P. Lorenz, S. Pisoni, S. Buecheler, A. N. Tiwari and K. Zimmer, *Appl. Surf. Sci.*, 2017, **416**, 112–117.

283 C. Schultz, M. Fenske, J. Dagar, A. Zeiser, A. Bartelt, R. Schlatmann, E. Unger and B. Stegemann, *Sol. Energy*, 2020, **198**, 410–418.

284 J. Zhao, N. Chai, X. Chen, Y. Yue, Y. B. Cheng, J. Qiu and X. Wang, *Nanophotonics*, 2022, **11**, 987–993.

285 N. N. Udalova, A. S. Tutantsev, Q. Chen, A. Kraskov, E. A. Goodilin and A. B. Tarasov, *ACS Appl. Mater. Interfaces*, 2020, **12**, 12755–12762.

286 B. Q. Lin, C. P. Huang, K. Y. Tian, P. H. Lee, W. F. Su and L. Xu, *Int. J. Precis. Eng. Manuf. – Green Technol.*, 2023, **10**, 123–139.

287 B. Misic, B. E. Pieters, U. Schweitzer, A. Gerber and U. Rau, *Phys. Status Solidi A*, 2015, **212**, 2877–2888.

288 B. Taheri, F. De Rossi, G. Lucarelli, L. A. Castriotta, A. Di Carlo, T. M. Brown and F. Brunetti, *ACS Appl. Energy Mater.*, 2021, **4**, 4507–4518.

289 M. Owen-Bellini, T. J. Silverman, M. G. Deceglie, P. Ndione, N. Kopidakis, I. Repins, M. Wilson, D. B. Sulas-Kern, J. Berry, L. T. Schelhas, C. Sillerud, J. Huang, M. J. Heben, Y. Yan, D. MacKenzie and J. S. Stein, *2022 IEEE 49th Photovoltaics Specialists Conference (PVSC)*, 2022, 0806.

290 K. E. A. Hooper, H. K. H. Lee, M. J. Newman, S. Meroni, J. Baker, T. M. Watson and W. C. Tsoi, *Phys. Chem. Chem. Phys.*, 2017, **19**, 5246–5253.

291 M. D. Kempe, G. J. Jorgensen, K. M. Terwilliger, T. J. McMahon, C. E. Kennedy and T. T. Borek, *Sol. Energy Mater. Sol. Cells*, 2007, **91**, 315–329.

292 J. Li, R. Xia, W. Qi, X. Zhou, J. Cheng, Y. Chen, G. Hou, Y. Ding, Y. Li, Y. Zhao and X. Zhang, *J. Power Sources*, 2021, **485**, 229313.

293 J. Werner, C. C. Boyd, T. Moot, E. J. Wolf, R. M. France, S. A. Johnson, M. F. A. M. Van Hest, J. M. Luther, K. Zhu, J. J. Berry and M. D. McGehee, *Energy Environ. Sci.*, 2020, **13**, 3393–3403.

294 Y. Hu, S. Si, A. Mei, Y. Rong, H. Liu, X. Li and H. Han, *Sol. RRL*, 2017, **1**, 1600019.

295 B. Chen, Z. Z. Yu, A. Onno, Z. Z. Yu, S. Chen, J. Wang, Z. C. Holman and J. Huang, *Sci. Adv.*, 2022, **8**, 1–12.

296 S. Hong, H. Kang, G. Kim, S. Lee, S. Kim, J. H. Lee, J. Lee, M. Yi, J. Kim, H. Back, J. R. Kim and K. Lee, *Nat. Commun.*, 2016, **7**, 3–8.

297 B. A. Kamino, B. Paviet-Salomon, S. J. Moon, N. Badel, J. Levrat, G. Christmann, A. Walter, A. Faes, L. Ding, J. J. Diaz Leon, A. Paracchino, M. Despeisse, C. Ballif and S. Nicolay, *ACS Appl. Energy Mater.*, 2019, **2**, 3815–3821.

298 E. J. Wolf, I. E. Gould, L. B. Bliss, J. J. Berry and M. D. McGehee, *Sol. RRL*, 2021, 2100239.

299 C. Peike, P. Hülsmann, M. Blüml, P. Schmid, K.-A. Weiß and M. Köhl, *Int. Sch. Res. Netw. ISRN Renew. Energy*, 2012, **2012**, 2356–7872.

300 C.-Y. Tsai, S.-Y. Lin and H.-C. Tsai, *Polymers*, 2018, **10**, 238.

301 L. Gnocchi, A. Virtuani, A. Fairbrother, E. Annigoni and C. Ballif, *Sol. Energy Mater. Sol. Cells*, 2023, **262**, 112526.

302 Y. Wang, I. Ahmad, T. Leung, J. Lin, W. Chen, F. Liu, A. M. C. Ng, Y. Zhang and A. B. Djurišić, *ACS Mater. Au*, 2022, **2**, 215–236.

303 F. Toniolo, H. Bristow, M. Babics, L. M. D. Loiola, J. Liu, A. A. Said, L. Xu, E. Aydin, T. G. Allen, M. Meneghetti, S. P. Nunes, M. De Bastiani and S. De Wolf, *Nanoscale*, 2023, **15**, 16984–16991.

304 C. Peike, C. Peike, I. Hädrich, K. Weiß, I. Dürr and F. Ise, *Pvi*, 2013, **22**, 85–92.

305 G. Oreski, A. Omazic, G. C. Eder, Y. Voronko, L. Neumaier, W. Mühleisen, C. Hirschl, G. Ujvari, R. Ebner and M. Edler, *Prog. Photovoltaics*, 2020, **28**, 1277–1288.

306 B. Adothu, P. Bhatt, S. Chattopadhyay, S. Zele, J. Oderkerk, H. P. Sagar, F. R. Costa and S. Mallick, *Sol. Energy*, 2019, **194**, 581–588.

307 G. Oreski, G. C. Eder, Y. Voronko, A. Omazic, L. Neumaier, W. Mühleisen, G. Ujvari, R. Ebner and M. Edler, *Sol. Energy Mater. Sol. Cells*, 2021, **223**, 110976.

308 B. Adothu, P. Bhatt, S. Zele, J. Oderkerk, F. R. Costa and S. Mallick, *Mater. Chem. Phys.*, 2020, **243**, 122660.

309 M. C. López-Escalante, L. J. Caballero, F. Martín, M. Gabás, A. Cuevas and J. R. Ramos-Barrado, *Sol. Energy Mater. Sol. Cells*, 2016, **144**, 691–699.

310 C. Barretta, G. Oreski, S. Feldbacher, K. Resch-Fauster and R. Pantani, *Polymers*, 2021, **13**, 271.

311 R. Heidrich, C. Barretta, A. Mordvinkin, G. Pinter, G. Oreski and R. Gottschalg, *Sol. Energy Mater. Sol. Cells*, 2024, **266**, 112674.

312 V. Fiandra, L. Sannino, C. Andreozzi, G. Flaminio and M. Pellegrino, *Polym. Degrad. Stab.*, 2024, **220**, 110643.

313 B. Adothu, F. R. Costa and S. Mallick, *Polym. Degrad. Stab.*, 2022, **201**, 109972.

314 L. Spinella, S. Uličná, A. Sinha, D. B. Sulas-Kern, M. Owen-Bellini, S. Johnston and L. T. Schelhas, *Prog. Photovoltaics Res. Appl.*, 2022, **30**, 1423–1432.

7598 | *Energy Environ. Sci.*, 2024, **17**, 7566–7599

This journal is © The Royal Society of Chemistry 2024

315 R. Meena, A. Pareek and R. Gupta, *Renewable Sustainable Energy Rev.*, 2024, **189**, 113944.

316 M. Tiefenthaler, G. M. Wallner and R. Pugstaller, *Sol. Energy Mater. Sol. Cells*, 2024, **264**, 112602.

317 K. Liu, P. Thornton, D. R. D'hooge and R. H. Dauskardt, *Prog. Photovoltaics Res. Appl.*, 2023, 317–329.

318 M. Hsian Saw, Y. Sheng Khoo, J. Prakash Singh, D. C. Jordan, N. Haegel, T. M. Barnes, A. Sinha, D. B. Sulas-Kern, M. Owen-Bellini, L. Spinella, S. Uličná, S. Ayala Pelaez, S. Johnston and L. T. Schelhas, *J. Phys. D: Appl. Phys.*, 2021, **54**, 413002.

319 J. Kettle, M. Aghaei, S. Ahmad, A. Fairbrother, S. Irvine, J. J. Jacobsson, S. Kazim, V. Kazukauskas, D. Lamb, K. Lobato, G. A. Mousdis, G. Oreski, A. Reinders, J. Schmitz, P. Yilmaz, M. J. Theelen and C. Jeff Kettle, *Prog. Photovoltaics Res. Appl.*, 2022, **30**, 1365–1392.

320 M. Knausz, G. Oreski, M. Schmidt, P. Guttmann, K. Berger, Y. Voronko, G. Eder, T. Koch and G. Pinter, *Polym. Test.*, 2015, **44**, 160–167.

321 N. Klasen, P. Romer, A. Beinert and A. Kraft, *AIP Conf.: Proc.*, 2019, **2156**, 020016.

322 M. Lang, G. Oreski, E. Helfer, P. Fuchs, A. Halm and M. Klenk, *24th International Conference on Thermal, Mechanical and Multi-Physics Simulation and Experiments in Microelectronics and*, *Microsystems (EuroSimE)*, 2023.

323 A. Virtuani, E. Annigoni and C. Ballif, *Prog. Photovoltaics Res. Appl.*, 2019, **27**, 13–21.

324 *IEC 62804: Test methods for the detection of potential-induced degradation – Part 1: Crystalline silicon*, International Electrotechnical Commission (IEC), Switzerland, 1st edn, 2014.

325 K. Brecl, M. Jošt, M. Bokalič, J. Ekar, J. Kovač and M. Topič, *Sol. RRL*, 2022, **6**, 2100815.

326 Z. Purohit, W. Song, J. Carolus, H. Chaliyawala, S. Lammar, T. Merckx, T. Aernouts, B. Tripathi and M. Daenen, *Sol. RRL*, 2021, **5**, 2100349.

327 J. Carolus, T. Merckx, Z. Purohit, B. Tripathi, H. G. Boyen, T. Aernouts, W. De Ceuninck, B. Conings and M. Daenen, *Sol. RRL*, 2019, **3**, 1900226.

328 M. A. Islam, M. Akhtaruzzaman, M. Mottakin, V. Selvanathan, M. Shahiduzzaman, M. N. I. Khan, A. F. M. Masum Rabbani, M. J. Rashid, M. A. Ibrahim, K. Sopian, K. Sobayel, M. Mottakin, V. Selvanathan, M. Shahiduzzaman, M. N. I. Khan, A. F. M. M. Rabbani, M. J. Rashid, M. A. Ibrahim, K. Sopian and K. Sobayel, *J. Electron. Mater.*, 2023, **52**, 3205–3218.

329 J. Dupuis, E. Saint-Sernin, O. Nichiporuk, P. Lefillastre, D. Bussery and R. Einhaus, *NICE module technology – From the concept to mass production: A 10 years review*, 2012.

330 A. Virtuani, M. Caccivio, E. Annigoni, G. Friesen, D. Chianese, C. Ballif and T. Sample, *Prog. Photovoltaics Res. Appl.*, 2019, **27**, 328–339.

331 E. Annigoni, A. Virtuani, M. Caccivio, G. Friesen, D. Chianese and C. Ballif, *Prog. Photovoltaics Res. Appl.*, 2019, **27**, 760–778.

332 *IEC 61730-1:2023: Photovoltaic (PV) module safety qualification – Part 1: Requirements for construction, VDE, 3.0.*, 2023.

333 I. Kafedjiska and D. Tune, *TandemPV Conference*, Amsterdam, 2024.

334 M. V. Khenkin, E. A. Katz, A. Abate, G. Bardizza, J. J. Berry, C. Brabec, F. Brunetti, V. Bulović, Q. Burlingame, A. Di Carlo, R. Cheacharoen, Y. B. Cheng, A. Colsmann, S. Cros, K. Domanski, M. Dusza, C. J. Fell, S. R. Forrest, Y. Galagan, D. Di Girolamo, M. Grätzel, A. Hagfeldt, E. von Hauff, H. Hoppe, J. Kettle, H. Köbler, M. S. Leite, S. (Frank) Liu, Y. L. Loo, J. M. Luther, C. Q. Ma, M. Madsen, M. Manceau, M. Matheron, M. McGehee, R. Meitzner, M. K. Nazeeruddin, A. F. Nogueira, Ç. Odabaşı, A. Osherov, N. G. Park, M. O. Reese, F. De Rossi, M. Saliba, U. S. Schubert, H. J. Snaith, S. D. Stranks, W. Tress, P. A. Troshin, V. Turkovic, S. Veenstra, I. Visoly-Fisher, A. Walsh, T. Watson, H. Xie, R. Yıldırım, S. M. Zakeeruddin, K. Zhu and M. Lira-Cantu, *Nat. Energy*, 2020, **5**, 35–49.

335 T. Song, D. J. Friedman and N. Kopidakis, *Adv. Energy Mater.*, 2021, **11**, 2100728.

336 G. Bardizza, H. Müllejans, D. Pavanello and E. D. Dunlop, *JPhys: Energy*, 2021, **3**, 21001.

337 T. Song, C. Mack, R. Williams, D. J. Friedman and N. Kopidakis, *Sol. RRL*, 2022, **6**, 2200800.

338 A. Mei, Y. Sheng, Y. Ming, Y. Hu, Y. Rong, W. Zhang, S. Luo, G. Na, C. Tian, X. Hou, Y. Xiong, Z. Zhang, S. Liu, S. Uchida, T. W. Kim, Y. Yuan, L. Zhang, Y. Zhou and H. Han, *Joule*, 2020, **4**, 2646–2660.

339 L. Duan, D. Walter, N. Chang, J. Bullock, D. Kang, S. P. Phang, K. Weber, T. White, D. Macdonald, K. Catchpole and H. Shen, *Nat. Rev. Mater.*, 2023, **8**, 261–281.

340 V. Paraskeva, M. Hadjipanayi, M. Norton, A. Aguirre, A. Hadipour, W. Song, T. Fontanot, S. Christiansen, R. Ebner and G. E. Georghiou, *Energies*, 2023, **16**, 2608.

341 M. Jošt, B. Lipovšek, B. Glažar, A. Al-Ashouri, K. Brecl, G. Matič, A. Magomedov, V. Getautis, M. Topič and S. Albrecht, *Adv. Energy Mater.*, 2020, **10**, 2000454.

342 J. Li, J. Dagar, O. Shargaieva, O. Maus, M. Remec, Q. Emery, M. Khenkin, C. Ulbrich, F. Akhundova, J. A. Márquez, T. Unold, M. Fenske, C. Schultz, B. Stegemann, A. Al-Ashouri, S. Albrecht, A. T. Esteves, L. Korte, H. Köbler, A. Abate, D. M. Többens, I. Zizak, E. J. W. List-Kratochvil, R. Schlatmann and E. Unger, *Adv. Energy Mater.*, 2023, **13**, 2203898.

343 M. Babics, M. De Bastiani, E. Ugur, L. Xu, H. Bristow, F. Toniolo, W. Raja, A. S. Subbiah, J. Liu, L. V. Torres Merino, E. Aydin, S. Sarwade, T. G. Allen, A. Razzaq, N. Wehbe, M. F. Salvador and S. De Wolf, *Cell Rep. Phys. Sci.*, 2023, **4**, 101280.

344 M. Khenkin, H. Kö, M. Remec, R. Roy, U. Erdil, J. Li, N. Phung, G. Adwan, G. Paramasivam, Q. Emery, E. Unger, R. Schlatmann, C. Ulbrich and A. Abate, *Energy Environ. Sci.*, 2024, **17**, 602–610.

This journal is © The Royal Society of Chemistry 2024

*Energy Environ. Sci.*, 2024, **17**, 7566–7599 | **7599**